GEOSYNTHETIC REINFORCED PILE SUPPORTED EMBANKMENTS

By

RUTUGANDHA GANGAKHEDKAR

A THESIS PRESENTED TO THE GRADUATE SCHOOL
OF THE UNIVERSITY OF FLORIDA IN PARTIAL FULFILLMENT
OF THE REQUIREMENTS FOR THE DEGREE OF
MASTER OF ENGINEERING

UNIVERSITY OF FLORIDA

2004

ACKNOWLEDGMENTS

I am indebted to Dr. Townsend, as the chairman of my committee for providing me great guidance in the research project. He has made this experience at U.F. a very pleasurable one. I would like to thank Dr. Davidson and Dr. Bloomquist for serving on my committee. Working with Dr. Davidson, as a teaching assistant, has been a very enjoyable learning experience.

I would like to express my gratitude to all the faculty members in the Geotechnical Department for making the master's program a pleasant experience.

I am grateful to my family back home for always standing by my side. I am thankful to all my friends back home and here who always have supported and encouraged me.

TABLE OF CONTENTS

page

LIST OF TABLES

LIST OF FIGURES

Abstract of Thesis Presented to the Graduate School
of the University of Florida in Partial Fulfillment of the
Requirements for the Degree of Master of Engineering

GEOSYNTHETIC REINFORCED PILE SUPPORTED EMBANKMENTS

By

Rutugandha Gangakhedkar

May 2004

Chair: Frank Townsend
Major Department: Civil and Coastal Engineering

The design of embankments on weak foundation soils is a challenge to the geotechnical engineer. There are several issues related to bearing capacity failures, intolerable settlements and slope instability that need to be addressed. The piled embankments with the inclusion of a geosynthetic layer have proved to be one of the economic and effective techniques to handle such problems.

The inclusion of the geosynthetic reinforcement eliminates the need for inclined piles used in conventional piled embankments for resisting large lateral pressures. The geosynthetic layer enhances the load transfer mechanism and considerably minimizes the differential and maximum settlements.

This study attempts to analyze the various methods available today for the design of these structures. A numerical study is carried out. The effects of certain factors like pile modulus, stiffness of the geosynthetic reinforcement, height of the embankment, effect of the soil layer directly below the geogrid which are not considered by other available methods are studied using a finite element program – Plaxis 2D. Plane strain

models of five case studies found in the literature are developed. The results from various methods are evaluated and compared with the results from Plaxis. It is found that numerical analysis was able to address many factors that were neglected by all the other available methods. It was also found to be more reliable than currently used methods.

CHAPTER 1
INTRODUCTION

1.1. Background

Weak foundation soils have always been a challenge to Geotechnical Engineers. When designing embankments over weak foundations, bearing capacity, slope stability, lateral pressures and movements and differential settlement are some of the major concerns. A variety of techniques are available to address these issues. They include preloading, deep mixing columns, stone columns, use of light weight fill, and soil replacement. Steel and concrete piles have also been used. Geosynthetic reinforced pile supported (GRPS) embankments, the subject of this thesis have also been very successful.

The conventional pile-supported (CPS) system (Figure 1) requires large pile caps and very closely spaced piles. This is essential to transfer the large embankment loads to the piles and to avoid surface deformations due to large differential settlement between the caps. The CPS requires inclined piles at the edges of the embankment to resist large lateral pressures. The Piled embankments with a concrete slab (Figure 2) are successful in transferring all the load, however they require a large amount of steel as reinforcement or very thick concrete slabs. This makes them very uneconomical and hence they are rarely used in practice.

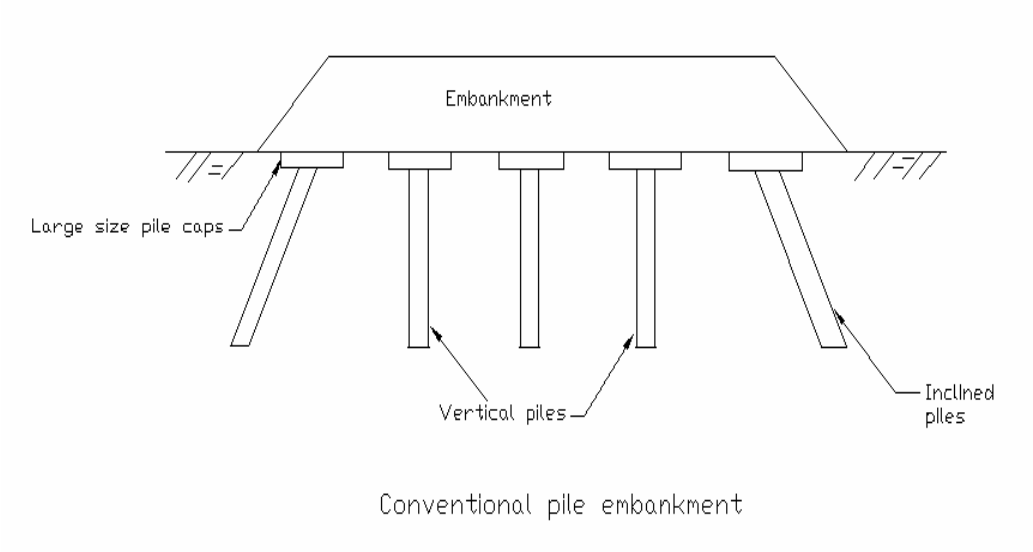

Figure1: Conventional pile-supported system

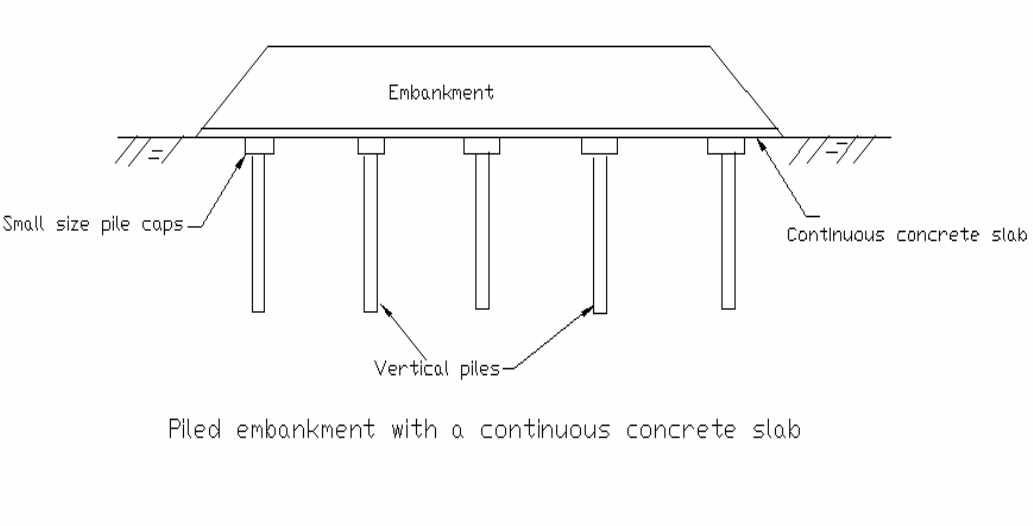

Figure 2: Piled embankments with concrete slab

Geosynthetics have a very high tensile strength which the soil lacks. Geosynthetics reduce the differential settlement, increase the bearing capacity, and the slope stability when used in soft soils. The GRPS system (Figure 3) has a geosynthetic reinforced platform or mat which increases the efficiency of transferring the load from the soil to the piles without giving rise to deflections between the pile caps. The geosynthetic layers

provide a resistance to the lateral thrust at the edges of the embankments. GRPS embankments can be more rapidly constructed than CPS embankments.

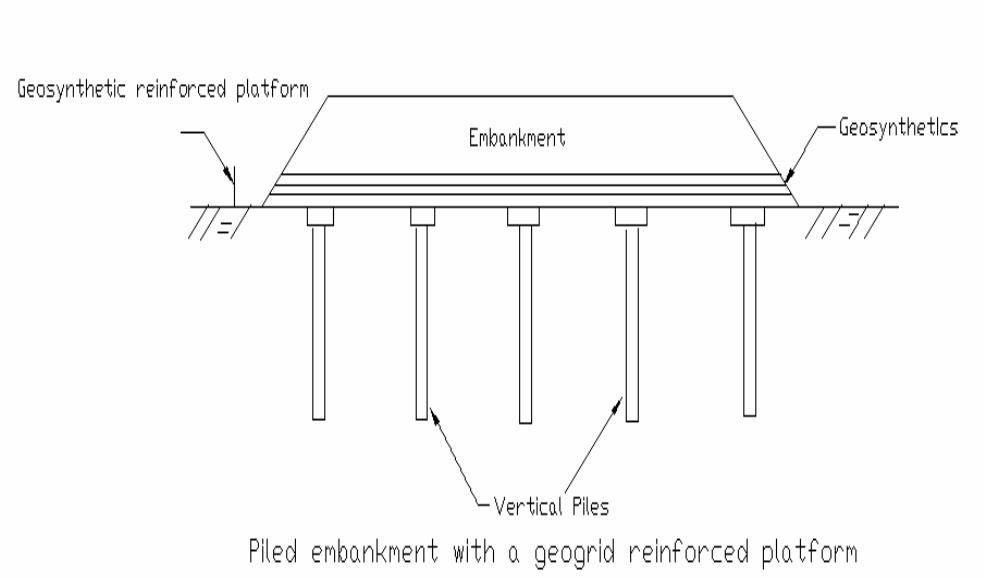

Figure 3: Geosynthetic reinforced piled supported embankments

From a survey of various projects (Han, 1999), it was found that in conventional piled embankments the percent coverage of the pile caps over the total foundation area is 60-70% whereas, in the GRPS system the percent coverage is reduced to about 10-20%. In this system, the pile size can also be reduced and larger pile caps can be used. This illustrates that this technique has technical and economical advantages over others.

Vibro-concrete columns, deep mixed columns, stone columns or any other columnar system used in ground improvement can be used to support the embankment. Such columns, commonly have larger diameters than the piles. The column heads act as pile caps and help in transferring the load. The deformation of the soil between the pile caps induces negative skin friction in the piles. This is eliminated in the columnar system. The columnar systems have a range of stiffness and their stiffness is less than the piles.

The columnar system can be installed in various patterns, grid, block, wall as per the specific requirements. The columnar system and soil act as a composite foundation and carry the load from the embankment. Hence, they can act as end bearing or a floating system unlike the piles which have to be seated on a firm strata.

GRPS embankments have several applications:

- Embankments over soft soils,
- Embankments approaching a bridge supported by deep foundations,
- To prevent differential settlement between a new embankment near existing structures or existing embankment where settlement has ceased.
- Sub-grade improvement

1.2. Statement of the Problem

A number of methods are available for the design of GRPS embankment systems. Limited guidelines are also available for columnar systems. This report addresses design issues and compares the various methods available. A finite element model is developed for the case studies in Plaxis – finite element software.

The design issues of lateral movement, geosynthetic mattress design, pile design, slope stability and settlement will be handled here. The case studies will be discussed and comparison of various methods and the finite element model will be presented.

CHAPTER 2
LITERATURE REVIEW

2.1. Theory of Soil Arching

Arching is defined by McNulty (1965) (cited in Han, 1999) as "the ability of a material to transfer loads from one location to another in response to a relative displacement between the locations. A system of shear stresses is the mechanism by which the loads are transferred." Figure 4,5 and 6 illustrate this concept. Consider soil on a rigid base, there is no tendency for differential movement and hence no soil arching. The stress acting at a point **a** in Figure 4 is the overburden stress γH, where γ is the unit weight of the soil and H is the height of the soil prism. When one of the local supports at the point **a** is removed, the point **a** is in tension and a roof tension arch is formed. The true arch collapses as the soil is not in equilibrium. The soil settles in an inverted arch, the adjacent soil develops the required shear strength and the soil reaches equilibrium state. The transfer of pressure from the yielding portion to the stationary portion is called arching.

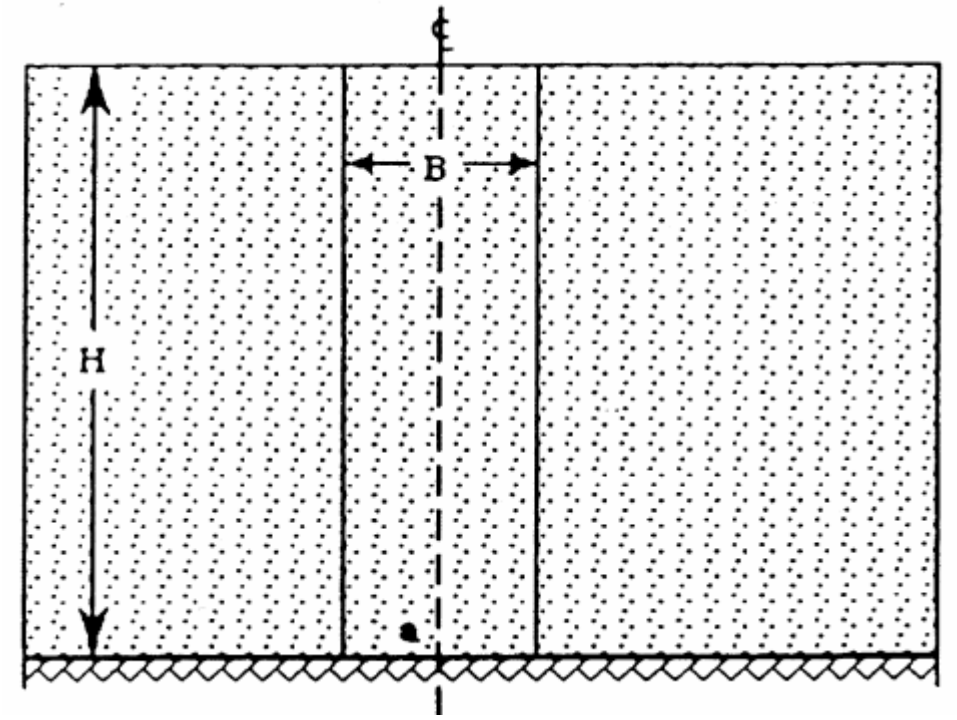

Figure 4: The soil mass overlying a potential void (McKelvey, 1994 - cited in Li et al., 2002)

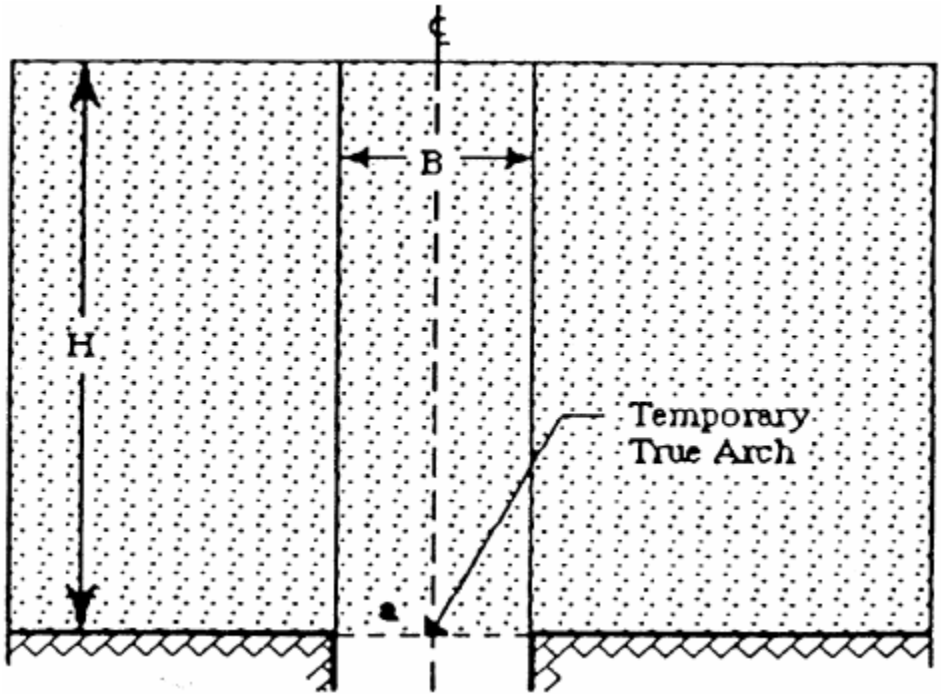

Figure 5: The formation of a true arch (Void under soil mass) (McKelvey, 1994 - cited in Li et al., 2002)

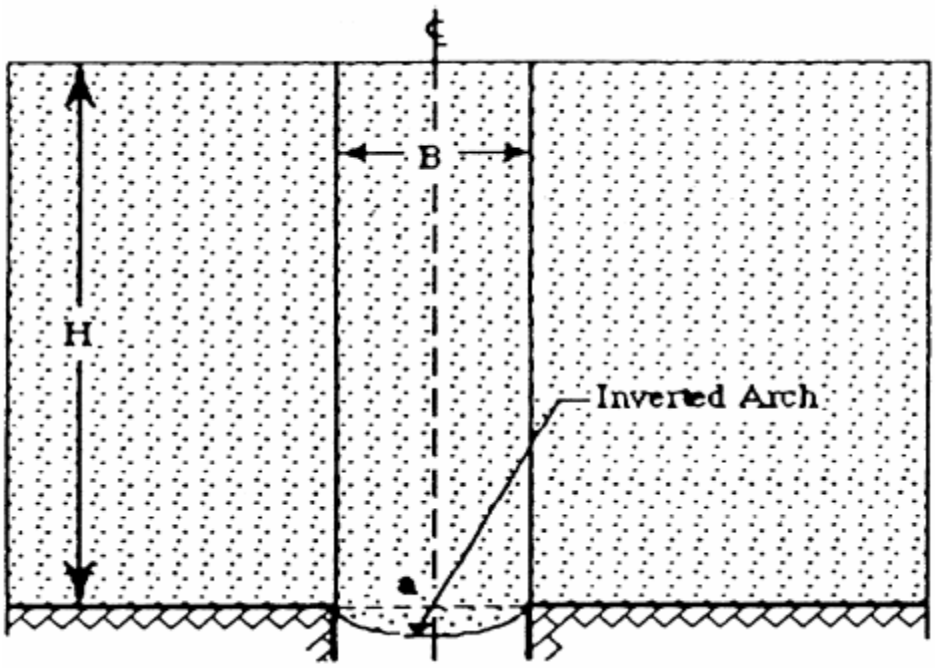

Figure 6: Soil mass collapses to form an inverted arch (McKelvey, 1994 - cited in Li et al., 2002)

Different methods have been proposed to model the soil arching effect. Terzaghi (1936) (cited in Han and Gabr, 2002) considered the shear strength along the soil prism which is mobilized to a certain height, at which the plane of equal settlement exists. Giroud et al. (1990) (cited in Han and Gabr, 2002) applied McNulty's model to deal with soil layer-geosynthetic systems overlying voids. Hewlett and Randolph (1988) (cited in Li et al., 2002) considered limit equilibrium in a domed region for the sand between the two piles. Most of the load above the crown was transferred onto the support through the crown. Schmertmann (1991) (cited in Han and Gabr, 2002) proposed that all the load within the triangular prism(plane strain) or conical prism(axisymmetric) is transferred directly onto the adjoining support. In all the above cases, it is assumed that all the pressure is to be carried by the geosynthetic; i.e., there is a cavity below the geosynthetic layer as shown in Figure 7.

2.1.1. Load Transfer Mechanism

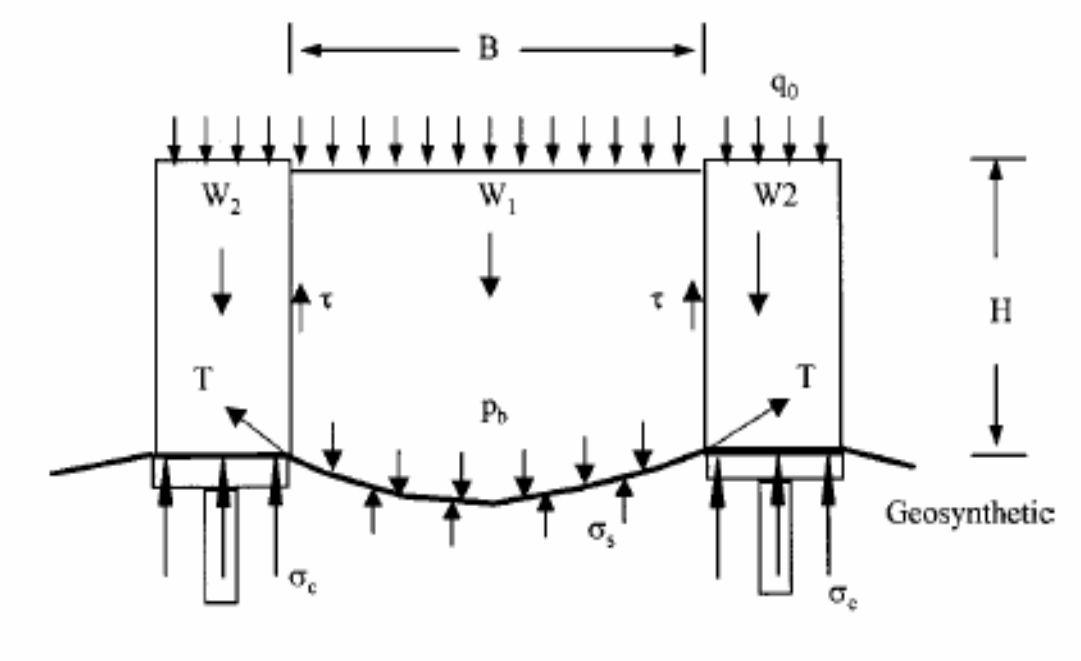

Figure 7: Load Transfer Mechanism (cited in Li et al., 2002)

Soil Arching $p_b=\rho(\gamma H+q_o)$

Tension in membrane T

Stress concentration ratio $n=\frac{\sigma_c}{\sigma_s}>1$

The geosynthetic layer and the embankment fill form a stiffened fill platform that supports load transfer mechanism. High quality fill is used for better interaction between the soil and pile. The weight of the fill tends to move downward due to the presence of soft soil below the geosynthetic layer. This downward motion is resisted by the shear resistance provided by the fill on the pile caps. The shear resistance reduces the pressure acting on the geosynthetic but increases the load acting on the caps.

The inclusion of the geosynthetic layer is expected to reduce the differential settlement between two pile caps. The reduction of the displacement reduces the shear stresses induced by soil arching. Hence, the load transfer by soil arching is reduced. This

also reduces the load transferred to the pile caps. The vertical component of the tension forces in the reinforcement(s) is however, transferred to the pile caps. A single geosynthetic layer acts as a tension membrane while a multi-layer system can interlock better with the surrounding soil and act as a stiffened “beam” or “plate”. The shear resistance from the reinforced mass is considered as apparent cohesion.

In the case, where the geosynthetic reinforced platform is perfectly rigid there is no differential settlement, tension in reinforcement, nor relative movement between the soil and reinforcement. Here, the mechanism of soil arching, tensioned membrane or apparent cohesion cannot be developed. This leads to the stress concentration on the pile caps which is due to the stiffness difference between the pile caps and soil.

2.1.2. Stress Concentration Ratio

The stress concentration ratio is a parameter that is used to quantify load transfer. It is defined as the ratio of the stress on the pile(caps) to the soil between the pile(caps). The stress concentration is a global index which incorporates the mechanism of soil arching, tension membrane or apparent cohesion effect and pile-soil stiffness difference. Ooi et al. (1987) (cited in Han, 1999) indicated that the value of n for conventional pile embankments ranged between 1.0 to 8.0. This ratio increased with the increase in the ratio of the embankment height to the net spacing between the two near edges of the caps on the piles. Based on studies by Reid et al. (1993) and Maddison et al. (1996) (cited in Han, 1999), the n values for the GRPS systems on vibro- concrete columns and concrete piles ranged from 8 to 25, which is much higher than the conventional piled embankments. This increase in n is due to the inclusion of the geosynthetic layer.

The n value depends on the stiffness or rigidity of the foundation. The stress concentration for a fully flexible foundation resting on a pile-soil composite foundation without soil arching is said to have a n value equal to one. The concentration ratio for a rigid foundation is very high. The GRPS system can be considered as an intermediate state between flexible and rigid foundations.

2.2. Design of Geosynthetic Reinforcement

In geosynthetic reinforced pile rafted embankments, the conventional rigid concrete mat resting on the piles is replaced by a layer of soil along with a geosynthetic reinforcement to provide the required tensile resistance. This layer is more flexible. Due to the flexibility of the geosynthetic layer, load transfer due to soil arching is seen. The degree of soil arching and hence the vertical stress on the reinforcement and pile(caps) needs to be evaluated.

The design of the reinforcement should consider:

- Vertical stress on the reinforcement after soil arching effect between the adjacent piles has taken place
- The tensile force developed in the reinforcement due to the vertical pressure of the embankment
- The tensile force in the reinforcement due to lateral spreading of the embankment.

The design methods that will be discussed here are: BS 8006, Terzaghi's theory, Helwett and Randolph theory and Guido's theory. The finite element method using Plaxis-finite element program will be discussed in Chapter 3. Most of the current design methods ignore the soil resistance below the geosynthetic layer; i.e., a void is considered below the geosynthetic layer. This makes the design conservative. Here we are considering piles arranged in a rectangular pattern.

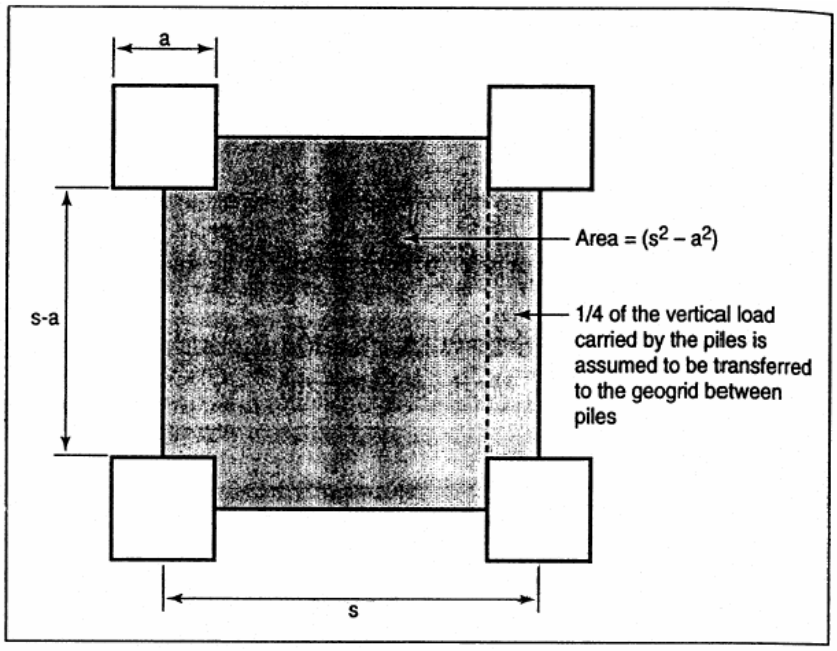

Figure 8: Unit Cell Utilization (Russell and Pierpoint, 1997 - cited in Li et al., 2002)

A unit cell supported at four ends on piles is considered (Russell and Pierpoint, 1997 - cited in Li et al., 2002). The area of the cell is s^2 and the area not supported by the pile is (s^2-a^2). A quarter of the load is assumed to be transferred to the reinforcement.

2.2.1. Stress Reduction Factor

In order to compare the various methods a stress reduction ratio denoted as S_3D is defined. It is defined as the ratio of the average vertical stress acting on the reinforcement to the overburden pressure due to the embankment fill.

$$S_{3D} = \frac{2W_T(s-a)}{\gamma H\left(s^2-a^2\right)} \qquad \text{Eqn.2.1}$$

2.2.1.1. BS8006(1995)

BS8006, (cited in British Standard 8006, 1995) is the British Standard method used for design of embankments with reinforced soil foundations on poor ground. This is the

most widely used method and is very conservative. The distributed vertical load acting on the reinforcement between the pile caps is W_T

For $H>1.4\times(s-a)$

$$W_T = \frac{1.4sf_{fs}\gamma(s-a)}{s^2-a^2}\times\left(s^2-a^2\left(\frac{p`_c}{\sigma`_v}\right)\right) \quad \text{Eqn.2.2}$$

For $0.7(s-a) \le H \le 1.4(s-a)$

$$W_T = \frac{s\times(f_{fs}\gamma H+f_q ws)}{s^2-a^2}\times\left(s^2-a^2\left(\frac{p`_c}{\sigma`_v}\right)\right) \quad \text{Eqn.2.3}$$

but $W_T = 0$ if $\frac{s^2}{a^2} \le \frac{p`_c}{\sigma`_v}$ Eqn.2.4

where

s the spacing between the piles

a the size of the pile caps

w_s the uniformly distributed surcharge loading

$p`_c$ the vertical stress on pile caps

$\sigma`_v$ the factored average vertical stress at the base of the embankment

$\sigma`_v = f_{fs}\gamma H + f_q w_s$

f_{fs} the partial load factor for soil unit weight

f_q the partial load factor for applied external loads

γ the unit weight of the soil

H the height of the embankment fill

This method considers the piles as buried rigid conduits. The vertical stress is given using Marston's formula for positive projecting conduits.

$$p`_c = \sigma`_v\left(\frac{C_c a}{H}\right)^2 \quad \text{Eqn.2.5}$$

BS8006 gives empirical equations for arching coefficient as follows

$$C_c = 1.95\frac{H}{a} - 0.18 \quad \text{for end-bearing piles(unyielding)} \qquad \text{Eqn.2.6}$$

$$C_c = 1.5\frac{H}{a} - 0.07 \quad \text{for friction and other piles} \qquad \text{Eqn.2.7}$$

Based on the above equations the stress reduction ratio is given by

$$S_{3D} = \frac{2.8s}{(s+a)^2 H}\left(s^2 - a^2\left(\frac{p_c}{\gamma H}\right)\right) \qquad \text{Eqn.2.8}$$

2.2.1.2. Terzaghi Method

Terzaghi's (1943) (cited in Li et al., 2002) method was based on results from trap door tests at large displacement. Terzaghi considered the problem as three dimensional. He considered the shear strength along a soil prism which is mobilized to a certain height where there exists a plane of equal settlement. The stress reduction ratio is given as

$$S_{3D} = \frac{(s^2 - a^2)}{4HaK\tan(\phi')} \times \left(1 - e^{\frac{-4aHK\tan(\phi')}{s^2 - a^2}}\right) \qquad \text{Eqn.2.9}$$

K is the ratio of the horizontal to vertical pressure. Terzaghi has taken K=1.

2.2.1.3. Hewlett and Randolph Theory

Hewlett and Randolph (1988) (cited in Li et al., 2002) found a theoretical solution for a granular, free draining soil based on model tests. It assumes the soil arching as a series of vaulted domes of hemispherical shape supported by the pile caps. In this case, the critical locations for failure would be at the crown of the domes or at the pile caps. The stress reduction factor is evaluated using limiting plastic equilibrium.

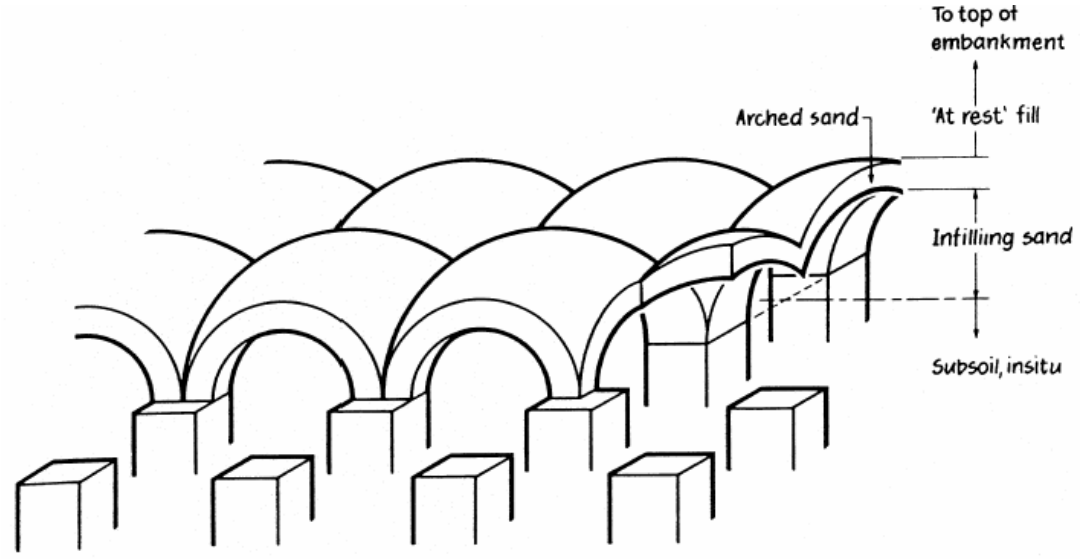

Figure 9: Hemispherical domes model (Hewlett & Randolph, 1988 – cited in Li et al., 2002)

The stress reduction ratio at the crown is given by

$$S_{3D}=\left(1-\frac{a}{s}\right)^{2(K_p-1)}\left(1-\frac{s}{2\sqrt{H}}\times\frac{2\left(K_p-1\right)}{\left(2K_p-3\right)}\right)+\frac{(s-a)}{\sqrt{2}H}\times\frac{2\left(K_p-1\right)}{(2K_p-3)} \qquad \text{Eqn.2.10}$$

The stress reduction ratio on the pile caps is given by

$$S_{3D}=\frac{1}{\left(\frac{2K_p}{K_p+1}\right)\left(\left(1-\frac{a}{s}\right)^{(1-K_p)}-\left(1-\frac{a}{s}\right)\left(1+\frac{a}{s}K_p\right)\right)+\left(1-\frac{a^2}{s^2}\right)} \qquad \text{Eqn.2.11}$$

Here, K_p is the passive earth pressure. The higher of the two stress reduction ratios is used for the calculations. Hence, it considers the worst case scenario.

2.2.1.4. Guido's Theory

Guido et al.(1987) (cited in Li et al., 2002) considered the effect of lateral spreading of the embankment. The reinforcement carries load from only a rectangular pyramid, that is not carried by the piles. The stress concentration ratio is given by

$$S_{3D}=\frac{(s-a)}{3\sqrt{2}H} \qquad \text{Eqn.2.12}$$

Schmertmann (1999) (cited in Han and Gabr, 2002), proposed a triangular load transfer model for soil arching. It was assumed that all the load above the triangle will be transferred onto the adjoining support. This was confirmed by finite element analysis by Gabr and Hunter(1994) (cited in Han and Gabr, 2002) . However, all the above models have neglected the effects of the difference in the stiffness of the geosynthetic layer and elastic modulus of the pile caps. The maximum tension in the geosynthetic is said to occur at the edge of the pile.

2.2.2. Tension in Reinforcement

The British Standard BS8006 (1995) suggests the following formula for an extensible reinforcement. The tensile load T_{rp} per metre "run" generated in the reinforcement resulting from the distributed load W_T is given by

$$T_{rp} = \frac{W_T(s\text{-}a)}{2a}\sqrt{1+\frac{1}{6\varepsilon}} \qquad \text{Eqn.2.13}$$

where

T_{rp} the tension in the reinforcement

ε the strain in the reinforcement.

The tension in the reinforcement is calculated taking into consideration the maximum allowable strain in the reinforcement. Six percent strain is considered the upper limit for transferring the load to the piles. The load/strain curve should be studied at different load levels. The upper limit should be reduced for shallow embankments to prevent differential movements on the surface of the embankment. To avoid long term localized deformations at the surface of the embankment, the long term strain should be kept to a minimum. A maximum creep strain of 2% is permitted for permanent construction.

This tensile load is developed as the reinforcement deforms during embankment construction. If it does not deform during construction, the tensile force is not developed; i.e., the load is not carried by the reinforcement till the foundation settles. Alternative equations should be used to determine the tensile strength of inextensible reinforcement.

Giroud et al. (1990) (cited in Li et al., 2002) proposed a membrane theory for a geosynthetic layer overlying an infinitely long void. This was also used to determine the tension in the reinforcement.

The formula can be stated as

$$T_{rp}=\sigma_s(s\text{-}a)\Omega \qquad \text{Eqn.2.14}$$

where

σ_s the stress placed on the geosynthetic reinforcement

Ω a dimensionless factor relating the geosynthetic strain to the geosynthetic deflection.

Ω can be defined as

$$\Omega=\frac{1}{4}\left[\frac{2y}{(s\text{-}a)}+\frac{(s\text{-}a)}{2y}\right] \qquad \text{Eqn.2.15}$$

where

y the geosynthetic deflection.

Many geosynthetics are anisotropic in nature. They have more strength in the machine or cross-machine direction. Giroud et al.(1990) (cited in Li et al., 2002) has two theories for the strength of the geosynthetic layer that is to be used. In the first approach the strength of the geosynthetic in the weak direction is assumed for the strength in all directions. The second approach is to limit the applied tension to half of the strength in

the strong direction. The more conservative approach is generally used in all designs. The actual value is generally close to the less conservative approach.

2.2.3. Soil Resistance

All the design methods stated above consider a void below the geosynthetic layer. The resistance from the soil below the GRPS platform is ignored. This leads to a conservative design. In practice, there will be some support provided by the soil below. This will considerably reduce the tension in the reinforcement. Reid and Buchman (1984) (cited in Han, 2003) found from their study that the resistance from the soil below the GRPS platform is $0.18\gamma H$ where γ is the unit weight of the embankment fill and H is the height of the embankment. John (1987) (cited in Han, 2003) found the soil resistance to be $0.15\gamma H$. Later, a finite element model by Jones et al. (1990) (cited in Han, 1999) proved that partial support from the reinforcement reduced the tensile force in the reinforcement significantly (Figure 10). This can be seen in the Plaxis model developed in Chapter 3.

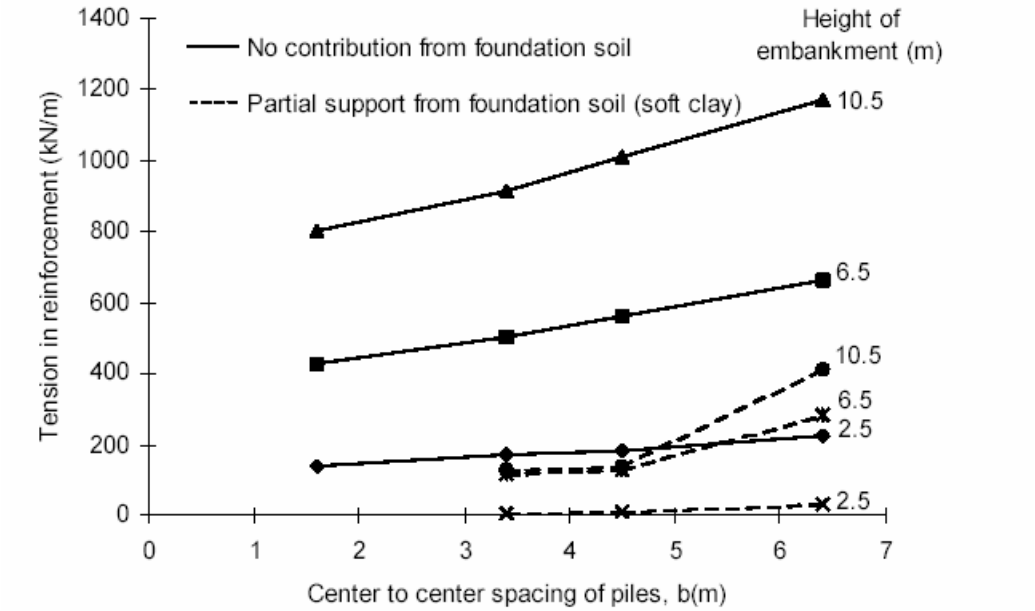

Figure 10: Tensile force in the reinforcement under embankment of medium dense soil (Jones et al. (1990) - cited in Han, 1999)

However, it seems to be reasonable to consider a cavity under the GRPS platform if the settlement below the platform is caused by factors other than the embankment loads. The settlement can be due to consolidation or under-consolidation of the soil, liquefaction, lowering of ground water, etc.

2.2.4. Tension in Reinforcement due to Lateral Sliding

The reinforcement should resist the horizontal force due to lateral sliding. This tensile load should be generated at a strain compatible with allowable lateral pile movements. The need for raking of the piles is eliminated. The reinforcement tensile load needed to resist the outward thrust on the embankment in accordance to BS8006 (1995) is

$$T_{ds}=0.5K_a(f_{fs}\gamma H+2f_q w_s)H \qquad \text{Eqn.2.16}$$

where

K_a the active earth pressure coefficient (Ka=tan2(45-□/2)).

w_s the uniformly distributed surcharge loading

f_{fs} the partial load factor for soil unit weight

f_q the partial load factor for applied external loads

γ the unit weight of the soil

H the height of the embankment fill.

To generate this tensile load the embankment fill should not slide outwards over the reinforcement. The reinforcement bond length should be

$$L_e \geq \frac{0.5K_aH(f_{fs}\gamma H+2f_q w_s)f_s f_n}{\gamma H\frac{\alpha`\tan(\varphi`)c}{f_{ms}}} \qquad \text{Eqn.2.17}$$

where

f_s the partial factor for reinforcement sliding resistance

f_n the partial factor governing the economic ramifications of failure

h the average height of the embankment fill above the reinforcement length L_e

α` the interaction coefficient relating the embankment fill/reinforcement bond angle to tan$\phi$`cv

$\phi`_{cv}$ the large strain angle of friction of the embankment fill under effective stress conditions

f_{ms} the partial material factor applied to tan $\phi`_{cv}$

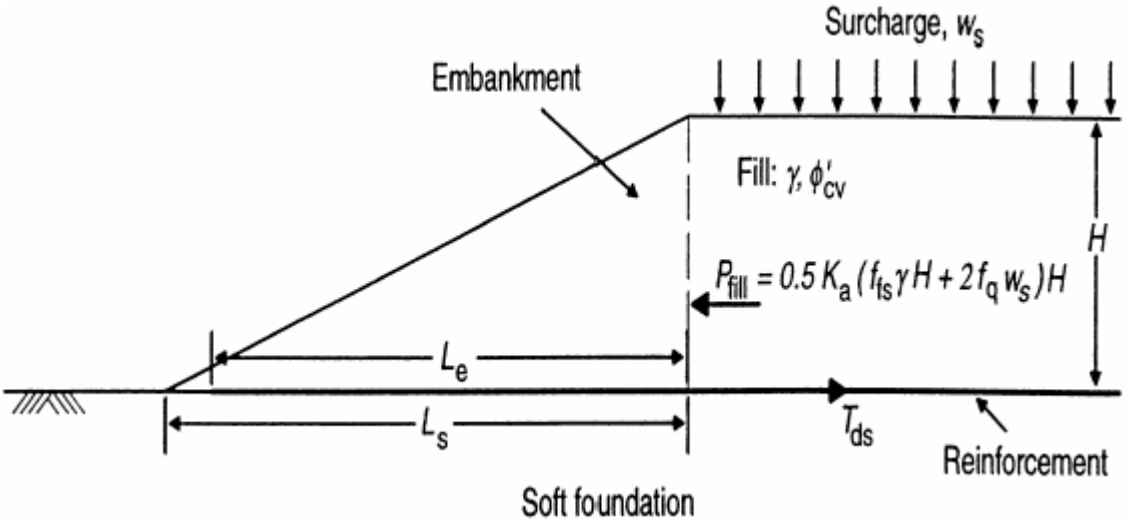

Figure 11: Lateral sliding stability at the interface of fill and reinforcement (BS8006, 1995)

2.2.5. Reinforcement Strain

According to BS 8006, the maximum allowable strain in the reinforcement should be limited to ensure that no differential settlement occurs at the surface of the embankment. In shallow embankments, however it might happen that the full soil arch cannot be formed within the embankment fill.

An initial tensile strain is required for transfer of load to the piles. An upper limit of about 6% is imposed to ensure that all the load is transferred to the piles. This upper limit can be reduced for shallow embankments to prevent differential movements.

In order to ensure that long term localized movements do not occur at the surface of the embankment, the long term strain should be kept to a minimum. A maximum creep strain of 2% is generally allowed over the design life of the reinforcement.

2.3. Plate Model Tests

Reinforced foundations have four possible modes of failure (Wayne et al., 1998, cited in Li et al., 2002). Variation in soil conditions and configuration of reinforcement result in these different modes. The failure modes are

- When soil beneath the reinforced soil is very soft.
- Dimension punching failure – failure above the uppermost reinforcement – it can occur when the topmost reinforcement layer is not placed close enough to the bottom of the reinforcement.
- Failure between the reinforcements – it can occur due to large spacing between two reinforcement layers.
- Deep punching failure – it occurs when the underlying soil is very soft and the reinforced mass is very strong but the reinforced mass does not have sufficient width or thickness to reduce the stress at the base of the reinforcement.

The actual failure of the foundation is controlled by the critical mode. The ultimate bearing capacity in the critical mode is less than that in any other types of failure.

Many model tests were performed by Wayne et al.(1998), Krishnaswamy et al.(2000) and Guido et al.(1997) (cited in Li et al., 2002) on reinforced foundation. These tests were performed to determine the influence of various factors on the bearing capacity of the foundation.

Wayne Model Test

Bearing capacity ratio(BCR) is used for convenience in comparing the test:

$$BCR=q_r/q_o \qquad \text{Eqn.2.18}$$

where

q_0 the ultimate bearing pressure for the unreinforced sand

q_r the bearing pressure of the geogrid-reinforced sand at a settlement corresponding to the settlement at the ultimate bearing pressure for the unreinforced sand.

Wayne recommended typical design parameters in order to keep the bearing capacity ratio in the range of 1.5 to 2.5. Generally a 0.1m thickness is placed below the lowest geogrid in order to have good interaction.

Table 1: Recommended values for design parameters

	Typical Values	Recommended (not greater than)
u	0.15B to 0.3B	0.5B
s	0.15B to 0.3B	0.5B
z	0.5B to 1.0B	2.0B
b	2.0B to 3.0B	4.0B
a	0.1B to 0.2B	0.3B
Δl	0.5B to 1.0B	2.0B
N	2 to 4	5

Note:

u = distance from the uppermost geogrid to the footing base

s = spacing between the geogrid layers

z = thickness of the reinforced fill

b = width of the reinforced fill

a = distance from the lowest geogrid to the bottom of the reinforced fill

Δl = length of the geogrid beyond each of the strip footing

N = number of geogrid layers

2.4. Pile Design

The pile reinforces the underlying subsoil. The piles give direct support to the embankment through soil arching. The embankment imposes a lateral thrust on the piles. In conventional pile supported embankments, inclined piles are included at the toe of the embankment. In GRPS, the geosynthetic membrane is laid on the pile caps. The tension provided by the membrane provides support and prevents lateral sliding of the embankment.

In geosynthetic reinforced pile supported embankments, the term pile is used not only for conventional piles but also for other soil improvement columns like stone columns, vibro concrete columns, soil-cement columns, etc.

The pile design incorporates

- lateral movement of the pile
- bending moment developed in the pile due to lateral movement
- axial bearing capacity of the pile
- settlement of the pile

The load carrying capacity of the pile or any other column used in soil improvement should be evaluated according to the methods developed for that type of soil improvement. The effect of group action should be considered. The spacing of the piles is maximized for economical reasons. An upper limit on the spacing of the piles is imposed (BS 8006) when the piles are installed in a square grid pattern.

$$s = \sqrt{\frac{Q_p}{\left(f_{fs}\gamma H + f_q w_s\right)}} \qquad \text{Eqn.2.19}$$

where

Q_p allowable load carrying capacity of each pile/column in pile group

f_{fs} partial factor for soil unit weight

g unit weight of the soil

H height of the embankment

f_q the partial load factor for external applied loads

w_s the external surcharge loading

2.4.1. Pile Group Extent

According to BS 8006(1995), the piled area should extend beyond the edge of the shoulder of the embankment. This is to ensure that any differential movement/settlement or instability outside the piled area does not affect the crest of the embankment. The outer edge limit for the outer pile cap can be given as

$$L_p = H\left(n - \tan\theta_p\right) \qquad \text{Eqn.2.20}$$

where

L_p the horizontal distance between the outer edge of the outer pile cap

H the height of the embankment

n the side slope of the embankment

θ_p the angle to the vertical between the shoulder of the embankment and the outer edge of the outer pile cap

$$\theta_p = 45^\circ - \frac{\varphi_{cv}}{2}$$

where

ϕ_{cv} describes the embankment fill

2.4.2. Lateral Movement of Pile and Bending Moment in the Pile

The pile prevents the ground soil from moving with the soil mass. This develops a lot of horizontal stresses on the pile. This horizontal stress is relieved partially when the

pile deflects from its original position. Hence, the soil experiences some earth pressure. This can be related to the difference between the movement of the pile and that of the soil.

The deformed shape of the soil depends on various factors like, the stiffness of the pile, the restraint provided by the embankment, the fixity provided by the lower stiff/firm layers, the depth of the deforming layer and the strength of the moving soil. The load applied on the pile will produce a lateral deflection and rotation at the level of the pile cap. Hence, horizontal displacement of the pile and the bending moment produced are of interest in this situation.

The behavior of the piles can be attributed to

- Strength of soil
- Relation of soil stiffness and strain
- Pile diameter
- Pile length
- Pile stiffness
- Pile group layout and spacing
- Lateral restraint provided by the deeper layers
- Relationship between the earth pressure on the pile and the soil strength
- Rate of movement of the soil

The pile-soil interaction is very complex in nature. There are various methods used for the determination of the lateral deflection of the piles

- Empirical relations
- Finite element analysis
- Displacement based methods

- Pressure based methods
- Centrifuge testing and large scale prototype testing

Goh et al.(1997) (cited in Li et al., 2002) used numerical methods to study the behavior of the lateral movement of a single pile. The piles are represented by beams to study the bending moments and the lateral movement. Hyperbolic soil springs are used to denote the soil-pile interaction. All the properties or input data for the soil are attained from experimental data. Initially, the lateral displacement due to the applied construction load of the embankment is analyzed. This "free-field" soil movement is applied in the second case, to an existing pile and its effect is studied. BCPILE was used to study this effect. According to Goh et al. (1997) (cited in Li et al., 2002) the difference between predicted and measured values was very small.

Goh et al. (1997) (cited in Li et al., 2002) developed some charts from experimental data. The empirical relations developed can be used for preliminary estimation of the bending moment induced in the piles located near the toe of the embankment and restrained from rotating at the pile head.

A dimensionless quantity M* is calculated from the following equations:

$$M^*=\frac{M_{max}}{c_u d h_s^2} \qquad M^*=\lambda e^{\left[\beta(q/c_u)\right]} \qquad \text{Eqn.2.21}$$

The values for λ and β can be obtained from the charts – Figure 13

$$\lambda=1.88\left(K_R\right)^{0.5} \qquad \beta=0.18\left(K_R\right)^{-0.1} \qquad \text{Eqn.2.22}$$

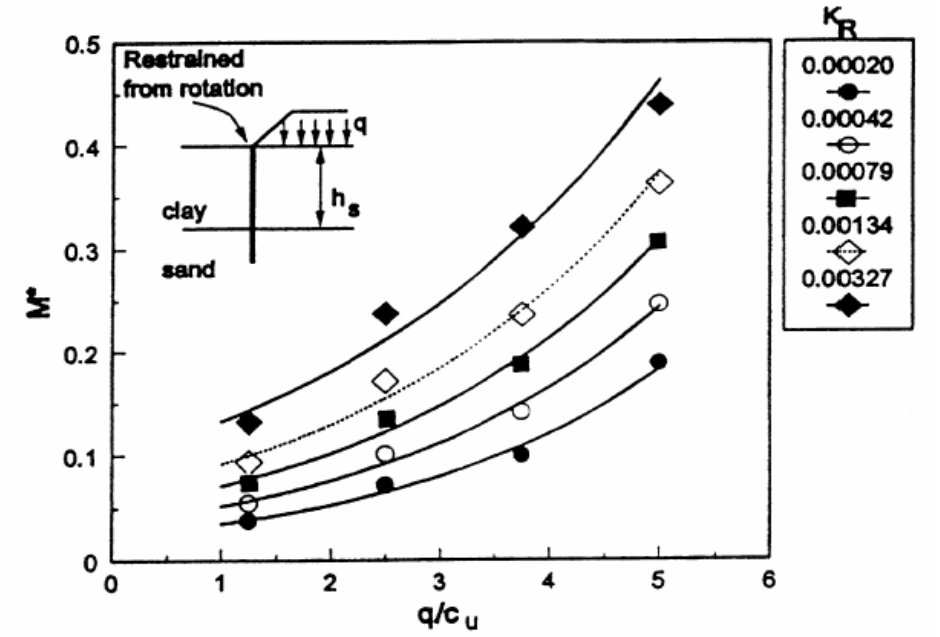

Figure 12: Plot of M* versus q/c_u (Goh et al., 1997 - cited in Li et al., 2002)

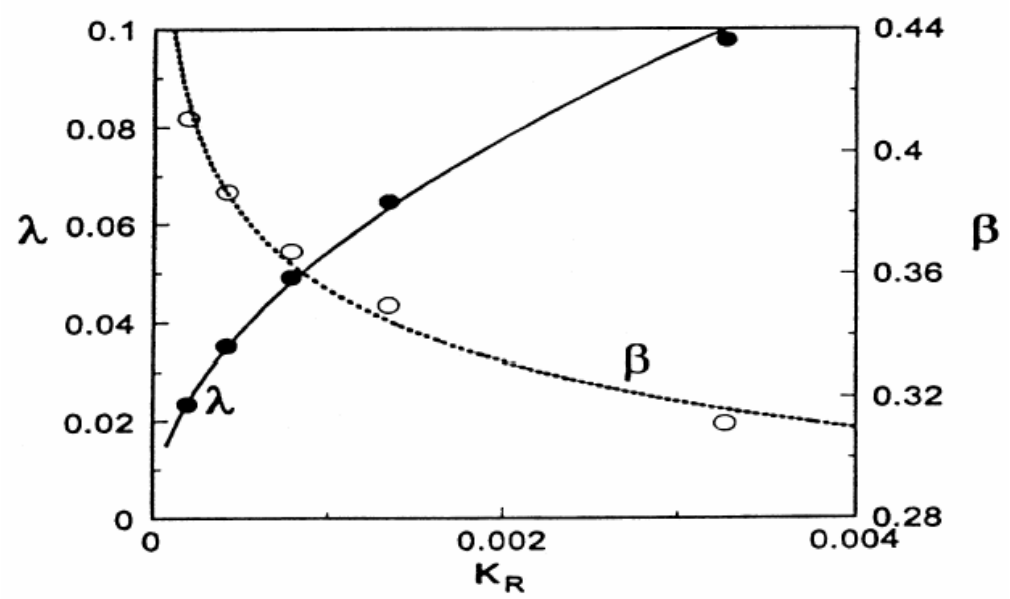

Figure 13: Values of λ and β derived from regression analysis (Goh et al., 1997 - cited in Li et al., 2002)

where

K_R relative pile-soil stiffness ratio; $K_R = \dfrac{E_p I_p}{E_{50} h_s^4}$

$E_p I_p$ bending stiffness of the pile

c_u undrained shear strength of the soil

d width of the pile

h_s thickness of the soft clay layer

E_{50} secant modulus at half ultimate stress in undrained test of soil

q applied embankment pressure

M_{max} maximum bending moment in the pile

Lee et al. (1991) (cited in Li et al., 2002) used a modified nonlinear boundary element approach to study the response of off-shore piles subjected to external soil movements. Finite element programs like PLAXIS can be used to analyze the response of piles to this type of system. The results from some PLAXIS models are presented in Chapter 4.

2.4.3. Pile Cap Punching Capacity

The pile caps can punch through the embankment fill if there is a concentration of stresses on the pile caps and if the embankment height is very low. The inclusion of a geosynthetic layer decreases the stress concentration on the pile caps (cited in Han and Gabr, 2000). This reduction of the stress on the pile cap can result in a smaller probability of punching failure of the pile caps. There is currently no design available for designing the punching failure of the pile caps. However, it can be simulated numerically.

2.4.4. Efficiency of the Piles

The efficiency of the pile support is the ratio of the weight of the embankment that the piles can carry.

$$E=1-\delta\left(1-\frac{s}{2H}\right)(1-\delta)^{(K_p-1)} \qquad \text{Eqn.2.23}$$

where

$$\delta=\frac{b}{s}$$

H height of the embankment

s c/c spacing between the piles

b width of the pile caps

K_p Rankine passive earth pressure

If the weight of the soil is considered then the crown will not be the only weakest position where failure will occur. The limited area on the pile cap is also prone to bearing failure at those points. The efficiency for this case can be expressed as

$$E=\frac{\beta}{1+\beta} \qquad \text{Eqn.2.24}$$

where

$$\beta=\frac{2K_p}{(K_p+1)}\times\frac{1}{(1+\delta)}\times\left((1-\delta)^{-K_p}-(1+\delta K_p)\right)$$

In normal conditions, K_p is assumed to be 3. The efficiency of the pile caps increases as the height of the embankment increases. When the embankment height, pile spacing and K_p are fixed then the efficiency of the piles depends on the width of the pile caps. When all other factors are kept constant, the efficiency of the piles depend on the angle of internal friction.

Piles in GRPS embankments need not be conventional piles. Vibroconcrete columns, stone columns, deep mixed columns are also considered here. Deep mixing columns initially popular in Asia and Europe are becoming more popular in America. The application of these deep mixed columns requires a thorough subsoil investigation.

Undrained shear strength of the soil and stiffness of the surrounding soil are very important properties. These columns can be made using a continuous flight displacement auger. They can be made up of dry or wet cement columns or lime. The degree of improvement of the soil depends on densification and pressurization. Load transfer depends on the soil conditions. Deep mixed columns can be installed in grid, wall, block or column type.

The load transfer to the deep mixed columns occurs due to the difference in the stiffness of the columns and the surrounding soil. Hence, there is more load concentration on the columns. This load transfer is controlled by

- Length of the column and its stiffness
- Ratio of the area covered by the columns to the total area
- Ratio of column stiffness to the stiffness of the surrounding soil
- The effects of the load spreading bearing layer or bearing layer on the top of the columns.

A detailed report of construction and analysis of the deep mixed columns in soft soil is found in a report of Coastal Caisson Corporation. Coastal Caisson installed five deep mixed columns in Jacksonville, Florida. There is much literature found on deep mixed columns written by Porbaha et al. (1998, 2000), Bruce et al.(2001) and Terashi et al.(2003) - cited in Interim Report by Han (2003).

2.5. Lateral Movement

Large lateral movements are seen when an embankment load is applied. This large lateral deflection is dangerous for the piles in the GRPS system. This causes excessive settlements in the system and can prove to be more dangerous than vertical settlements. The foundations or structures in the adjacent areas can be greatly affected by the lateral

movements caused. There are no methods available to estimate the lateral movements of geosynthetic reinforced pile supported embankments.

It is however essential to get an initial estimate of the lateral movements. This can be done by prototype testing. However, this is very uneconomical. Initial predictive methods should be used to determine lateral ground movements. The design method used will depend on the sensitivity of the structure to the soil movements.

Seaman(1994) (cited in Li et al., 2002) investigated the effects of various factors on lateral movements. The increase in certain factors that tend to increase the lateral movements are:

- Vertical stress applied on the soil due to the embankment fill
- Length of the embankment
- Width of the embankment
- Embankment slope
- Poisson's ratio of the soil

The increase in certain factors that tend to decrease the lateral movements are

- Thickness and stiffness of the fill
- The distance from the embankment toe
- Stiffness of the soil
- Strength of the soil
- Adhesion between the soil and the fill

The lateral movements caused by application of the embankment load can be estimated using

- Empirical relations with the soil properties and the observed behavior of the soil on the site.

- Theoretical Analysis
- Prototype Testing

All three methods listed above do not consider the effect of piles and geosynthetic reinforcement.

The prototype testing method is one of the best and most reliable methods. However, it is not an economical method for initial estimation. Empirical methods seem to be the simplest for estimation for the lateral movements.

2.5.1. Empirical Methods

The maximum lateral deflection was related to the thickness of the deforming layer by Bourges and Mieussens(1979) (cited in Li et al., 2002)

$$\lambda = \frac{y_{max}}{D} \qquad \text{Eqn.2.25}$$

This value of λ is related to the stability factor

$$F = (\pi + 2)\frac{c_u}{q} \qquad \text{Eqn.2.26}$$

where

c_u average undrained shear strength along failure surface of the soil

q average overburden pressure applied by the embankment load

Figure 14 shows Bourges and Mieussens results. The data points indicate the distance from the crest of the embankment. The results show that greater displacements are found with an increase in the width of the embankment.

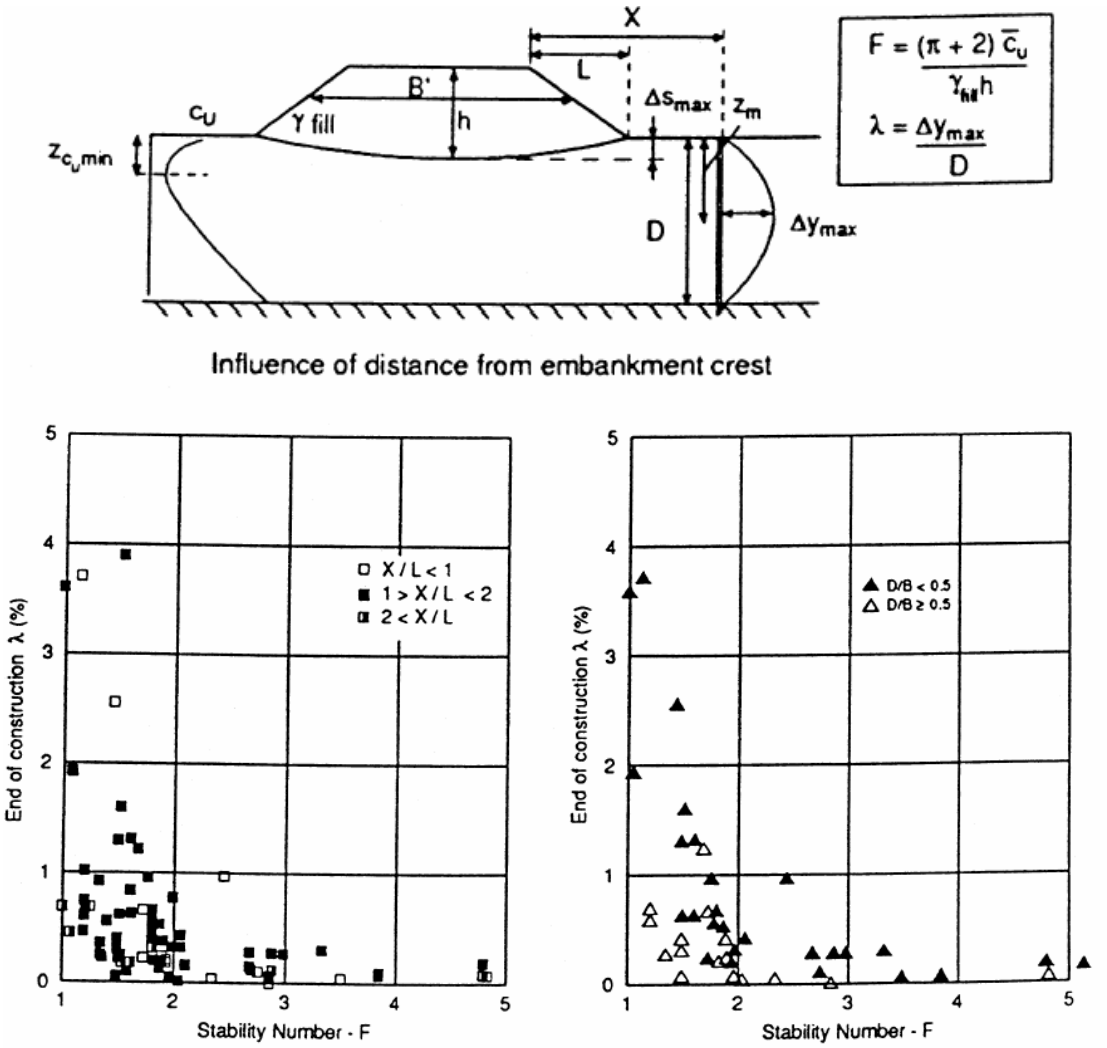

Figure 14: Relation between the maximum stability and maximum lateral movement (Bourges and Mieussens, 1979 - cited in Li et al., 2002)

Marche and Chapuis(1974) (cited in Li et al., 2002) compared displacement factor, $R = \frac{y_{max} E_u}{qB}$ with a D/B ratio (Figure 15). This method considers the relation of the undrained modulus of the soil, the width of the embankment and the depth of the deforming soil. E_u is generally found from empirical relations with the undrained shear strength.

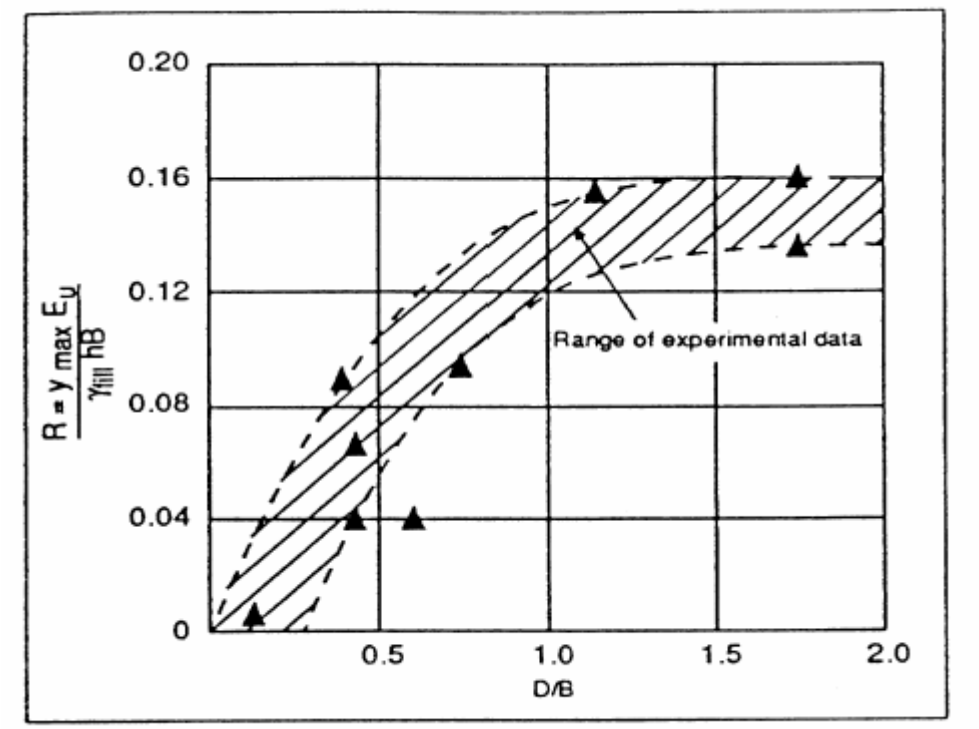

Figure 15: Impact of soil stiffness and embankment geometry on lateral movements (Marche and Chapuis, 1974 - cited in Li et al., 2002)

The magnitude of lateral movement with depth varies with the stiffness and the strength of the soil. The ratio of the deforming soil layer to the embankment width also influences the lateral movements. Tavenas et al. (1979) (cited in Li et al., 2002) determined that the maximum lateral movements occur at a depth of minimum shear strength of the weak soil (Figure 16). However, Suzuki(1988) (cited in Li et al., 2002) concluded that the maximum lateral movements occur at a distance of 2-3m below the depth of minimum shear strength (Figure 17). Suzuki concluded that the width of the embankment had a very strong effect on this value. These conclusions were drawn for the weak clay overlain by a stronger soil.

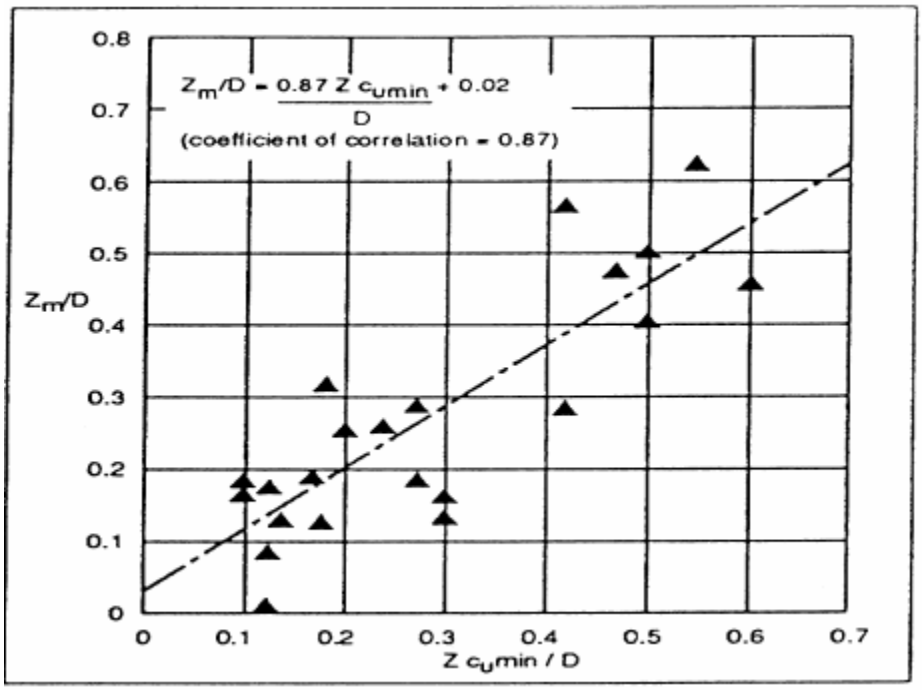

Figure 16: Relation between the depth of maximum lateral movement to minimum shear strength (Tavenas et al., 1979 - cited in Li et al., 2002)

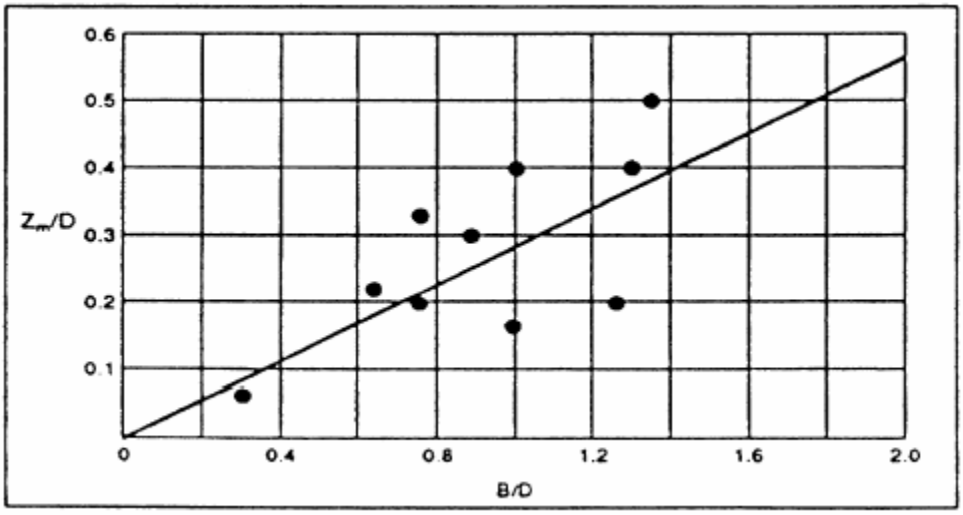

Figure 17: Relation between depth of maximum lateral movement and the embankment width (Suzuki, 1988 - cited in Li et al., 2002)

2.5.2. Theoretical Methods

The most commonly used theoretical methods to predict the lateral movement of the soil are

- Volume conservation method
- Elastic continuum methods

These methods give results which are more reliable than the empirical methods.

The lateral movements can be predicted using finite element methods. The prediction of lateral movements using Plaxis-Finite element program will be dealt with in the Chapter 3.

2.6. Slope Stability

2.6.1. BS8006

The stability of GRPS embankments can be carried out by using conventional slip circle methods. However, the presence of piles and basal reinforcement should be taken into consideration (Figure 18). According to BS8006, the analysis can be performed using effective stress parameters taking account for the pore water pressures. An analysis for short term stability should assume undrained conditions.

To ensure stability the following relationship should be satisfied at all locations along the base of the embankment:

$$M_D \leq M_{RS} + M_{RP} + M_{RR} \qquad \text{Eqn.2.27}$$

where

M_D the factored distributing moment at all locations along the base of the embankment

M_{RS} the factored restoring moment due to the soil at all locations along the base of the embankment

M_{RP} the resisting moment due to the axial load in the piles along the base of the embankment

M_{RR} the restoring moment due to the reinforcement at all locations along the base of the embankment

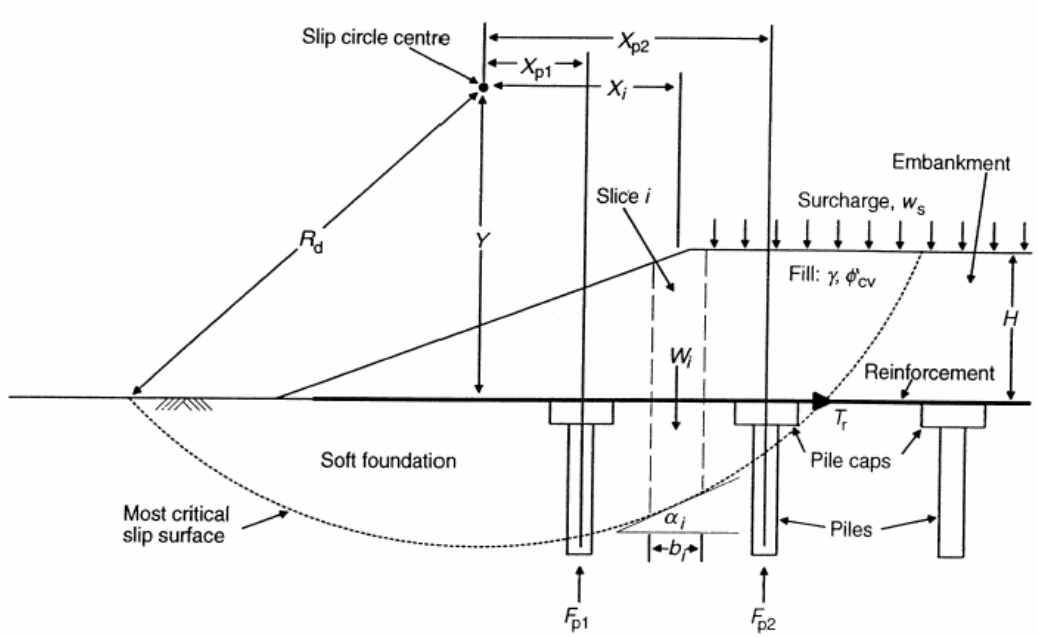

Disturbing moment due to soil and loading:

$$M_D = \left[\sum \left(f_{fs} W_i + f_q b_i w_{si}\right) \sin \alpha_i\right] R_d$$

Restoring moment due to soil:

$$M_{RS} = \left[\sum \left\{ \frac{c_i'}{f_{ms}} b_i \sec \alpha_i + \left((W_i + b_i w_{si}) \cos \alpha_i - u_i b_i \sec \alpha_i\right) \frac{\tan \phi'_{cvi}}{f_{ms}} \right\}\right] R_d$$

Restoring moment due to piles:

$$M_{RP} = F_{p1} X_{p1} + F_{p2} X_{p2}$$

Restoring moment due to reinforcement:

$$M_{RR} = T_r Y$$

Figure 18: Variables required for the stability analysis of GRPS embankments (cited in BS 8006, 1995)

2.6.2. Modified Boundary Element Method

Lee et al. (1995) (cited in Li et al., 2002) studied the effect of piles on slope stability. The Bishop circle method was used to find the stability of the slope. The effect of the piles was studied separately by a modified boundary element method.

Lee et al. defined the improvement ratio as

$$N_{ps} = \frac{F_p}{F_s} \qquad \text{Eqn.2.28}$$

where

F_p factor of safety of the pile-sloped problem

F_s minimum factor of safety of the problem without piles

Lee et al. presented charts for the behavior of cast-in-situ reinforced concrete piles in homogenous (Figure 19 to 22) and layered slopes (Figure 23 to 26).

2.6.2.1. Homogenous Slopes

- The most effective position of the piles is near the crest or near the toe. If the pile is close to middle of the slope the improvement ratio is reduced to 1.0. If the pile head is fixed against rotation it has no effect on the stability of the slope.
- As the pile spacing increases the improvement ratio reduces.
- The larger the diameter of the pile, the greater is the improvement ratio. In this case, when d/ds is greater than 1.0 toe piles are more effective.
- The soil modulus and the pile stiffness have little or no effect on the stability of the slope.
- The piled-slope improvement ratio increases linearly with increase in pile – soil limiting pressure

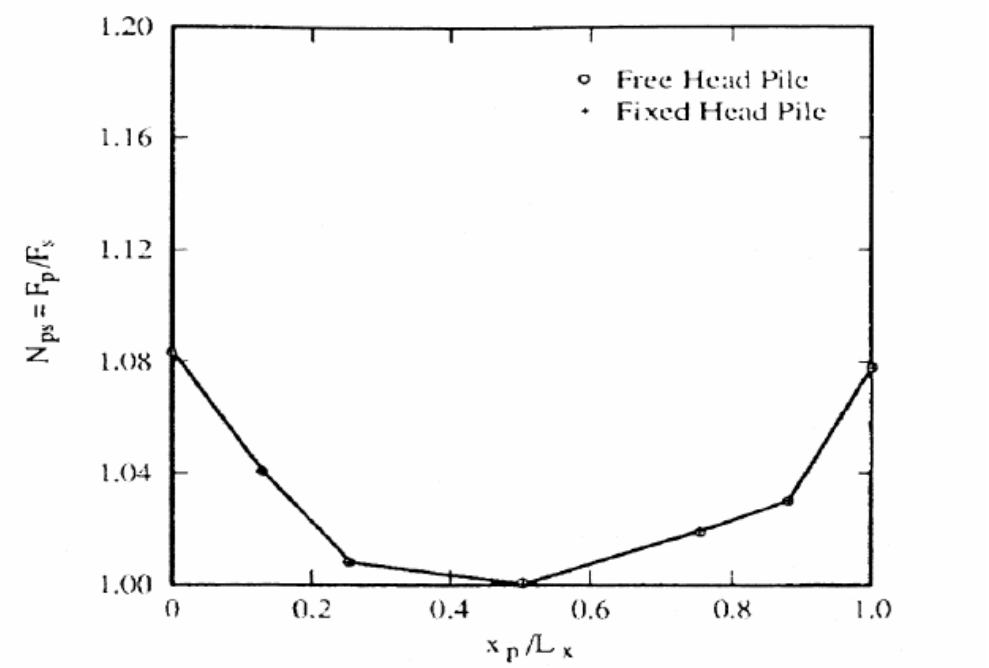

Figure 19: Effect of pile position on the homogenous slope (Lee et al., 1995 - cited in Li et al., 2002)

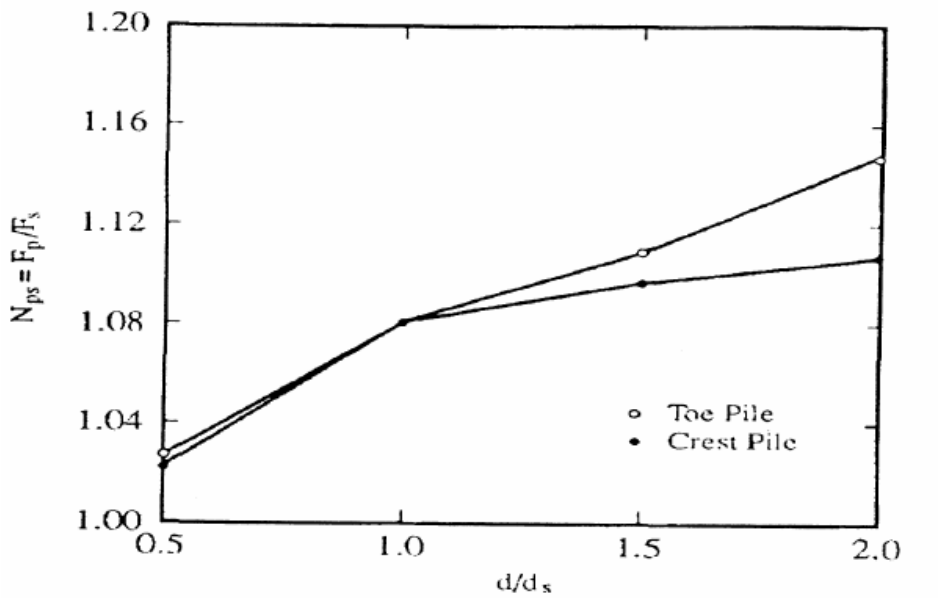

Figure 20: Effect of pile diameter on the homogenous slope (Lee et al., 1995 - cited in Li et al., 2002)

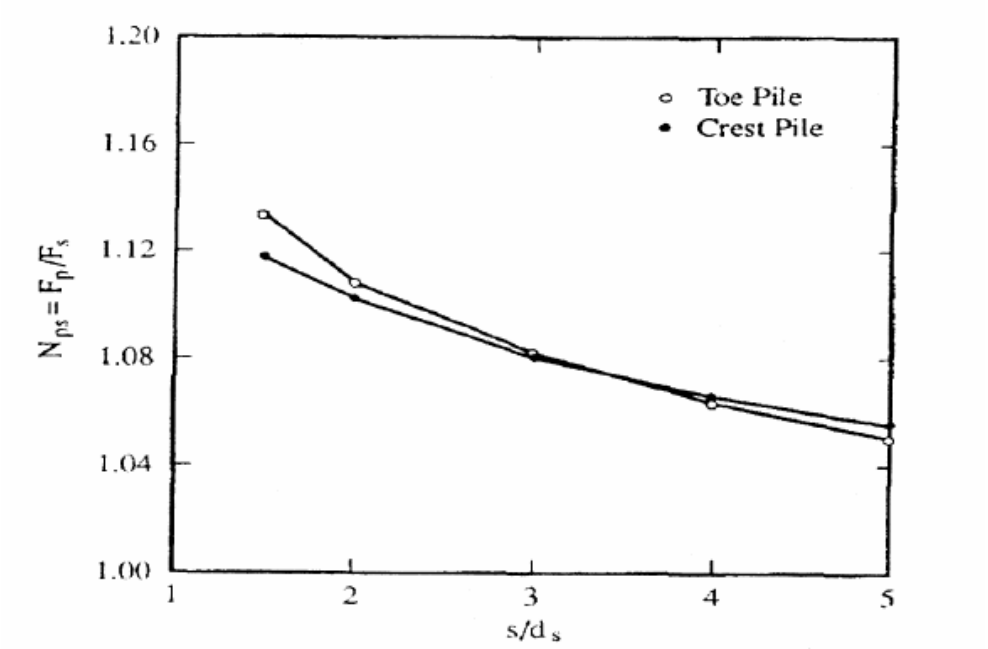

Figure 21: Effect of pile spacing on homogenous slope (Lee et al., 1995 - cited in Li et al., 2002)

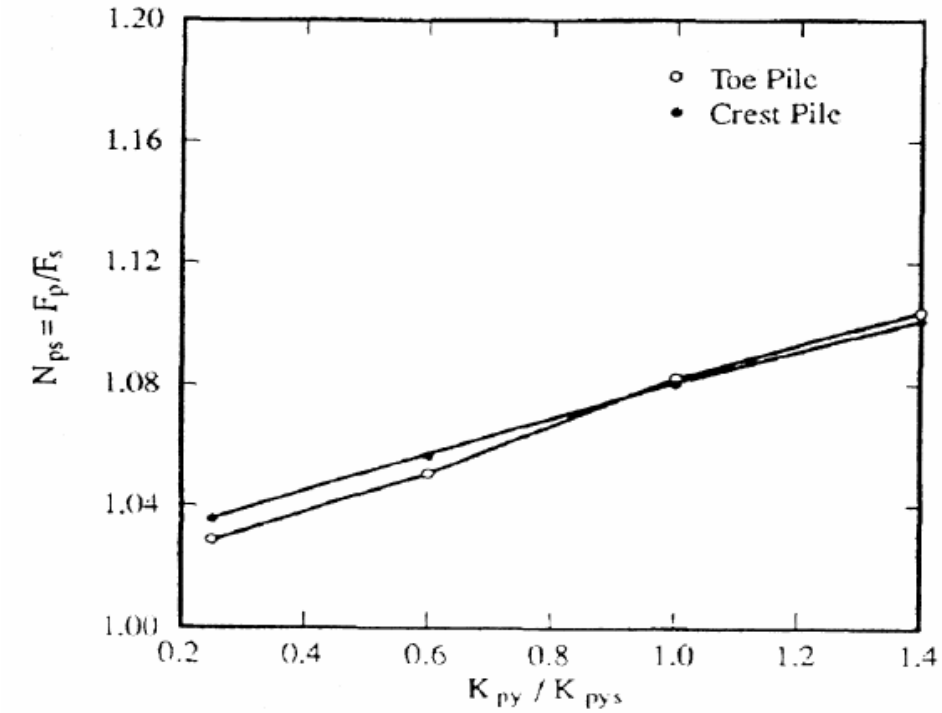

Figure 22: Effect of pile-soil limiting pressure on homogenous slope (Lee et al., 1995 - cited in Li et al., 2002)

2.6.2.2. Two Layer Soil Slope

CASE 1: An upper soft layer is underlain by a stiff layer

CASE 2: A lower soft layer is overlain by a stiff layer

It is generally preferred to have the pile embedded through the soft layer into the firm lower layers.

- The most effective position of the piles for Case1 is between the crest and the middle of the slope. For Case 2, the most effective position is at the toe or at the crest.
- The larger the diameter, the greater the pile improvement ratio. This effect is seen more vividly in Case1.
- The greater the spacing, the smaller the pile improvement ratio. This effect is more evident in Case 1 than Case 2.
- The improvement ratio increases with increase in the pile-soil limiting pressure. This ratio is higher in Case1 than in Case 2.

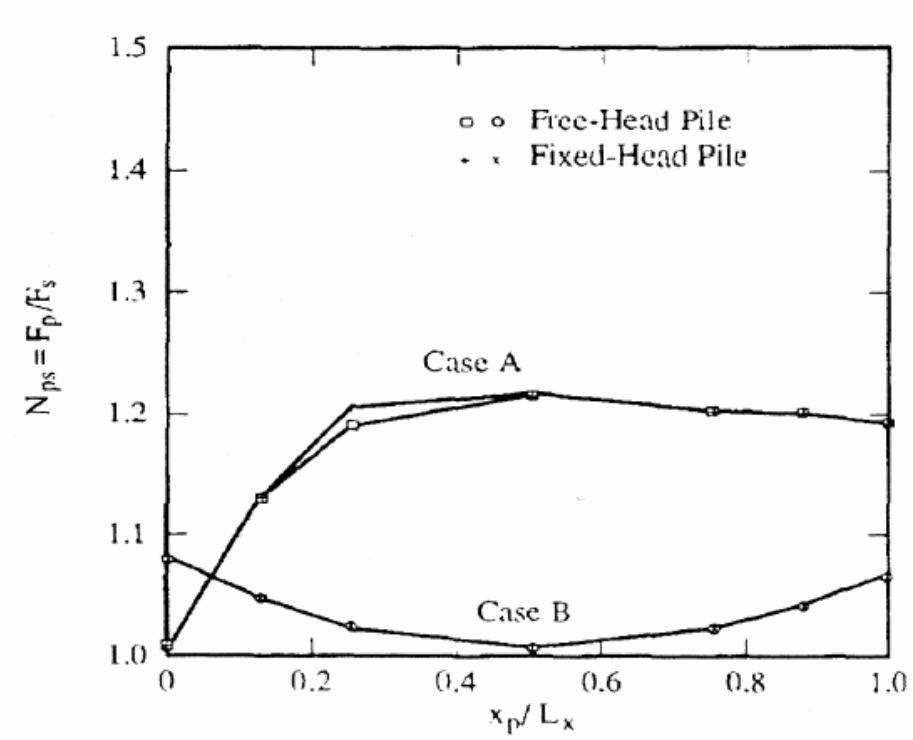

Figure 23: Effect of pile position on two - layer slope (Lee et al., 1995 - cited in Li et al., 2002)

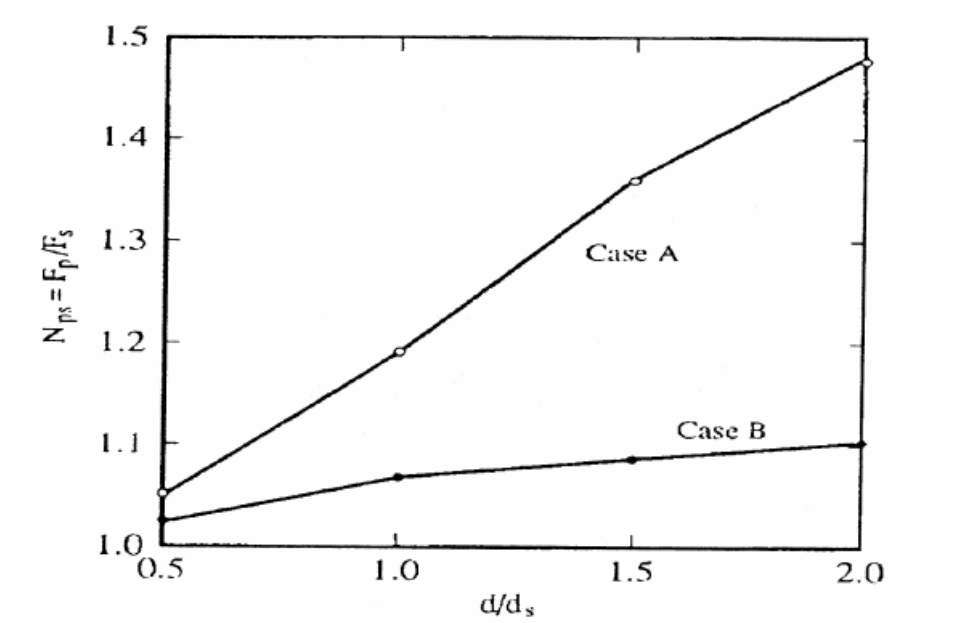

Figure 24: Effect of pile diameter on a two-layer slope (Lee et al., 1995 - cited in Li et al., 2002)

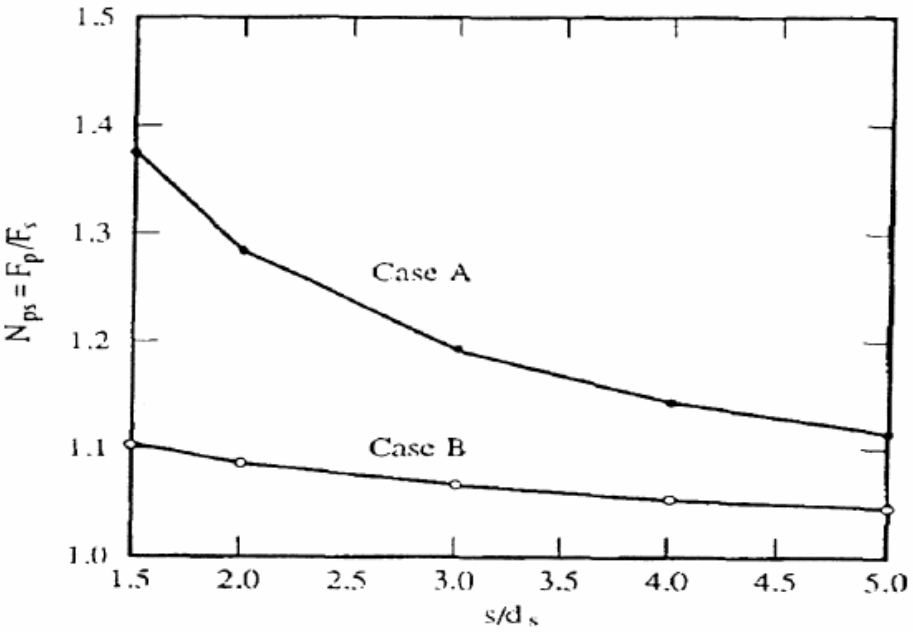

Figure 25: Effect of pile spacing on the two-layer slope (Lee et al., 1995 - cited in Li et al., 2002)

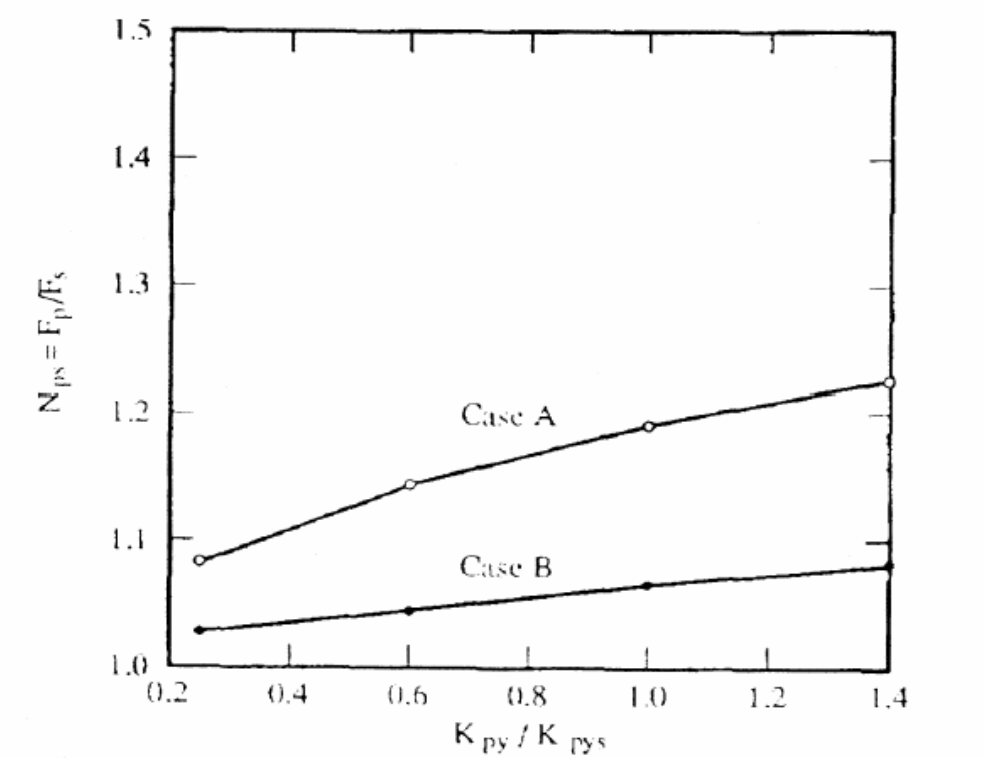

Figure 26: Effect of pile-soil limiting pressure multiplier on the two-layer slope (Lee et al., 1995 - cited in Li et al., 2002)

2.6.3. Friction Circle Method

The Friction Circle method is very useful for homogenous slopes. This method is found to be very convenient for pile reinforced slopes. The method is generally used when both cohesive and frictional components are to be used. Using the Mohr – Coulomb criterion, the factor of safety can be defined as the available shear strength to the required shear strength.

Factor of safety with respect to friction F_φ and cohesion F_c are as follows:

$$F_c = \frac{c_a}{c_r} \qquad F_\varphi = \frac{\tan\varphi_a}{\tan\varphi_r} \qquad \text{Eqn.2.29}$$

The forces that maintain the equilibrium of the system are weight of the mass, cohesion force C_r required to maintain equilibrium and the resultant of the normal and frictional component of strength mobilized along the failure surface (Figure 27). The

direction of the resultant corresponds to the line that forms a tangent to the friction circle, with a radius, $R_f = R\sin\varphi_m$.

Taylor(1937) (cited in Li et al., 2002) derived two expressions for the stability number

For toe failure:

$$\frac{c_a}{F_c\gamma H} = \frac{(1/2)\,\mathrm{cosec}^2 x\left(y\,\mathrm{cosec}^2 y - \mathrm{cot}y\right) + \mathrm{cot}x - \mathrm{cot}i}{2\,\mathrm{cot}x\,\mathrm{cot}v + 2} \qquad \text{Eqn.2.30}$$

For base failure:

$$\frac{c_a}{F_c\gamma H} = \frac{(1/2)\,\mathrm{cosec}^2 x\left(y\,\mathrm{cosec}^2 y - \mathrm{cot}y\right) + \mathrm{cot}x - \mathrm{cot}i - 2\eta}{2\,\mathrm{cot}x\,\mathrm{cot}v + 2} \qquad \text{Eqn.2.31}$$

In this method, a value for F_φ is assumed and a surface is defined by angles x and y. The angle v is obtained from its relation with φ_r. A number of iterations are carried out using the above equations, until F_c is obtained equal to F_φ. The critical surface is the one which has a minimum factor of safety.

When a number of piles are introduced into the system, the critical surface and the factor of safety will change. The forces acting in this system are similar to those above with the exception of the force acting on the slope due to the piles, F_p (Figure 28). This resulting force F_p can be incorporated into the system. This results in two new expressions for toe failure and base failure.

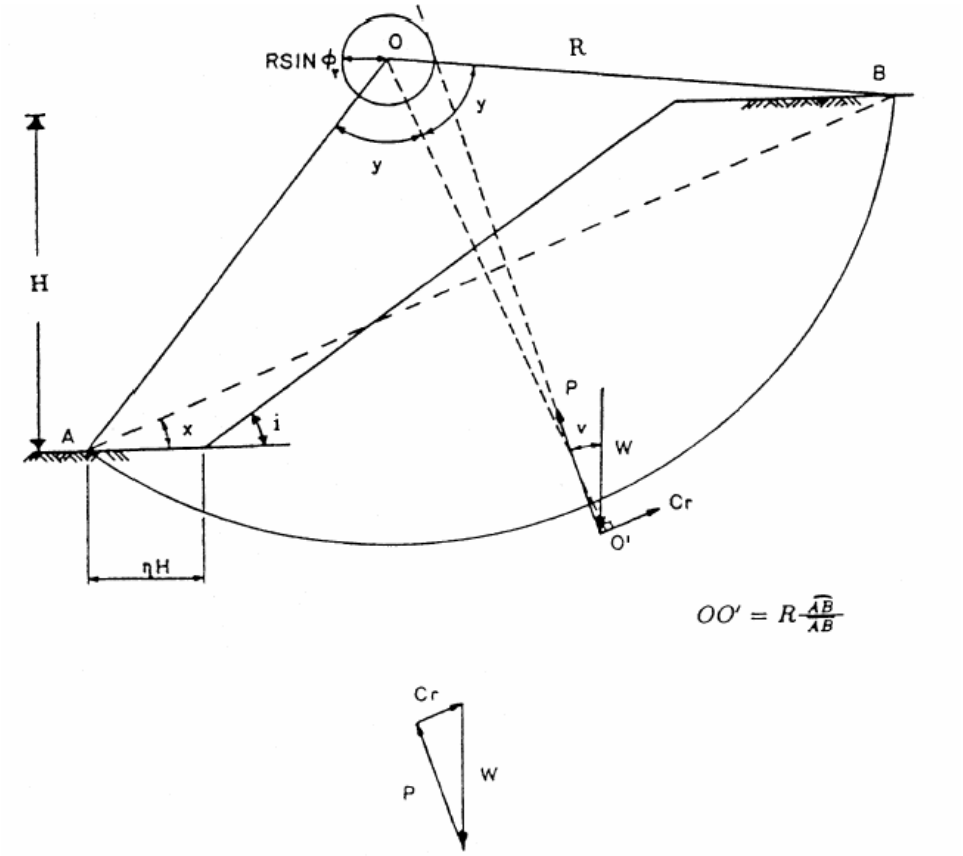

Figure 27: Forces on slopes without piles (Taylor,1937 - cited in Li et al., 2002)

$$\frac{c_a}{F_c\gamma H}=\frac{E-\frac{12F_p}{\gamma H^3}\left[\frac{\cos(CEO)}{\sin v}\frac{H}{2}\operatorname{cosec}x\times\operatorname{cosec}y\times\sin\varphi+OG\right]}{6\operatorname{cosec}^2x\times\operatorname{cosec}y\times\sin\varphi\left[\frac{\cos x}{\sin v}+\operatorname{cosec}(u-v)\cos(x-v)\right]} \qquad \text{Eqn.2.32}$$

$$\frac{c_a}{F_c\gamma H}=\frac{\left(E+6\eta^2-6\eta\sin\varphi\times\operatorname{cosec}x\times\operatorname{cosec}y\right)-\frac{12F_p}{\gamma H^3}A}{6\operatorname{cosec}^2x\times\operatorname{cosec}y\times\sin\varphi\left[\frac{\cos x}{\sin v}+\operatorname{cosec}(u-v)\cos(x-v)\right]} \qquad \text{Eqn.2.33}$$

where

$$E=1-2\left(\cot^2 i+3\cot i\times\cot x-3\cot i\times\cot y+3\cot x\times\cot y\right) \qquad \text{Eqn.2.34}$$

where CEO is the angle formed by F_p and horizontal, OG is the moment of F_p. The above equations can be used for calculation of factor of safety of the slope.

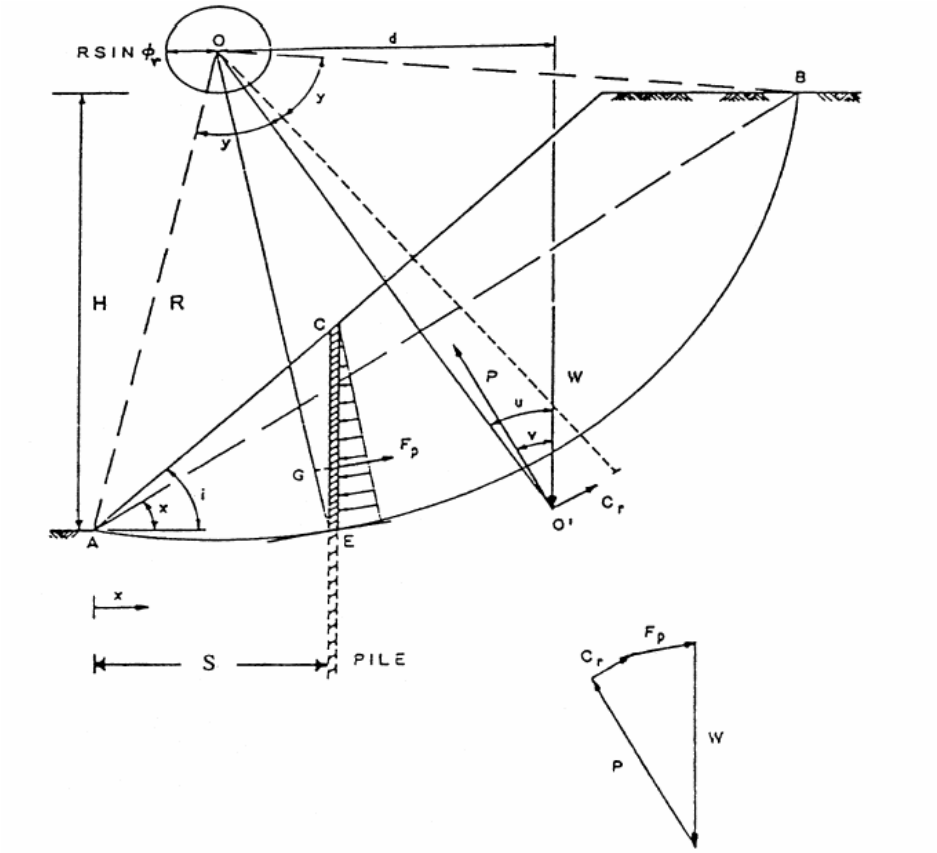

Figure 28: Forces acting on a slope reinforced with piles (Taylor, 1937 - cited in Li et al., 2002)

2.7. Settlements

Soft clay and other compressible soils have a tendency to settle under heavy loading. There are various soil improvement techniques used to prevent these settlements. The technique used in any particular case depends on soil conditions, the availability of equipment and the cost required for improvement.

Piles, stone columns, vibroconcrete columns, deep mixed columns are some of the commonly used techniques. The GRPS system is gaining popularity in embankment construction over such soils. Settlement is greatly reduced with the inclusion of a geosynthetic layer. The greater the stiffness of the geosynthetic reinforcement, the

smaller the settlement. The settlement also decreases with an increase in the stiffness of the piles.

Due to the complex nature of the system, no analytical method has been developed to determine the settlement of GRPS embankments. The settlement analysis is carried out as for the unreinforced case. In the case of rigid piles, it is assumed that the entire load of the embankment is taken by the piles. Settlement calculations are carried out by available methods. In the case of other ground improvement techniques, settlement calculations are carried out on the basis of methods available for those techniques.

BS8006(1995) states that a plane of equal settlement exists at a height of 1.4(s-a) from the top of the pile caps in which s is spacing of the pile caps and a is the width of the pile cap. Terzaghi(1943) (cited in Han, 1999) carried out laboratory tests and found that the plane of equal settlements exists at 1.5-2.5 times the width of the void. If the height of the embankment is greater than this height then there is no problem of local depressions. However, if the height is less than 1.4(s-a) the method for estimating the surface depression due to the existence of a void can be used. When two or more geogrids are used in the system, the differential settlement is effectively reduced. The strain in the upper reinforcement is 30% of the strain in the lower geogrid (Jenner et al., 1998 - cited in Han, 1999) although the upper geogrid is weaker than the lower one. The height of the equal settlement plane is reduced significantly by soil resistance. Soil resistance when increased to a certain limit can result in the equal settlement plane being lowered to the top of the upper geosynthetic layer in a multi layer system.

PWRC (2000) and Ogisako (2002) (cited in Han, 2003) have developed methods to determine the settlement of geosynthetic reinforced embankments on deep mixed

columns. Finite element or finite difference methods provide a measure of the settlement expected in a GRPS embankment. This can be seen in the Plaxis models developed and discussed in Chapter 3.

2.7.1. Public Work Research Center Method

The PWRC-Geosynthetic reinforced Earth Committee (2000) (cited in Han, 2003) has come up with a design method for reinforced embankments on deep mixed columns.

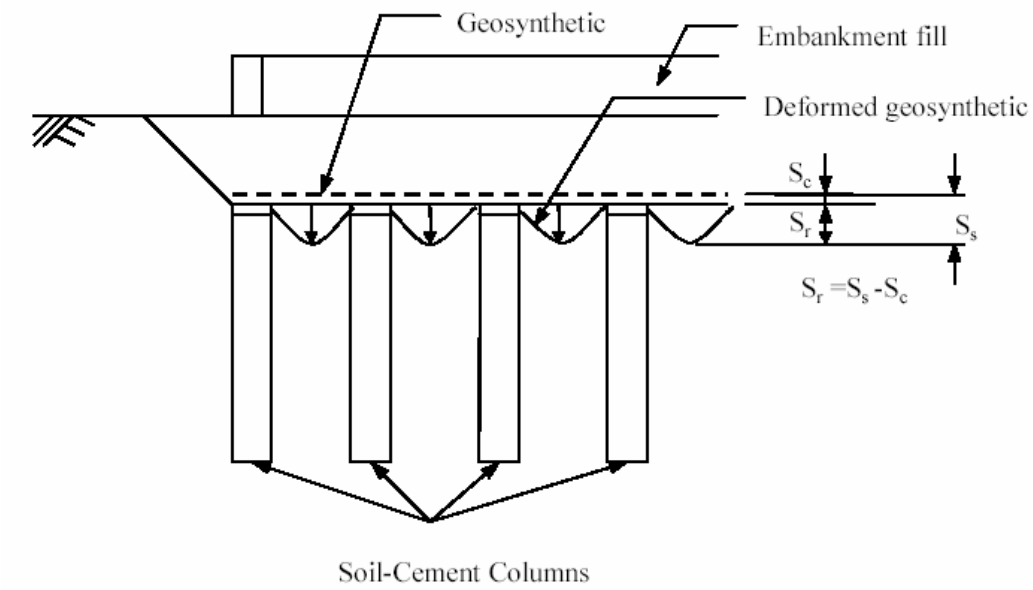

Figure 29: Settlement and differential settlement of soil embankment on deep mixed columns.

The settlement of the deep mixed columns is given as

$$S_c = \frac{\sigma_c}{E_c} L \qquad \text{Eqn.2.35}$$

where

S_c settlement of the deep mixed column

σ_c stress on the deep mixed columns

L length of the deep mixed columns

E_c modulus of deformation of the deep mixed columns

The modulus of deformation is given as

$$E_c = 100 q_u \qquad \text{Eqn.2.36}$$

where

q_u unconfined compression strength of the deep mixed columns

The settlement of the untreated soil is given by

$$S_s = S_0 \frac{\sigma_s}{p} \qquad \text{Eqn.2.37}$$

where

S_s settlement of the untreated soil subjected to reduced pressure σ_s

S_0 settlement of the untreated soil subjected to the actual load of the embankment p

σ_s reduced pressure on the untreated soil due to the embankment

p total applied pressure of the embankment

The differential settlement between the soil and the columns in the absence of geosynthetic reinforcement is given by

$$\Delta S = S_s - S_c$$

When there is a inclusion of geosynthetic layer present, the differential settlement can be given taking into account an influence factor due to the inclusion of the reinforcement.

$$\Delta S_r = \frac{S_s}{\left(1 + 2\alpha\left(\frac{S_s}{p}\right)\right)} \qquad \text{Eqn.2.38}$$

where

ΔS_r differential settlement between the columns and the untreated soil

α influence factor due to the presence of geosynthetic reinforcement layer

This influence factor is related to the tensile stiffness of the geosynthetic reinforcement. The relation between the two factors can be seen in the Figure 30.

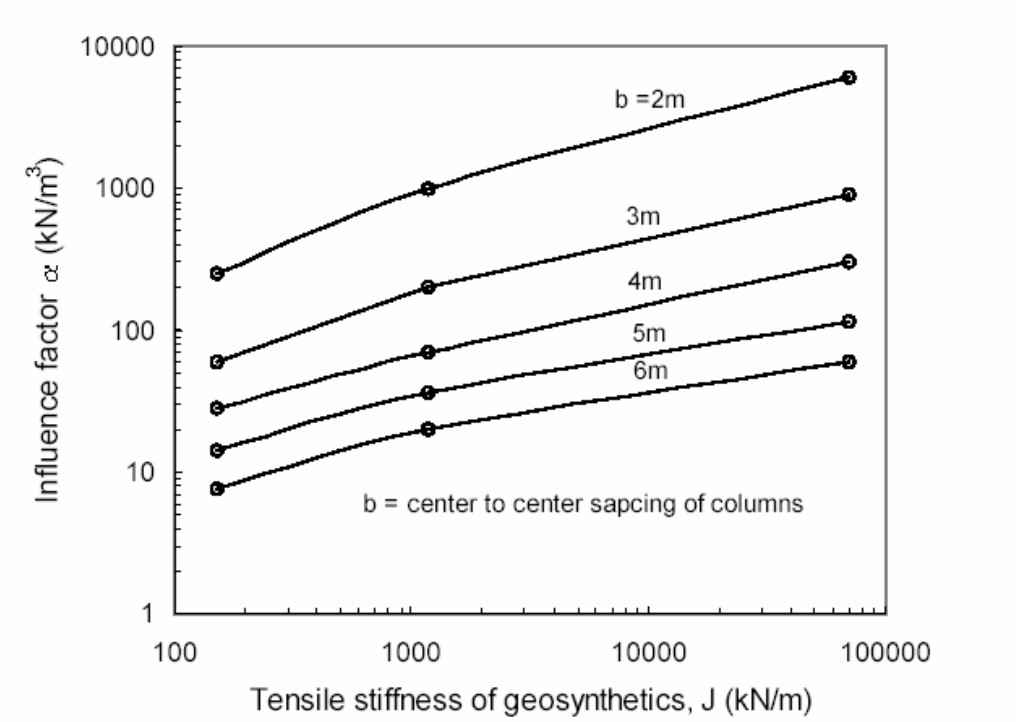

Figure 30: Determination of the influence factor

2.7.2. Ogisako's Method

Ogisako (2000) (cited in Han, 2003) used the finite element method to study the relation between tensile stiffness, improvement ratio, stress concentration ratio and the ratio of the volumetric compression modulus of the untreated soil to the columns. He developed a 2D problem considering the deep mixed columns as a continuous wall.

In the absence of the geosynthetic reinforcement, the settlements can be estimated as follows. The settlement of the untreated soil between the deep mixed columns is given by

$$S_s = m_{vs} L \sigma_s \qquad \text{Eqn.2.39}$$

where

m_{vs} volumetric compression modulus of the untreated soil

L length of the deep mixed column

σ_s average vertical stress acting on the untreated soil

The settlement of the deep mixed column is given by

$$S_c = m_{vc} L \sigma_c = \frac{n}{R_m} S_s \qquad \text{Eqn.2.40}$$

where

m_{vc} volumetric compression modulus of the deep mixed columns

L length of the deep mixed column

n stress concentration ratio $n = \frac{\sigma_p}{\sigma_s}$

R_m ratio of the volumetric compression modulus of the untreated soil to the deep mixed columns $R_m = \frac{m_{vs}}{m_{vc}}$

σ_c stress acting on the deep mixed column

The differential settlement is given as

$$\Delta S = S_s - S_c = \left(1 - \frac{n}{R_m}\right) m_{vs} L \sigma_s \qquad \text{Eqn.2.41}$$

The inclusion of the geosynthetic reinforcement can be taken care of by using the stress concentration ratio calculated in the presence of the geosynthetic reinforcement.

$$\Delta S_r = \left(1 - \frac{n_r}{R_m}\right) m_{vs} L \sigma_s \qquad \text{Eqn.2.42}$$

The average stress acting on the untreated soil between the columns is given by

$$\sigma_s = \frac{p}{1 + a_s (n-1)} \qquad \text{Eqn.2.43}$$

This can be included into the above equation, and the differential settlement is given as

$$\Delta S_r = \left(1 - \frac{n_r}{R_m}\right) \frac{m_{vs} Lp}{1 + a_s (n_r - 1)} \qquad \text{Eqn.2.44}$$

Ogisako found the relation between the stress concentration with and without the reinforcement. This can be related to the tensile stiffness of the reinforcement.

$$\frac{n_r}{n} = \frac{J}{C_1 + C_2 J} + 1 \qquad \text{Eqn.2.45}$$

where

n_r stress concentration ratio in the presence of the geosynthetic reinforcement

n stress concentration ratio without the inclusion of geosynthetic reinforcement

J tensile stiffness of the geosynthetic reinforcement

C_1 and C_2 coefficients which can be determined from the following charts

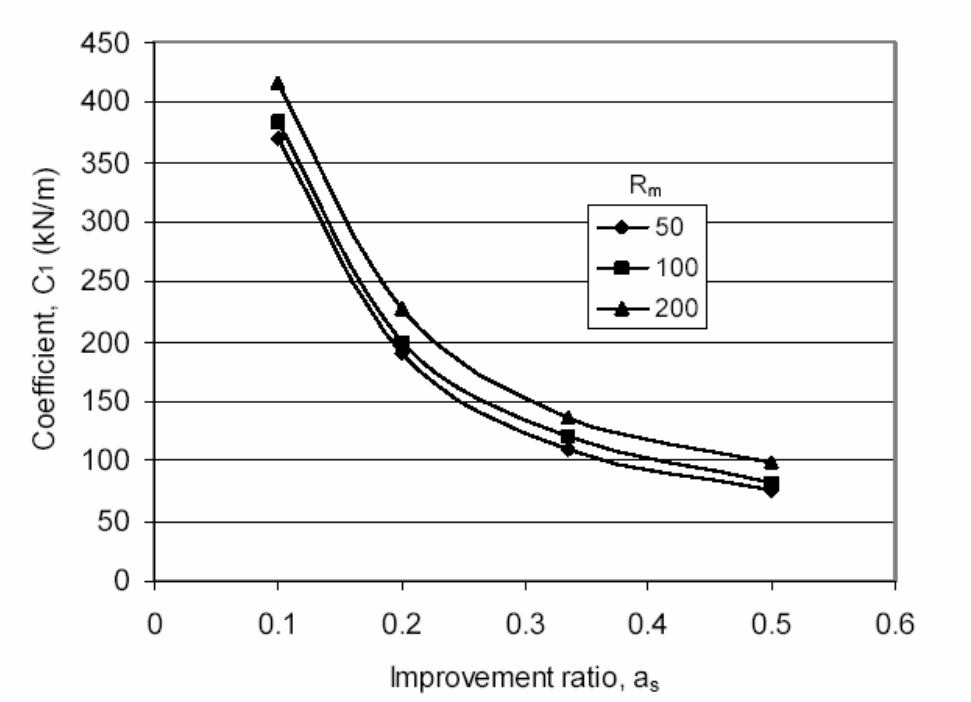

Figure 31: Coefficient C_1 versus the improvement ratio, a_s

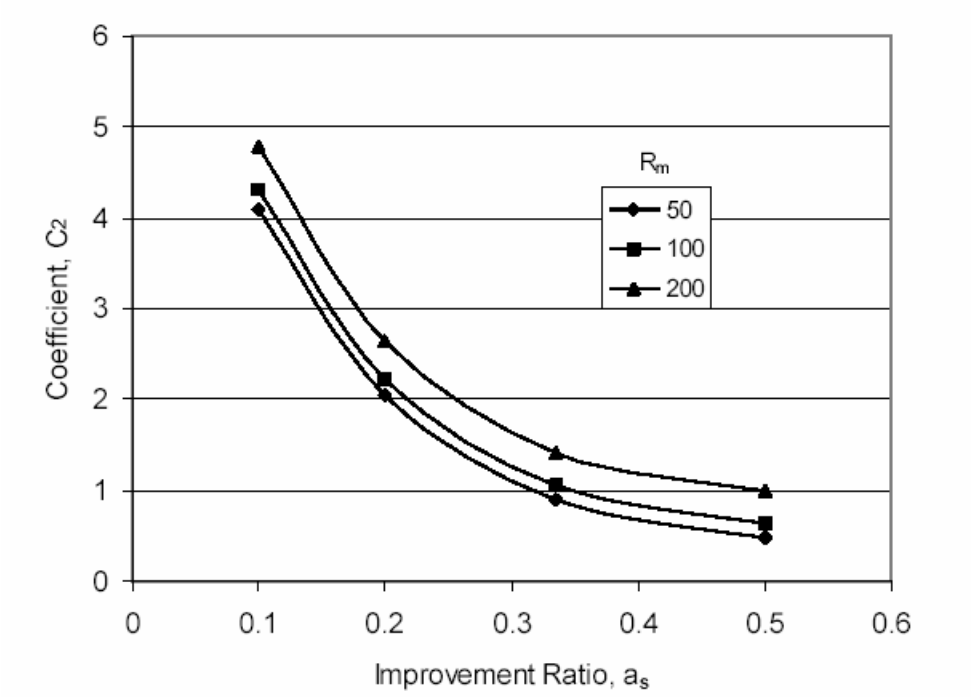

Figure 32: Relation between the coefficient C_2 and improvement ratio a_s

Much research has been carried out on determining of the settlements in situations involving deep mixed columns. No direct methods have been developed for settlements for other type of soil improvement techniques. However, conventional settlement methods give approximately close estimates of settlement.

CHAPTER 3
MODELLING IN PLAXIS

Numerical modeling of the geosynthetic reinforced pile supported embankments was performed in PLAXIS 7.2 – finite element software. Numerical modeling enables the designer to study the effects of embankment loading, the soil behavior in various conditions without resorting to simplified assumptions. An attempt was made to design the system in Plaxis 3D. However, Plaxis 3D was unable to simulate the field conditions.3D cannot simulate the condition of a void below the geogrid. Updated mesh analysis is required for this analysis. This is not available in Plaxis 3D. Hence, the experimentation was then carried out in Plaxis 2D.

The study comprised two parts. The axisymmetric unit cell was used to determine the strength of the geogrid, considering an infinitely long embankment. This axisymmetric model was utilized to show the effect of the soil support below the geosynthetic layer. A parametric study was performed on this model. Large plane strain models were built. These comprised of all the elements which had an influence on the behavior of the system. The various aspects like lateral movements, tensile strength of geogrid, bending moment in the piles and the total settlements were studied.

3.1. Axisymmetric Model

The piles in the GRPS embankments were arranged in a rectangular or triangular pattern. A rectangular arrangement of the piles was taken into consideration. For this analysis, one pile was considered. In order to simplify the analysis, each pile was

assumed to have its own zone of influence. A pile with a diameter of 0.7m was used for the analysis. A review of constructed GRPS embankments indicated that the typical spacing used in many projects is 1.5 to 4.5m (Han, 1999). An average spacing of 3m was used for this study. The geogrid was placed on the top of the pile. This model was used to perform parametric study.

The four important materials involved in this complex system are the piles, the geogrids, the foundation soil and the embankment soil. A drained condition was considered for the analysis. Simplified constitutive models were used to model these complex components. The "Soft soil model" in Plaxis was used to represent the weak foundation soil. This model is a Cam Clay type model used to simulate the behavior of normally consolidated clay or peat. The most important characteristic of the soft soil model is the stress dependent stiffness, which corresponds to the soft soil behavior. A logarithmic relation between the volumetric strain ε_v and mean effective stress, p' is assumed. As the model uses volumetric strain instead of void ratio, modified compression index λ^* is used in place of λ (Burland, 1965) (cited in Brinkgreve & Vermeer, 1998). For virgin isotropic compression it yields

$$\varepsilon_v - \varepsilon_v^0 = -\lambda^* \ln\left(\frac{p`}{p^0}\right) \qquad \text{Eqn.3.1}$$

For isotropic loading/reloading the elastic volume strain is formulated as

$$\varepsilon_v^{\ e} - \varepsilon_v^{e0} = -\kappa^* \ln\left(\frac{p`}{p^0}\right) \qquad \text{Eqn.3.2}$$

These modified compression index and modified swelling index can be related to Cam clay parameters and internationally normalized parameters as below:

Relation to Cam clay parameters

$$\lambda^* = \frac{\lambda}{1+e} \qquad \kappa^* = \frac{\kappa}{1+e} \qquad \text{Eqn.3.3}$$

Relation to normalized parameters

$$\lambda^* = \frac{C_c}{2.3(1+e)} \qquad \kappa^* = 1.3\frac{1-\nu_{ur}}{1+\nu_{ur}}\frac{C_s}{1+e} \qquad \text{Eqn.3.4}$$

Other input parameters for the soft soil model are c,ϕ and ψ. The yield function can be described by an ellipse in p`-q plane. The M-line is referred to as the critical state line. The tops of all ellipses pass through this line which is inclined at slope M. The failure is described by the Mohr- Coulomb criterion with ϕ` can c` parameters. Both the M line and the failure line are given at a shift of c`cotϕ`(Brinkgreve & Vermeer, 1998).

The total yield contour is the boundary of the elastic area (Figure 33). The failure line is fixed. However, the cap may increase due to primary compression.

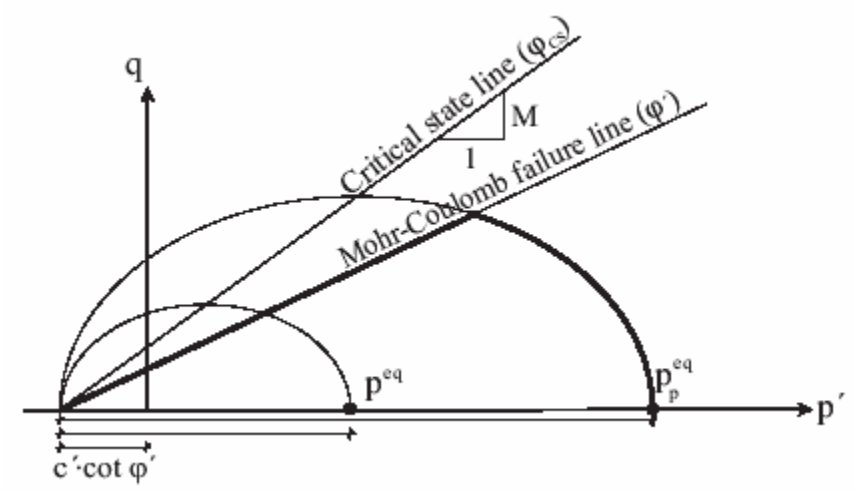

Figure 33: Yield surfaces of soft soil model in p`-q plane

The "Mohr-Coulomb Model" was used for the embankment fill. The geogrid was represented by a geotextile element in Plaxis. These are flexible elastic elements that represent sheet of fabric in out of plane direction. They can sustain tensile forces but not

compression. A linear elastic model was applied to the pile. It is important to model the interface between the geosynthetic-soil and the pile-soil. The influence of the interface is reduced when the deformations are very small. For this study, a fully bonded interface between the soil-pile and soil-geogrid was assumed. The factors that were varied in the parametric study were geosynthetic stiffness, height of the embankment, position of the geosynthetic layer and modulus of elasticity of the pile.

All the analytical methods used for the determination of tensile strength in the geogrid assume that there is a void below the geogrid. The axisymmetric model is used to prove the importance of the supporting behavior of the underlying soil. The tension in the reinforcement in the presence of the underlying soft soil is noted. Later, the soil below the geogrid was removed to represent the existence of a void. The change in the tension of the reinforcement was studied.

The elastic normal stiffness of the geogrid was varied to study its impact on the system. The geogrid undergoes creep which result in an increase in the strains. This will cause a reduction in the tensile strength to a certain extent. For simplicity, it was also assumed that the geogrid had identical properties in all horizontal directions.

The finite element model for the above described model can be seen in Figure 34.

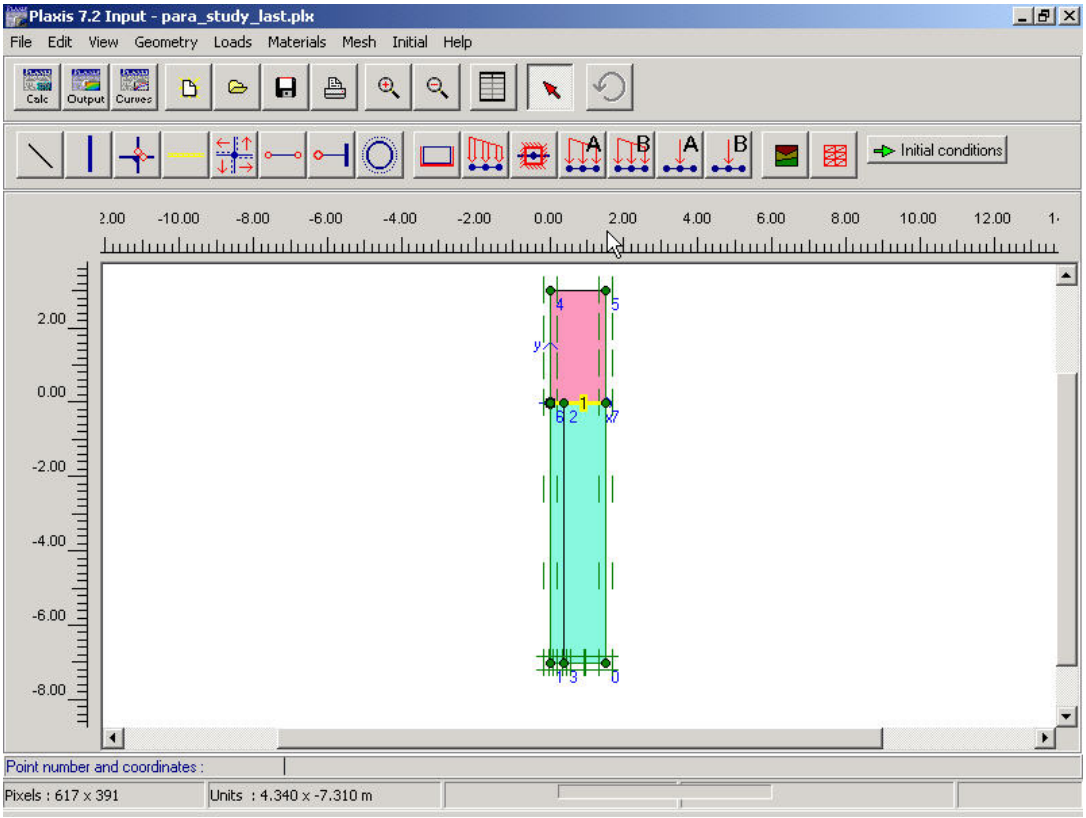

Figure 34: Axisymmetric model

Table 2: Soil properties for axisymmetric model

Material	Unit weight (kN/m^3)	Modulus of elasticity (kN/m^2)	Angle of internal friction (degrees)	Cohesion	Poisson's ratio
Embankment fill	19	20000	30	1	0.3
Foundation soil			22	5	

1) soft soil parameters are lambda*=0.2, kappa*=0.05, nu_{ur}=0.15

Once the geometry of the model was developed, initial situation and initial stress state should be stated. This was done in the initial conditions part of the input program. The elements that are not active in the initial situation can be deselected. Initial stresses are developed by the K_0-procedure. The water conditions can also be specified in the Geometry configuration mode (Figure 35).

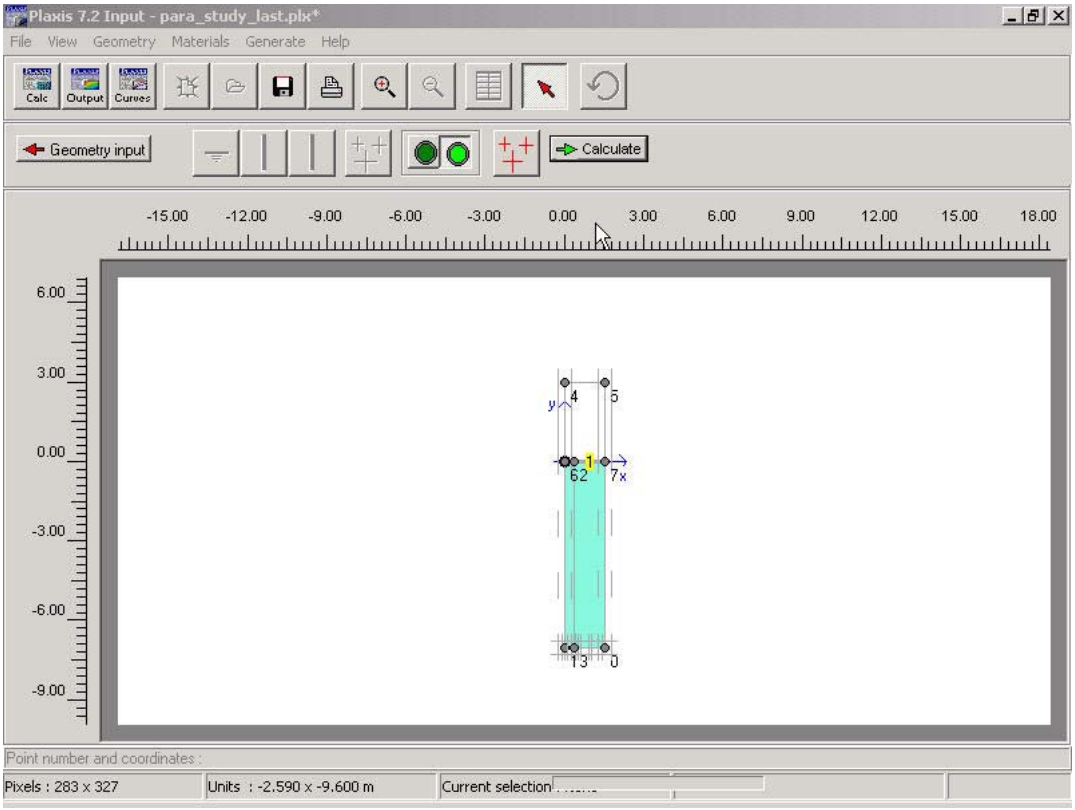

Figure 35: Initial Stresses are developed

The generation of the finite element model was followed by the calculations phase. An updated mesh analysis was applied. In the finite element analysis it is generally assumed that the change in the geometry of the mesh does not significantly affect the equilibrium conditions. However, in cases of reinforced soil structures and the cases where the soft soils cause large deformations the influence of change in the geometry of the model has to be taken into consideration. Updated mesh analysis was used in such cases (Figure 36). A staged construction procedure was used for simulation of realistic process of construction. This option enabled activating and deactivating of elements, changing geometry configuration, changing properties of materials and changing water pressures. The phases of construction can be given as

- Soil in place prior to construction
- Installation of pile + geogrid

- Application of embankment load
- Removal of soil below the geogrid if the void below the geogrid is to be represented

In the parametric study, the last phase is not considered.

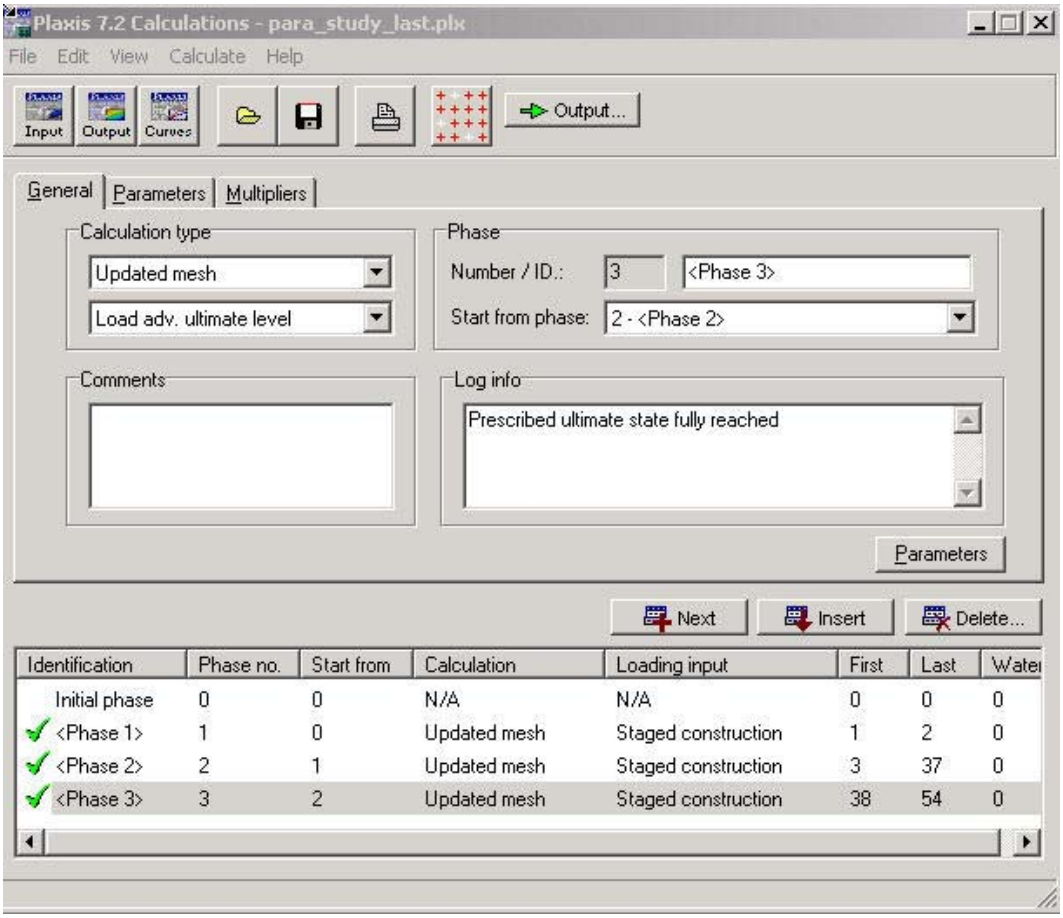

Figure 36: Stages of construction

The axisymmetric model helped in estimating the tensile strength in the geogrid assuming an infinitely long embankment. However, in order to study the entire system plane strain models of the entire system need to be developed. The results obtained from the axisymmetric analysis are presented in Chapter 4.

3.2. Plane Strain Model

The plane strain model considers all the important elements during construction of the embankment. This helps to understand the behavior of the displacement and stresses in the piles, total lateral movement of the soil, axial forces in the pile caps and tension in the various geogrids used in the system. It however requires a lot of modeling efforts. The plane strain models for five case histories were developed.

In each of the five case studies, a different type of embankment fill was used. In order to present a comparison between the predictions from the various analytical methods described in Chapter 2 and numerical analysis performed using Plaxis an embankment fill having the following properties was used. The Mohr Coulomb model was used for the embankment fill.

Table 3: Soil properties for the embankment fill

Unit weight of embankment fill (kN/m^3)	Angle of internal friction (degrees)	Elasticity modulus of the fill (kN/m^2)
19	30	20000

For numerical considerations, the value of cohesion of the embankment fill was set to $1kN/m^2$.

The plane strain models use beam elements to represent the piles. The “Soft soil model” represents the weak clay. Plastic analysis can be performed on the plane strain models. There are no guidelines provided to indicate when the updated mesh analysis should be performed. One of the approaches suggested by the Plaxis manual is to inspect the deformed mesh after conventional plastic analysis. If large geometric deformations are seen, updated mesh analysis might be needed. Plastic and updated mesh analysis was performed on all models. The effect of geometry was not observed to be as significant in

the large plane strain models as in the axisymmetric model. However, only a plastic analysis was performed on the fifth case history of Polk Parkway in Florida. This model has a large number of elements. Updated mesh analysis takes a large amount of computer time. Due to large deformations it updates the stiffness matrix at the beginning of every calculation stage. Plaxis failed to perform updated mesh analysis on such a complex structure.

In order to give consideration to the interaction between the various elements of the system, interfaces between the pile-soil and soil-geosynthetic should be introduced. The maximum shear force on one side of the geogrid is determined by the Mohr-Coulomb strength multiplied by a factor R_{inter}. This factor was taken as 0.9 for calculations. In cases where the geogrid lay on the pile cap, the contact surface between the pile cap and the geogrid was a complicated problem. The assumption was made that no slip occured at this contact surface. In practice, a layer of non-woven geotextile was placed between the pile cap and the geogrid. A small slip might occur at this location, which would result in a small decrease in the tensile strength of the geogrid. The introduction of the interfaces largely increases the number of elements. In the Polk County case study, there were a large number of elements placed very close to each other. Such cases were difficult and time consuming to model with interfaces. Two case studies were presented with interfaces so as to get an estimate of the difference that would be caused by the presence of interfaces.

Figure 37 shows the plane strain problem of a case study of timber pile-in-situ soil reinforcement at the Polk Parkway, a multilane toll facility at Lakeland, Florida.

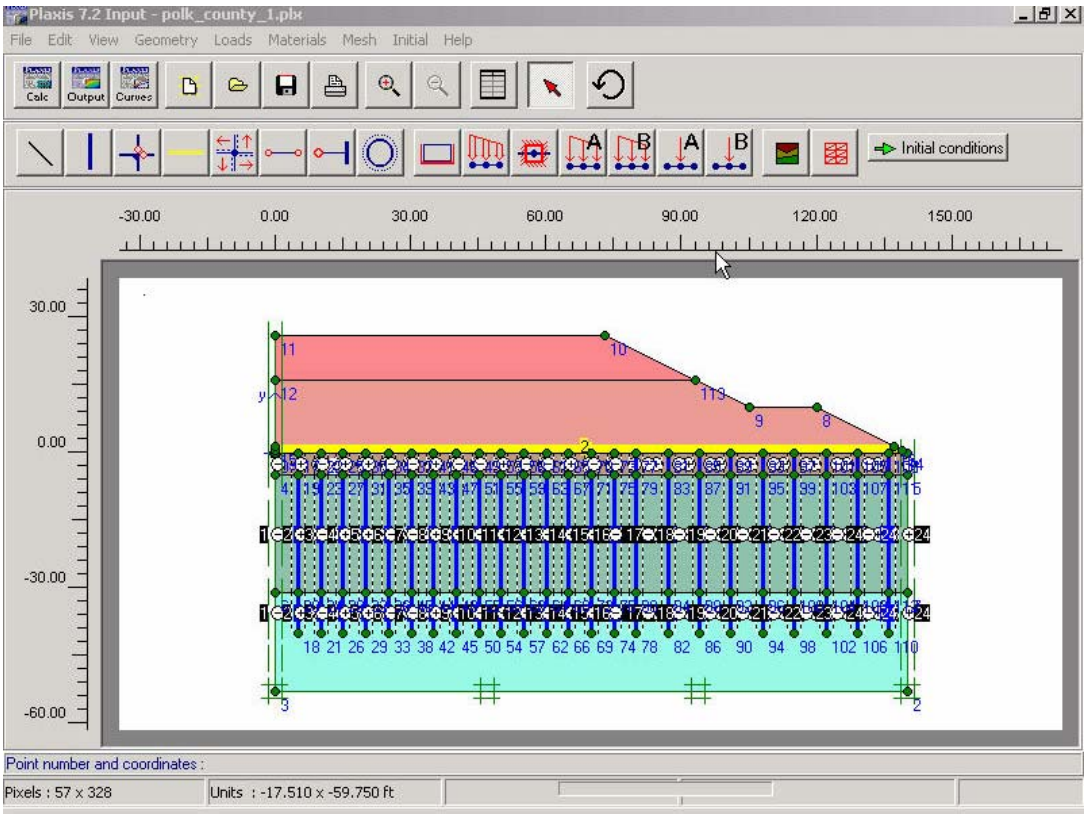

Figure 37: Plane strain model for Polk County project

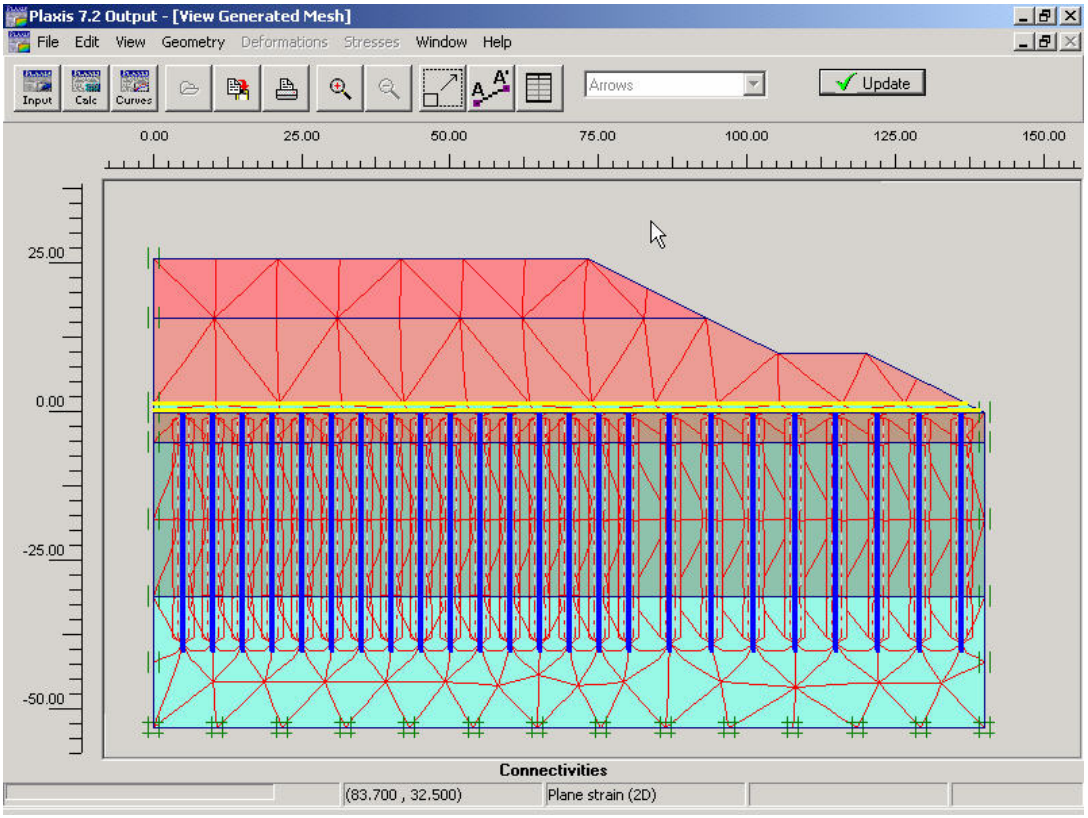

Figure 38: Mesh generated for the Polk County Project.

The calculation phases were applied as in the axisymmetry model analysis. Any traffic or wheel loads that were to be applied were modeled as an equivalent soil layer. There is an assumption that there is no horizontal or vertical movement due to the consolidation of the soft soil. In cases where there were pile caps, they were modeled as linear elastic cushions of known thickness.

Slope stability analysis which is one of the important aspects of design of GRPS embankments can be handled using Plaxis. The slope stability analysis for one of the case studies was performed. In order to perform stability analysis, initially gravity loading was applied. Plastic analysis was performed. Safety analysis can be executed by reducing the strength parameters of the soil until failure of the structure occurs. This can be achieved using a Phi-c reduction type of loading. The strength of the structural objects like beams or geotextiles is not affected in the Phi-c reduction. This type of loading can be performed only using Number of steps procedure in the calculation mode of Plaxis. The stress dependent behavior and hardening effects are removed from the safety analysis. Hence, when the Phi-c reduction analysis is applied to advanced soil models, these models follow the standard Mohr-Coulomb failure. Figure 39 shows the calculation phases in the slope stability analysis. The safety analysis is done after every stage of construction. Thus, the slope stability of the GRPS embankments can be handled using Plaxis.

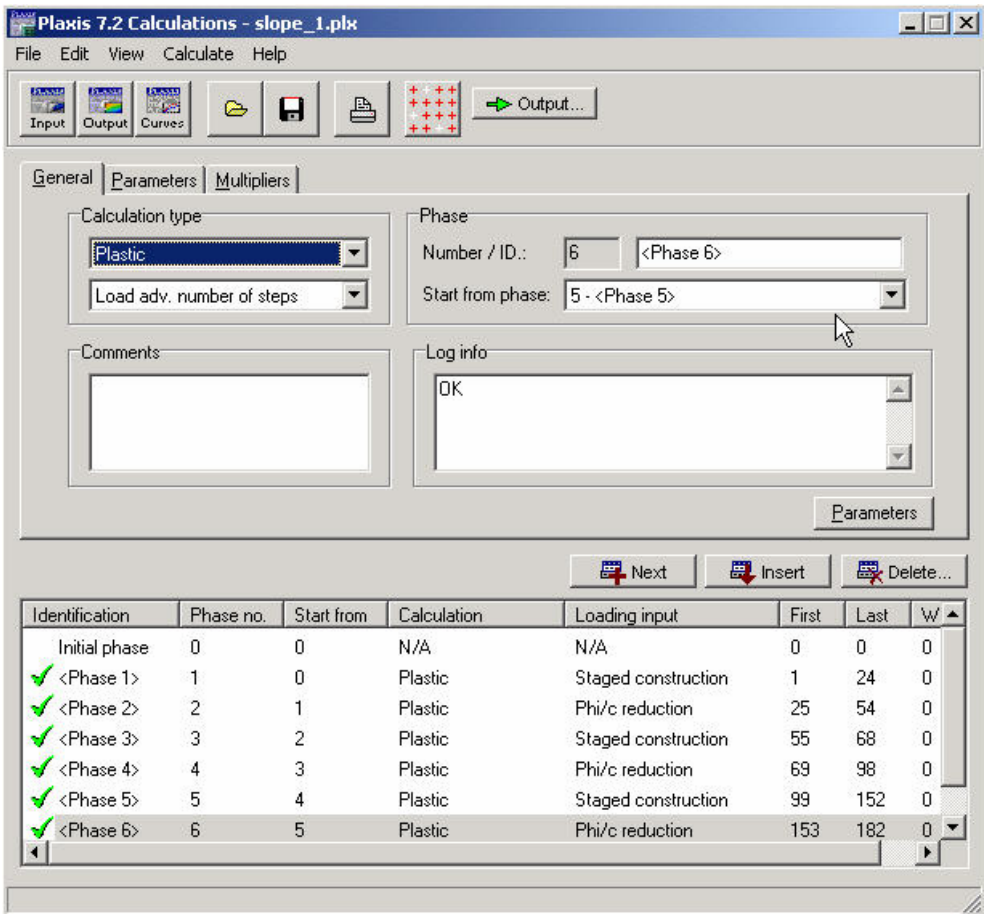

Figure 39: Stability analysis using Plaxis Phi-c reduction method

The results of the five case studies are presented in Chapter 5. A comparison of results from all available methods and Plaxis program is presented.

CHAPTER 4
CASE HISTORIES, COMPARISON OF VARIOUS METHODS

4.1. Axisymmetric Model Analysis

Plaxis 2D was used for the numerical modeling of the GRPS embankments. In most GRPS embankments, the piles are arranged in a triangular or square grid pattern. A square grid pattern was chosen for the analysis. The axisymmetric model was used to study the impact of varying various factors on the system. A pile having a diameter of 0.7m was selected for the study. Typical spacing between piles in GRPS embankment systems ranges between 1.5 to 4.5m (Han, 1999). A spacing of 3m was chosen. An embankment height of 3m was considered. After considering the various case studies available, eight meters of soft soil was assumed to be underlain by a stiff layer. No displacements were expected beyond the depth of this layer. One layer of geogrid was laid on the top of the pile.

4.1.1. Maximum Settlements

Maximum settlements at the pile head were studied. The maximum settlement increased with a reduction in the pile modulus. It can also be seen in Figure 40 that the inclusion of the geosynthetic layer reduced the maximum settlements greatly. The stress concentration ratio was improved with the inclusion of the geosynthetic layer, due to the stiffness difference between the pile and the soil. The maximum settlements at the pile head decreased with an increase in the tensile stiffness of the geogrid (Figure 41). The maximum settlement increased with an increase in the height of the embankment (Figure

42). It can be proved again that the presence of the geogrid helps in reducing the maximum settlements.

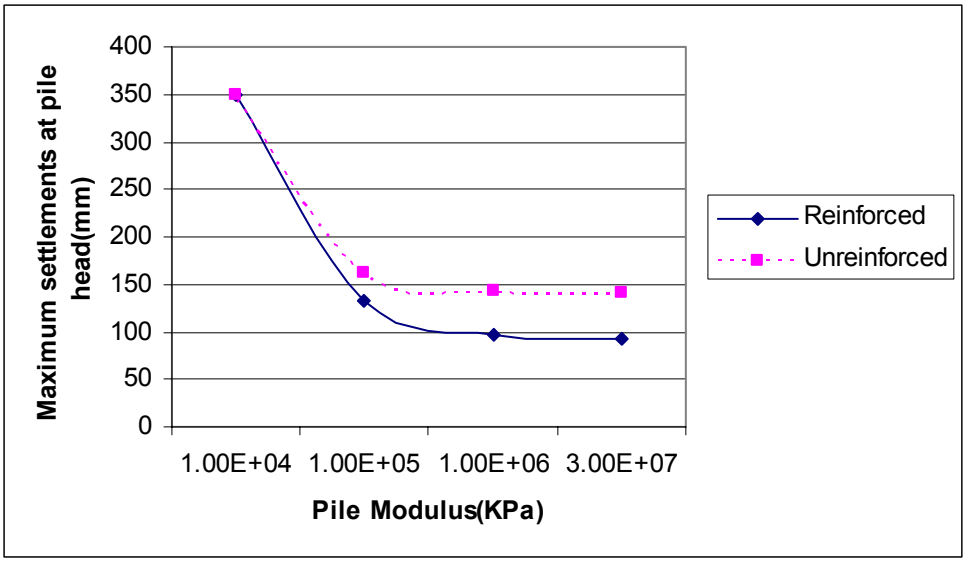

Figure 40: Influence of pile modulus on the maximum settlements at pile head

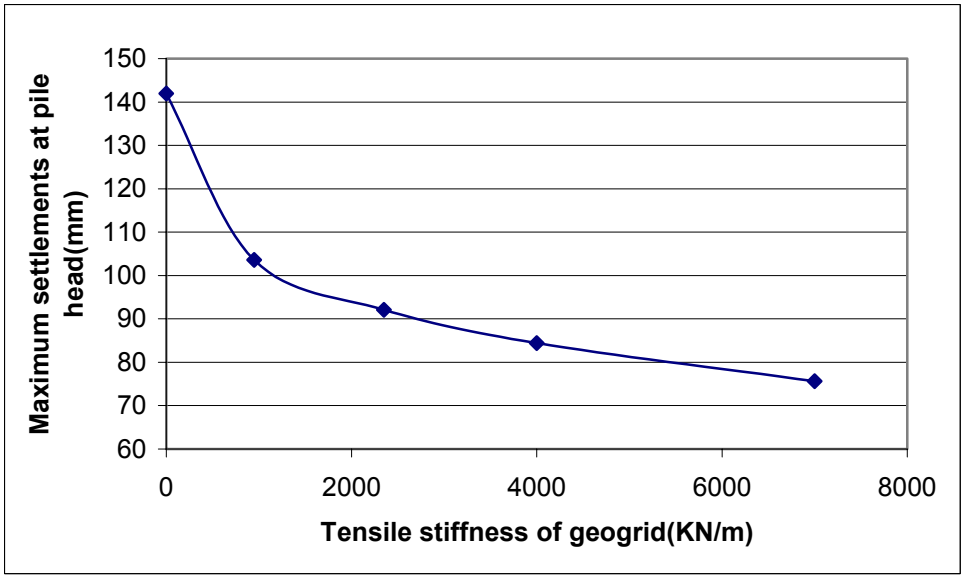

Figure 41: Influence of tensile stiffness on the maximum settlements at pile head

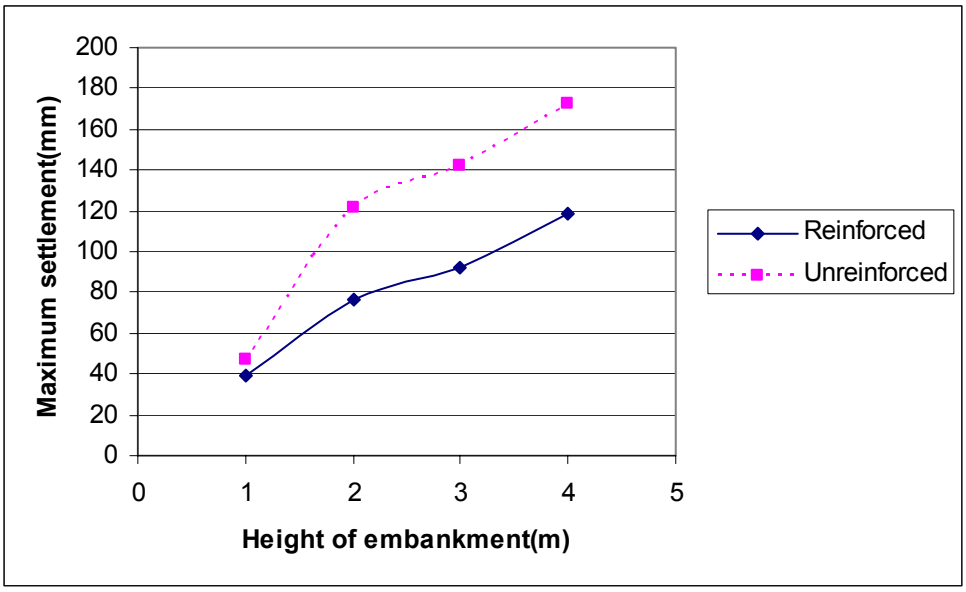

Figure 42: Influence of height of embankment on maximum settlements at pile head

4.1.2. Differential Settlements

Differential settlement can be defined as the difference in the settlement at the center of the pile and at the midspan of the pile spacing. Differential settlements at the pile head increase with an increase in the modulus of the pile (Figure 43). This is due to the increase in the difference between the stiffness of the soil and the pile. The large modulus difference promotes more differential settlement. The differential settlement would be zero if the soil and pile had the same modulus.

The differential settlement decreased with an increase in the tensile stiffness, similar to the maximum settlements (Figure 44). Similarly, with an increase in the height of the embankment the differential settlement at the pile head increased (Figure 45).

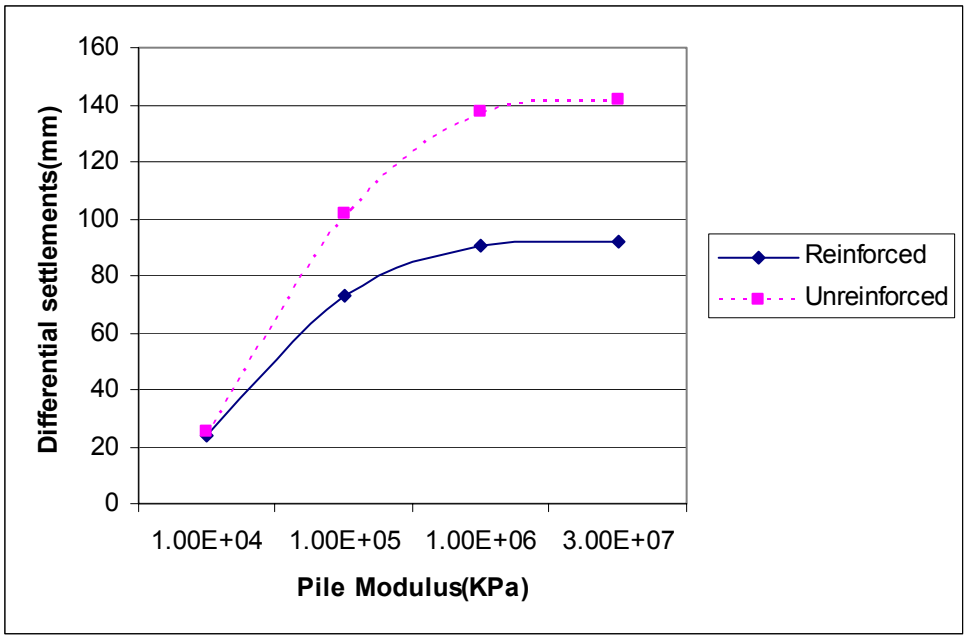

Figure 43: Influence of pile modulus on differential settlement at pile head

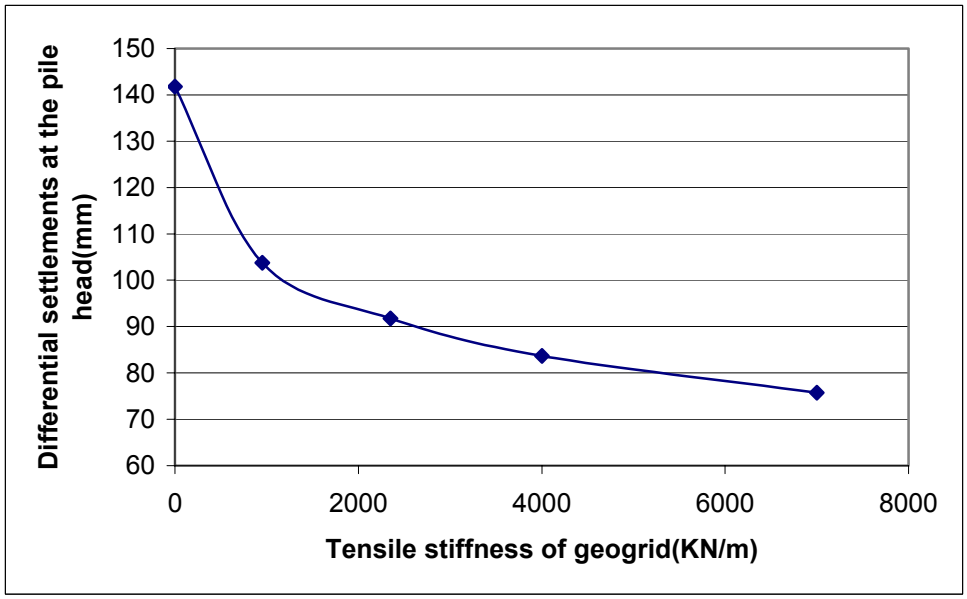

Figure 44: Influence of tensile stiffness on differential settlement at pile head

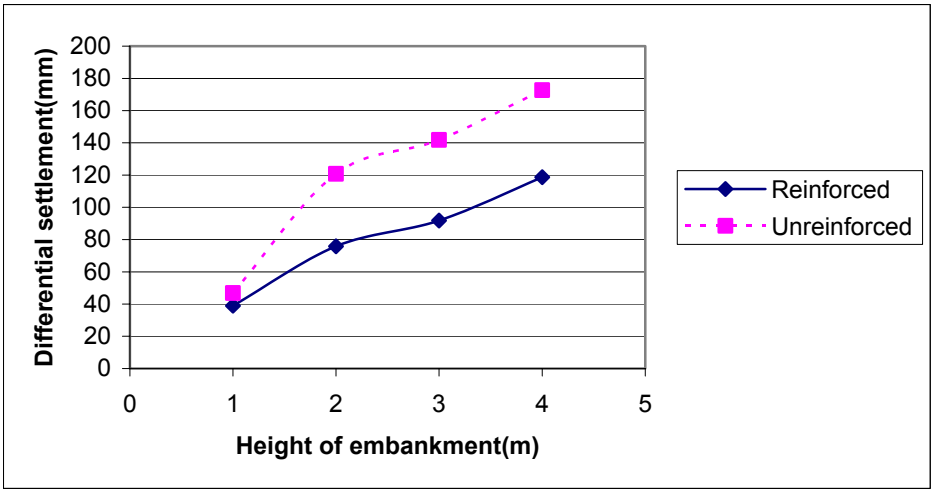

Figure 45: Influence of height of embankment on the differential settlement at pile head

4.1.3. Tensile Strength of the Geogrid

The tensile strength of the geogrid occurs at the edge of the pile. The maximum tensile strength increases with increased geogrid tensile stiffness (Figure 47). The increase in the tensile stiffness of the geogrid promotes in the early mobilization of the tensile strength for very small increase in differential settlements. The tensile strength in the geogrid increases with an increase in the pile modulus (Figure 46). The increase in the pile modulus causes an increase in the difference in the stiffness between the pile and soil. This causes more differential settlements and eventually increases the tensile strength in the geogrid. The increase in the height of the embankment causes an increase in the differential settlement at the pile head. This again mobilizes more tensile strength in the geogrid (Figure 48).

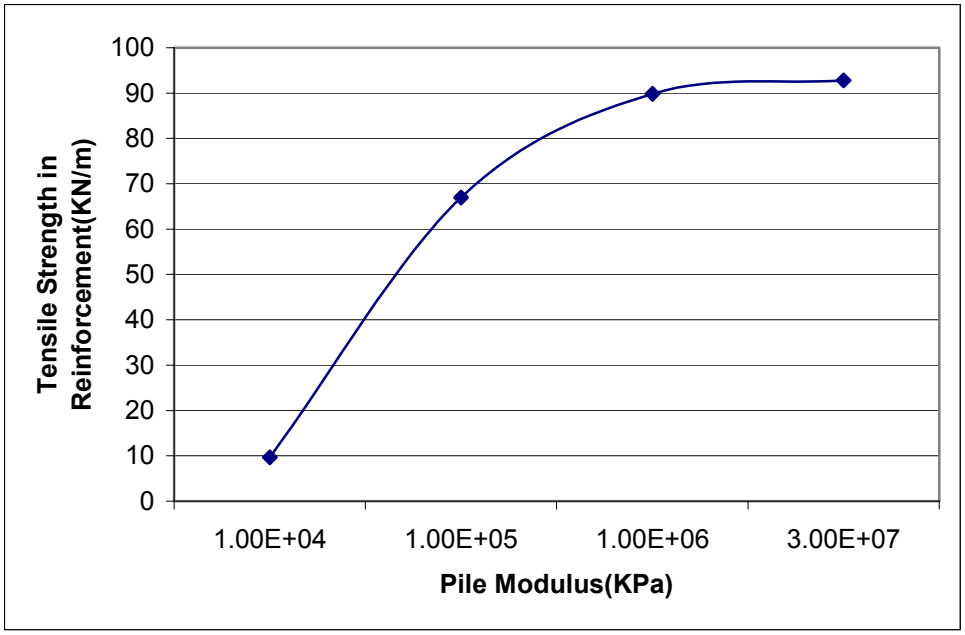

Figure 46: Influence of pile modulus on tensile strength of geogrid

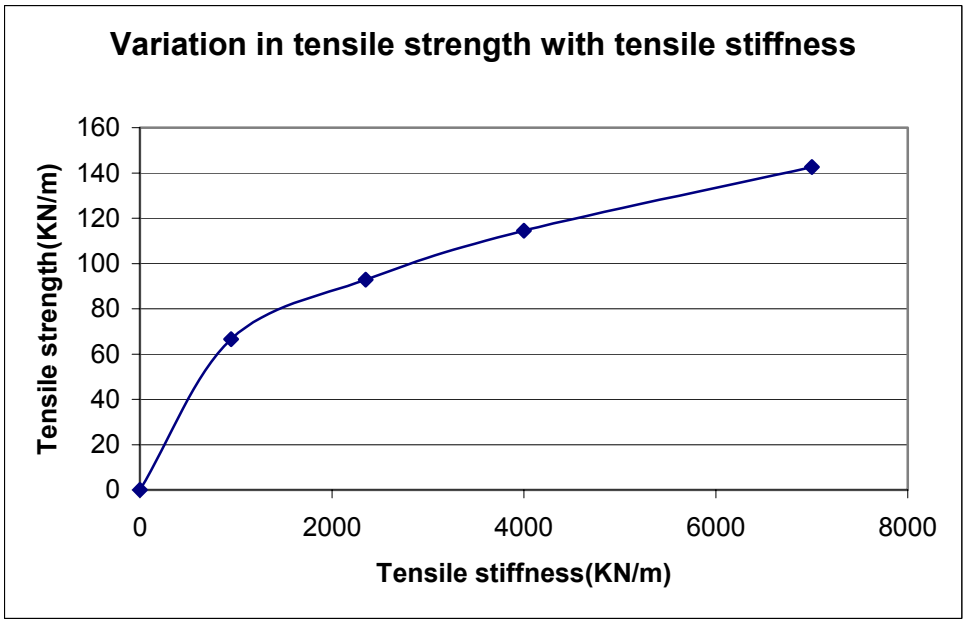

Figure 47: Influence of tensile stiffness of geogrid on tensile strength of geogrid

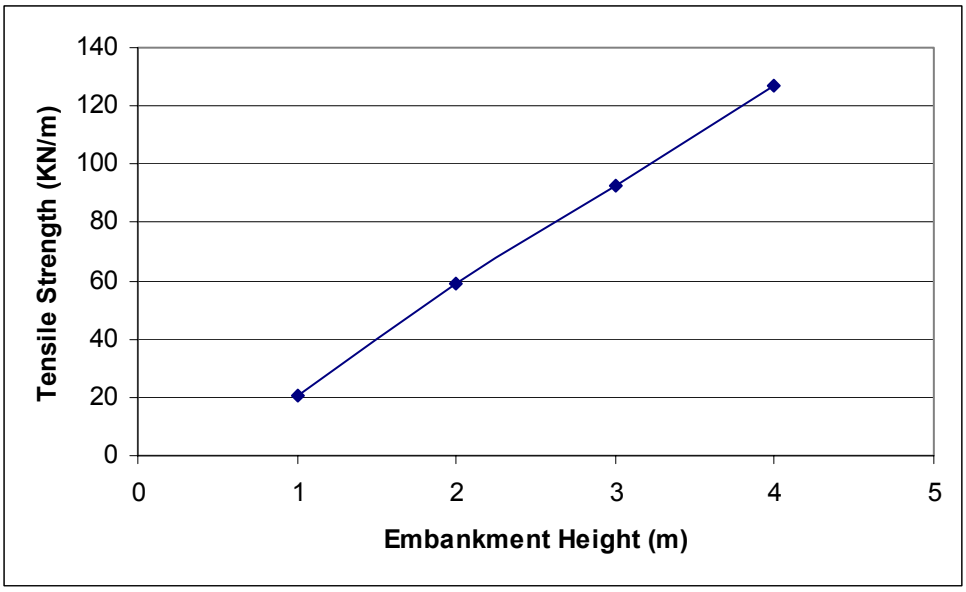

Figure 48: Influence of height of embankment on tensile strength of geogrid

4.1.4. Stress Concentration Ratio

The stress concentration ratio is the measure of the load transfer from the soil to the piles. The stress concentration ratio increases with the increase in the modulus of the pile. The stress concentration is nearly constant after the modulus reaches 3E7 KPa (Figure 49). The stress concentration ratio increases with an increase in the tensile stiffness of the geosynthetic layer (Figure 50). For an unreinforced systems the stress concentration ratio is generally between 1–8. The inclusion of the geosynthetic layer increases the transfer of stresses from the soil to the pile. There is a sharp increase in the stress concentration ratio with an increase in the height of the embankment (Figure 51).

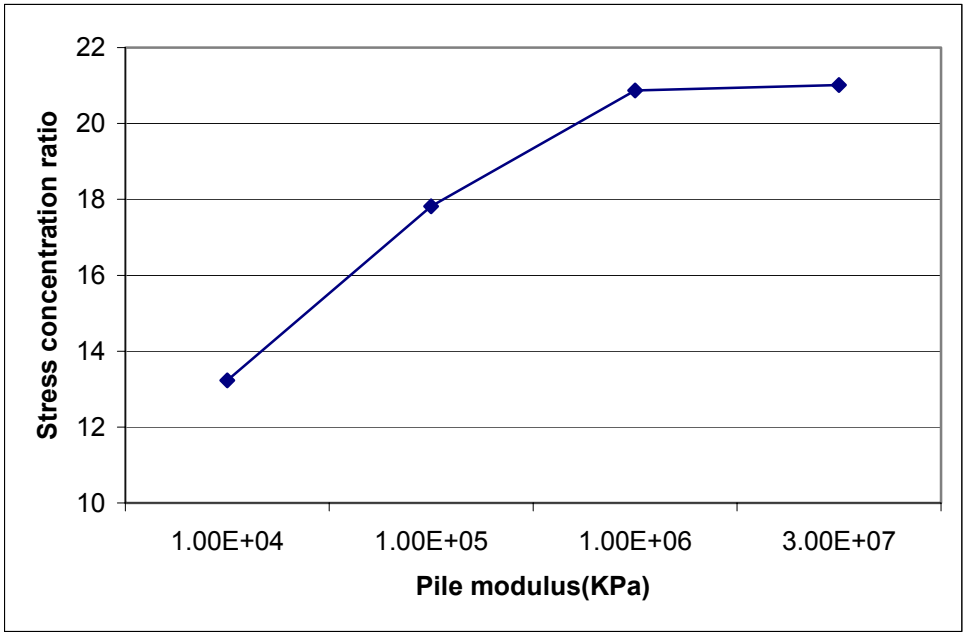

Figure 49: Influence of pile modulus on stress concentration ratio

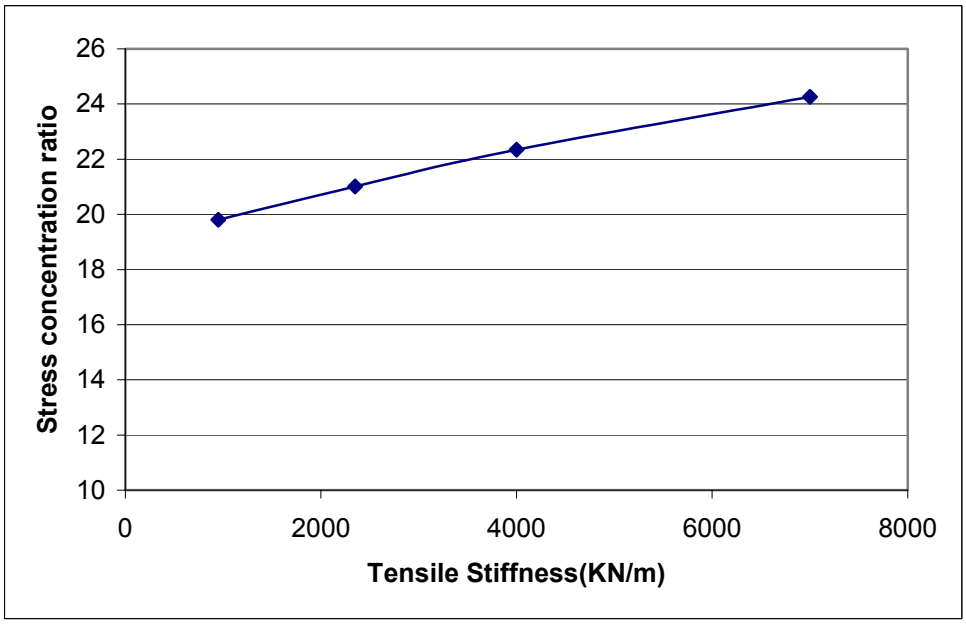

Figure 50: Influence of tensile stiffness of geogrid on stress concentration ratio

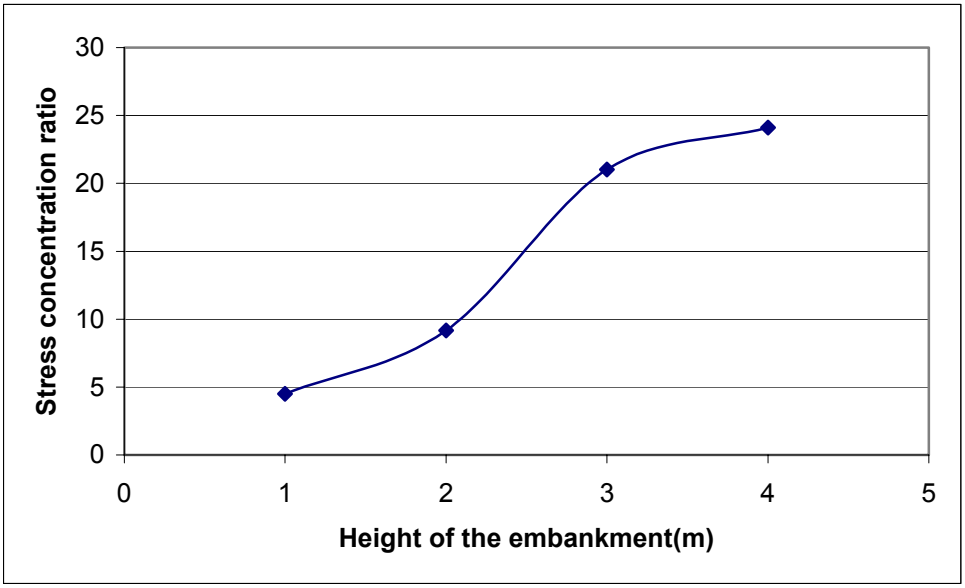

Figure 51: Influence of height of the embankment on stress concentration ratio

4.1.5. Position of the Geotextile

The position of the geotextile with respect to the pile head was considered (Table 4). The geotextiles were placed on the top of the pile head or at some distance from the top of the pile head. It is seen that as the position of the geogrid from the pile head increases, the maximum and differential settlements continue to increase. However, there is a decrease in the tensile stress in the geogrid.

Table 4: The effect of position of the geogrid

Position of geogrid	Pile modulus (kN/m^2)	Maximum settlement (mm)	Differential Settlement (mm)	Tension in reinforcement (mm)
Geogrid on pile	3.00E+07	92.06	91.78	92.83
Geogrid 0.1 m above pile head		93.93	93.78	62.27
Geogrid 0.2 m above pile head		108.77	108.78	44.59

All the analytical methods assume that the weak foundation soil settles and hence, there is no contact between the geogrid and the soil directly under the geogrid. However,

the tension in the geogrid greatly increases if the presence of a void is considered. This is demonstrated in Table 5.

Table 5: Effect of support of underlying soil

Pile modulus (kN/m^2)	Maximum settlement (mm)	Differential Settlement (mm)	Tension in reinforcement (kN/m)	
3.00E+07	92.06	91.78	92.83	with support
3.00E+07	292.91	292.75	256.61	support from underlying soil removed

All the factors, pile modulus, tensile stiffness of geogrid, height of the embankment and the position of the geogrid affect the system greatly. However, these effects have not been incorporated into any of the analytical methods.

4.2. Case Histories

Several case histories of GRPS embankments were found in the literature. Five were chosen for numerical analysis using Plaxis. The reference, application and design parameters of the case studies are presented below. The results from Plaxis will be discussed along with the other methods in the Section 4.3.

4.2.1. Timber Pile in-Situ Soil Reinforcement (Ostensen and Bennett, 2002 and Kuo et al., 1998)

The Turnpike District of the Florida Department of Transportation constructed the Polk Parkway, which is a multi-lane facility expressway looping around the southern extent of Lakeland, Florida. Owing to the uncertain soil conditions in Section 3A a surcharge program was designed to eliminate potential excessive differential and total displacements before construction of a Mechanically Stabilized Wall.

A localized slope failure occurred during the construction. This was due to the presence of a deposit of phosphatic waste clay which was not detected in the original field exploration program. Various engineering methods were evaluated for soil

improvement. In considering the long term performance of the proposed MSE wall, construction cost, schedule, constructibility and reliability, timber pile reinforcement was selected. The final configuration consisted of a 5 foot square grid system supporting a fill height of 20-26 feet. The spacing was increased to 7 feet under the South Frontage Road, where the fill height was 5-10 feet. 1100 treated piles, 40 feet long were installed and each pile was subjected to a design load of 30 tons. The pile tip diameter was 7 inches.

A six inch layer of sand was placed after the installation of the piles. This was followed by 12 inches of sand and a second layer of geotextile in the orthogonal direction. The long term allowable design strength of the geotextile was 1550 lb/in(18.6 kips per foot). The function of the two geotextiles was to transfer the weight of the MSE wall to the timber piles and prevent stability and settlement problems. The finite element model for the case study can be seen in Figure 52.

The performance of the pile supported reinforcement system was evaluated using one vertical inclinometer and four vibrating wire settlement cells. A lateral movement of 0.7 inches was recorded by the inclinometer. Two settlement cells were installed below the MSE wall and two were installed below the South Frontage road. Two of the cells were damaged. The other two showed a total settlement of 3-4 inches in 6 months. These values indicate that the pile supporting system was successful in improving the sub surface conditions.

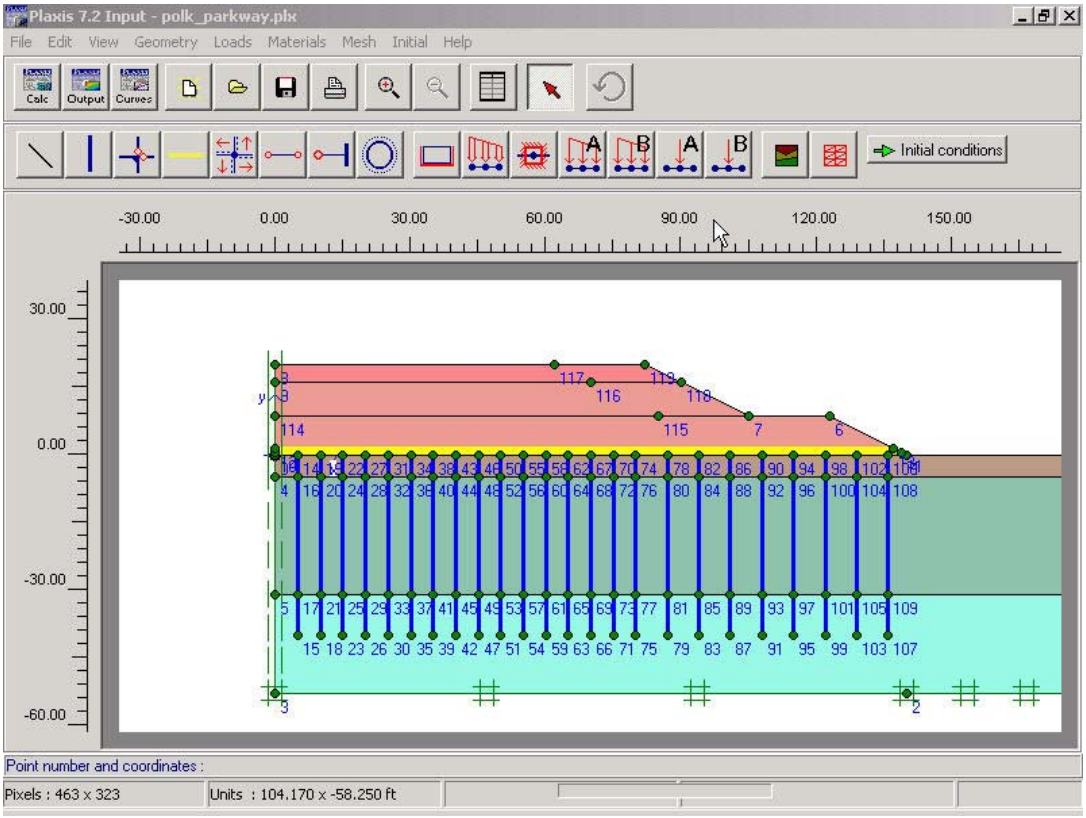

Figure 52: Model for Polk Parkway –Timber pile in-situ soil reinforcement

4.2.2. Route 403 – Niitsu Bypass Japan (Ohtani and Miki, 2002) (cited in Han, 2003)

The route 403 Niitsu Bypass located 15 km from Nigatta City, Japan, was constructed on a 5 m thick peat layer. A low embankment was built with an average height of 1.5m. The finite element model for this study had a maximum height of 2.6m (Figure 53). Deep mixed(DM) columns were used for ground improvement. In order to prevent differential settlement between the DM columns two layers of biaxial geogrid were placed before the construction of the embankment. The peat had the following properties: water content – 160-668% , liquid limit – 367%, plastic limit – 157%, moist unit weight – 9.60 -10.39 KN/m^3, void ratio 9.64-16.41, compression index – 2.1, undrained shear strength – 6.86KPa.

The design parameters of the geogrid and the DM columns were available. The geogrid had a tensile stiffness of 490kN/m and an elongation of 1.5% was used. The design tensile strength of the geogrid was 7.35kN/m. The DM columns were end bearing columns made of Portland blast – furnace cement B. The columns were 5.5m long and 1m in diameter. They were placed in a 2.3×2.3m square grid pattern throughout the embankment width. The unconfined compression strength of the DM columns was 598 KPa.

To monitor the performance of the system instrumentation devices were installed. Settlement and earth pressure gauges were used on top and between the columns. Strain gauges were installed below the geogrids. The observed results during and after construction of the embankment can be seen in Figure 54.

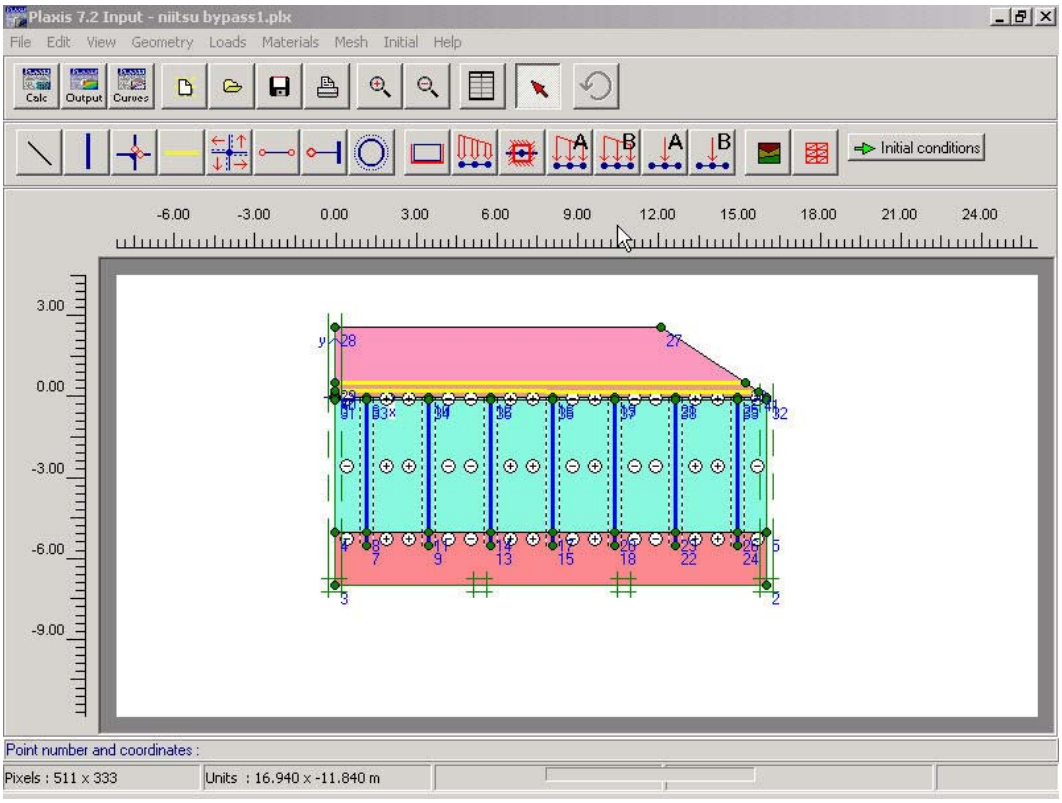

Figure 53: Model for Niitsu Bypass, Japan

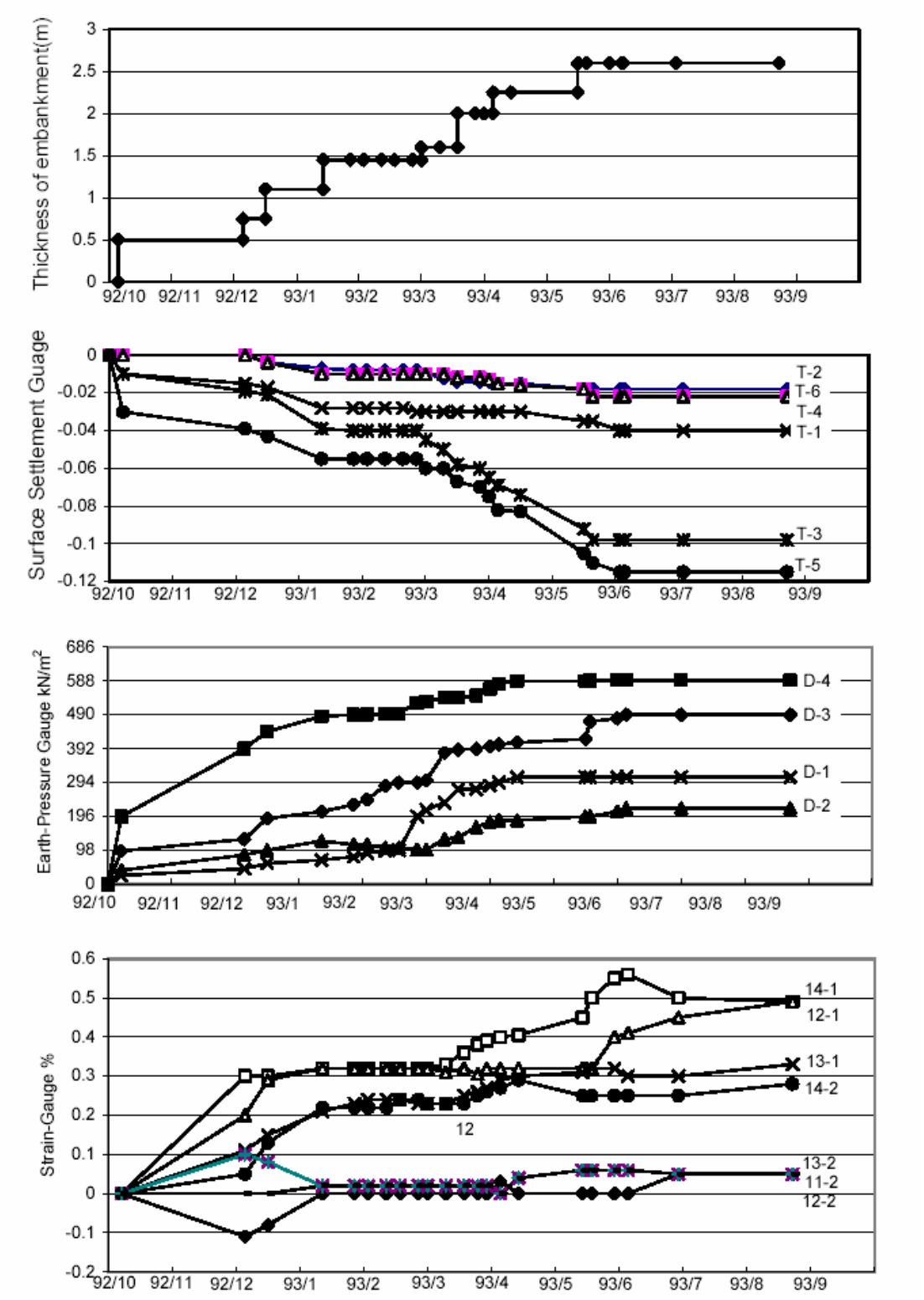

Figure 54: Results of geotechnical monitoring on the Niitsu-Bypass site.

4.2.3. Yono City, Japan – Geogrid Reinforced Low Height Embankment on Deep Mixed Columns (Tsukada et al., 1993) (cited in Li et al., 2002)

A 10 m wide street with 2m wide sidewalks on each side accommodates two lane traffic. The subsoil is very soft, consisting of a 4m thick peat layer underlain by a 4m thick clay layer. The surrounding area was already developed. Hence, ground improvement techniques like PV drains and sand drains could not be applied. The deep mixed columns technique was selected for the improvement.

Deep mixed columns of 800mm diameter having an unconfined compression strength of 1MPa were used. The DM columns were spaced at a distance of 2.1m. A low height embankment of 1.5m was constructed on the DM columns. Finite element model for the case study can be seen in Figure 55. Due to the large spacing between the columns large differential settlements were expected at the surface. A layer of geogrid Tensar SS2 was laid on top of the columns to reduce the effect of differential settlement. The improvement ratio used on this project was about 11%. This is far less than the expected 50-70% pile cap coverage in conventional piled embankments.

After the installation of the DM columns, the surface soil was excavated. The soil was replaced by the subgrade and the geogrid was sandwiched between the two subgrade layers. The pavement was then laid on top of the subgrade.

The differential settlement that was observed on the site was about 15mm. Almost all the settlement occurred during construction. There was an increase in the strain of the geogrid. However, it did not exceed 0.5%.

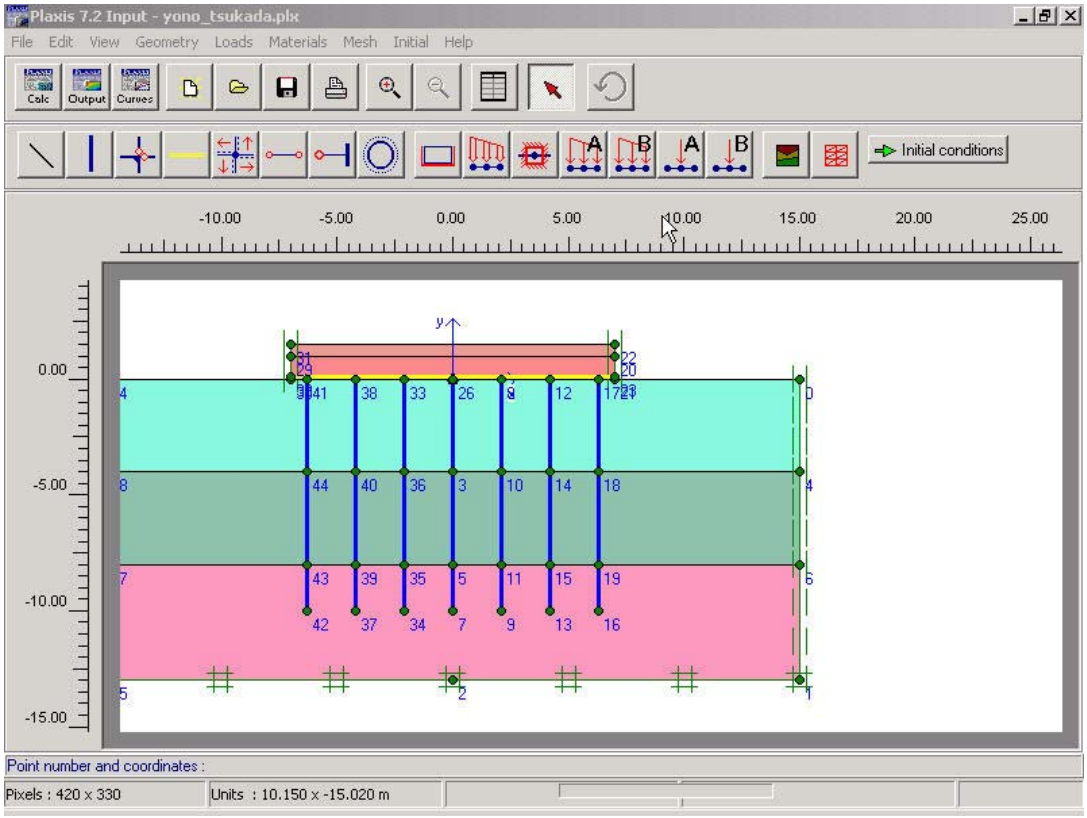

Figure 55: The model for street in Japan, Yono city

4.2.4. Stansted Airport Piled Embankment (Jones et al., 1990) (cited in Li et al., 2002)

The rail link between Stansted Airport terminal and the London-Cambridge mainline was constructed on a geogrid reinforced piled embankment. The subsoil was weak and consisted of a 5-13m deep peat layer, underlain by 1-10m of stiff glacial till. This rested on a chalk stratum. The top layers of the chalk stratum were found to be weak. The water level at the site was very high. It existed at about 1-1.5m below the ground level.

The undrained shear strength of peat was between 10 and 20 kN/m^2. The embankment of the London-Cambridge mainline was stable and all settlement was completed. It was very important that no differential settlement occur between the mainline and the new spur line. In order to accomplish that many methods could be

employed. However, considering the time constraint and feasibility of other ground improvement techniques, a geogrid reinforced piled embankment was found to be the most suitable.

Precast piles were used. 1500 piles were placed in a square grid of 2.75m. The pile caps were 1.4m in diameter and 0.5m thick. The embankment of 3-5m was constructed. The embankment consisted of locally available boulder clay. The properties of the fill were c=25KPa, ϕ=25◦, γ=20 kN/m^3.

Paralink geogrid having an ultimate tensile strength of 350kN/m was used along the length of the embankment and of 425kN/m was used across the embankment. The geogrid was wrapped around gabions in order to create the required tension. A finite element model for the case study can be seen in Figure 56.

There has been no discernible differential settlement noticed at the site since the construction.

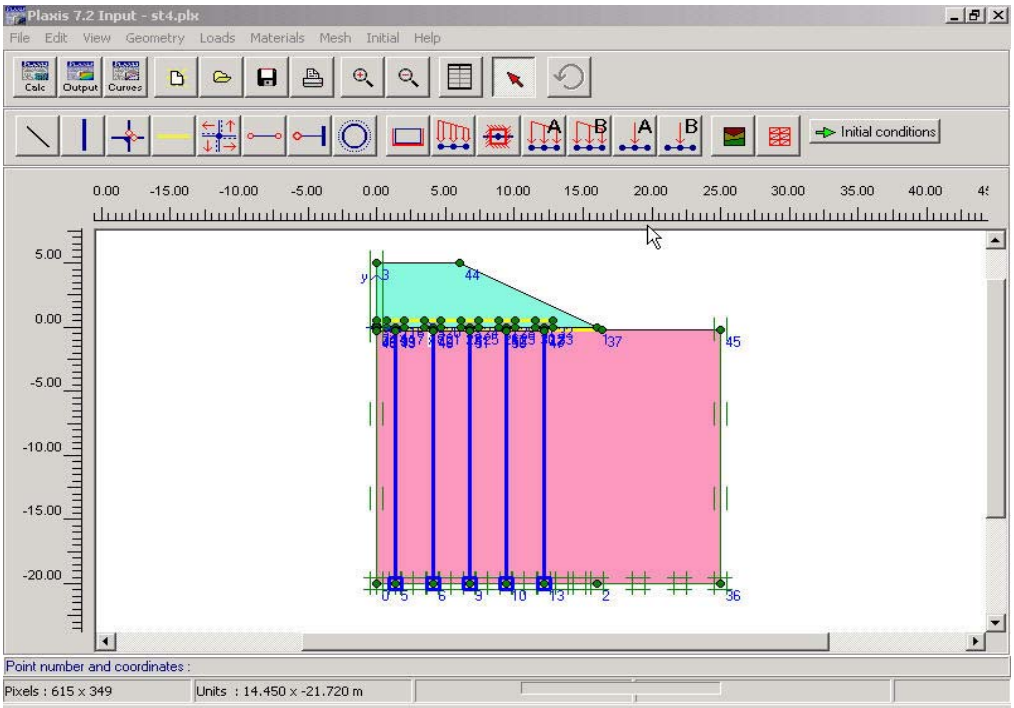

Figure 56: Embankment from Stansted airport terminal to Cambridge-London mainline

4.2.5. AuGeo Piled Embankment for Double Track Railway Rawang-Bidor (Cortlever & Gutter, 2002)

The AuGeo Piled Embankment was built in some sections of the proposed double railway track Rawang – Bidor. The AuGeo piled embankment system consisted of lightweight piles with enlarged pile caps and pile tips. The subsoil consisted of about 6m of soft clay. The piles were founded in the stable layer of sand, gravel or silt below the soft clay. A Fortrac 250 mattress was placed on top of the pile caps to transfer the embankment loads. A 0.6m layer of gravel was laid on the geotextile and was followed by another layer of geotextile –Comtrac 110. The Comtrac 110 was used to avoid migration of fines from the fill to the lower layers.

A one meter layer of sand was placed before the installation of the piles. The AuGeo piles of 0.15m diameter were placed at a distance of 1m center-to-center in the direction perpendicular to the track. In the direction parallel to the track the spacing varied from 0.96m to 4.0m with the height of the embankment. The pile caps were square in shape, 300mm×300mm with rounded edges on top. A height of 2.5m was used for analysis. The finite element model for the case study can be seen in Figure 57.

No differential settlements were seen on the site. Cofra's design was available to us. The results obtained from the analysis were compared with those.

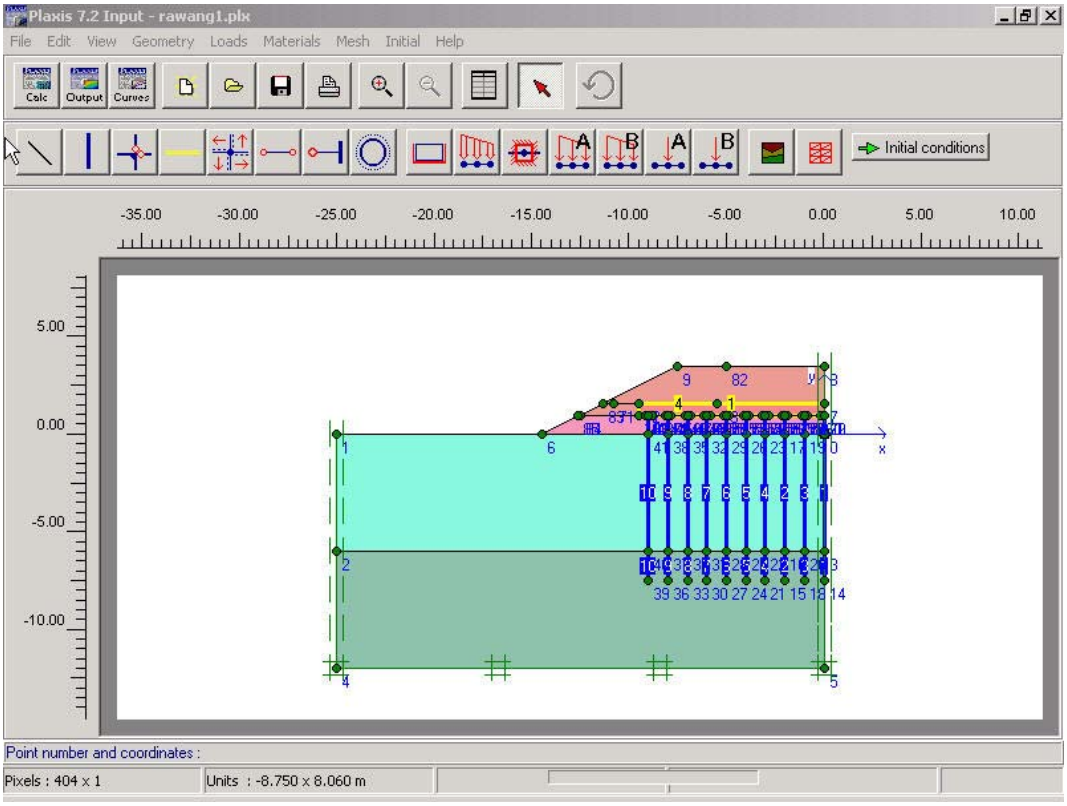

Figure 57: The model of AuGeo piled embankment for double track railway Rawang - Bidor

4.3. Comparisons

The various methods discussed in the literature are used. Lateral movements, bending moments in the pile and the geosynthetic tensile strength are compared with the results from Plaxis.

4.3.1. Lateral Movements

Existing methods for predicting lateral movements, are only for embankments without piles and geosynthetics. Plaxis gives due consideration to the presence of piles and geosynthetic layers. All the predictions given below are for movement at the toe of the embankment.

The Bourges and Mieussens method is conservative. Briaud and Gibbens method could not be used in all case studies as sufficient data were not available. Lateral movements increase if a void below the geogrid is considered in the Plaxis analysis (Table 7). The comparison of the various methods can be seen in Table 6.

Table 6: Comparison between maximum lateral movements

	Bourges & Mieussens(m)	Marche & Chapuis(m)	Briaud & Gibbens(m)	Plaxis 2D w/o void below geogrid(m)
4.1	0.24-0.36	0-0.022	0.0038	0.067
4.2	-[1)]	0-0.023		0.0844
4.3	-[2)]	-[2)]		0.003503
4.4	0.275	0.067-0.077		0.02448
4.5	-[2)]	-[2)]		0.0306

1) stability factor was found to be less than one. So no calculations could be made.

2) The undrained shear strength for the soil was not known. Hence, lateral movements could not be estimated.

Table 7: The lateral movements in Case 4.5 in various conditions

	Lateral movement w/o void	Lateral movement with void
Updated Mesh Analysis	0.0306	0.0357
Updated Mesh Analysis with interfaces	0.0448	0.04588

This shows that the introduction of interfaces impacts the lateral settlements significantly.

4.3.2. Geogrid Strength

All the analytical methods used to calculate the tensile strength in the geotextile assume that the soft soil below the geotextile settles. Hence, a void is formed. However, the Plaxis plane strain model does not allow a void to be created in all the cases. It cannot handle very small elements formed and the stiffness matrix fails. This can be taken care of by using a small axisymmetric model. The axisymmetric model gives an estimate of the increase in the tensile strength of the geotextile due to the formation of a void. This

void formation does not affect any of the other factors significantly. Hence, the expected lateral movements, bending moment in the piles and settlements will not vary much from the values obtained from the plane strain model, which does not assume a void below the geotextile.

One drawback of Plaxis is that it cannot by itself calculate the force in the geotextile along the width of the embankment. However, Gutter (2002) in their study found that the extra tensile force due to sliding could be evaluated with the aid of a program Grond. Grond calculates the forces and displacements in a horizontally loaded pile. The interaction between the pile and the geogrid is represented by a horizontal spring in Plaxis. The horizontal spring constant for maximum pile cap force was evaluated. From this value, the maximum tension in the geogrid was found. This force due to horizontal sliding is assumed to be equal in both directions. The value for the tensile strength obtained from the axisymmetric model is the combination of the horizontal sliding and the geogrid interaction with the individual pile. A unit cell model similar to the one in the axisymmetric analysis is made for the case study. The ratio of the tensile strength for the axisymmetric model to the plane strain model, and horizontal sliding force determined help in calculating the tensile strength along the width of the embankment. This portion is not within the scope of this study. More research is required in this area, especially in cases where the geogrid does not lie on the top of the pile head.

It can be seen from Table 8 that the values obtained from the updated mesh analysis and the plastic analysis are comparable. Hence, for the Polk County case study, the values can be obtained from the plastic analysis. For all other case studies the updated

mesh analysis can be considered. The results also show that with the inclusion of the interfaces there is a decrease in the tensile strength of the geotextile by about 10 percent.

Table 8: Comparison between the tensile strength of the geosynthetic reinforcement for the case of no void below geogrid

Case No.	Plastic Analysis(kN/m)	Updated Mesh Analysis (kN/m)	Updated Mesh Analysis with interfaces (kN/m)
4.1	Bottom – 31.083 Top – 26.997	Soil body failed	Soil body failed
4.2	Bottom – 5.64 Top – 4.13	Bottom – 6.38 Top – 4.14	Soil body failed
4.3	4.16	4.23	2.93
4.4	27.19	33.45	32.67
4.5	Fortrac – 17.21 Comtrac – 4.73	Fortrac – 17.63 Comtrac – 4.42	Fortrac – 14.84 Comtrac – 4.20

A comparison between the predicted values from the various methods can be seen in Table 9. BS8006 is not consistent. Guido's method under estimates the tensile strength of the geogrid greatly. Terzaghi and Hewlett's methods seem to give results close to those given by Plaxis.

Table 9: Comparison between observed and predicted values for tensile strength of the geogrid along the length of the embankment

Case No	BS8006 (kN/m)	Terzaghi (kN/m)	Hewlett & Randolph (kN/m)	Guido (kN/m)	Plaxis Without void below the geogrid (kN/m)	Plaxis with void below the geogrid (kN/m)	Observed Tensile Strength Along length of Embankment (kN/m)
4.1	168.69	402.33	407.87	19.24	31.083	297.117	182
4.2	41.052	55.425	50.288	12.136	Top-4.14 Bottom–6.38	Top-24.18 Bottom–28.91	
4.3	67.23	46.213	50.259	13.331	4.23	67.19	
4.4	3.436	55.153	47.717	10.77	33.45	59.15	140
4.5	30.87	31.3	35.427	4.621	Fortrac - 17.63 Comtrac – 4.38	Fortrac - 37.73 Comtrac – 4.42	

The comparison between the tensile strength along the width of the embankment calculated using the different analytical methods are presented in Table 10.

Table 10: Comparison between observed and predicted values for tensile strength of the geogrid along the width of the embankment

Case No	BS8006 (kN/m)	Terzaghi (kN/m)	Hewlett & Randolph (kN/m)	Guido (kN/m)	Observed Tensile Strength Along the width of Embankment(kN/m)
4.1	285.44	519.07	524.62	135.99	182
4.2	80.148	94.52	89.384	51.231	
4.3	76.492	55.476	59.521	22.594	
4.4	82.603	134.32	126.883	89.937	170
4.5	50.661	51.092	55.219	24.412	

4.3.3. Bending Moment in the Piles

The maximum bending moments that are developed in the system are of importance in the design of the system. The maximum bending moment is found in the pile located at the embankment toe.

The results in Table 11 show no significant difference between the plastic and the Updated Mesh analysis. This shows that the geometry does not affect the analysis. The values for the Updated Mesh analysis are used for the comparison. However, in the case the of Polk Parkway, due to the large number of elements, the Updated Mesh analysis failed. However, results of the plastic analysis can be used as the geometry effect is not significant. The table also shows that the inclusion of interfaces decreases the bending moment. Due consideration should be given to that. However, the computer time increases drastically with the inclusion of the interfaces. So, using an estimate from the updated mesh analysis after applying certain corrections is more practicable.

Table 11: Prediction of maximum bending moment in piles near the toe of the embankment

Case No.	Max. Bending Moment Plastic Analysis(kNm)	Max Bending Moment - Updated Mesh Analysis (kNm)	Max. Bending Moment - Updated Mesh with interfaces (kNm)
4.1	10.818	Soil body crashed	Soil body crashed
4.2	16.468	19.642	Soil body crashed
4.3	21.63	22.89	18.501
4.4	568.232	552.557	531.822
4.5	8.211	8.843	8.9355

The maximum moments calculated using empirical relations given by Goh et al seem to be very high compared to the results obtained from Plaxis (Table 12). However, no data were available on the actual bending moments in the piles. Hence, it is difficult to draw any conclusions.

Table 12: Prediction of maximum bending moment in piles near the toe of the embankment

Case No	Maximum Bending Moment predicted in Piles(kNm)Goh et al.	Maximum Bending Moment predicted by Plaxis(kNm)
4.1	244.517	10.818
4.2	279.924	19.642
4.3	-[1)]	22.89
4.4	3020	552.557
4.5	-[1)]	7.153 – with void 8.843 – without void

1)The maximum bending moments for cases 4.3 and 4.5 could not be calculated as the value of undrained shear strength are not known.

4.3.4. Pile Efficiency

The efficiency of the piles is defined as the proportion of the embankment weight carried by the piles. The efficiency of the piles stated in Table 13 considers the weight of the soil. The calculations for pile efficiency can be found in Appendix A.

Table 13: Efficiency of the piles

Case No	Pile Efficiency (%)
4.1	30.8%
4.2	77.2%
4.3	69.2%
4.4	85.5%
4.5	54%

4.3.5. Slope Stability

The slope stability of the Rawang - Bidor Case was studied. The slope stability was computed after every step in the construction. Plaxis considers the presence of the piles and the geotextile unlike many of the other methods used. The only drawback is that the soft soil follows the Mohr-Coulomb failure criterion.

The results of the slope stability analysis performed on Case 4.5 can be seen in Figure 58. The safety factor can be evaluated by plotting the displacements against the parameter $\sum M_{sf}$ for two points. One point is the toe of the slope, the other point on the slope at the level of the pile heads. The maximum settlements seen in this graph are not significant as we set displacements to zero at the beginning of every Phi-c reduction calculation.

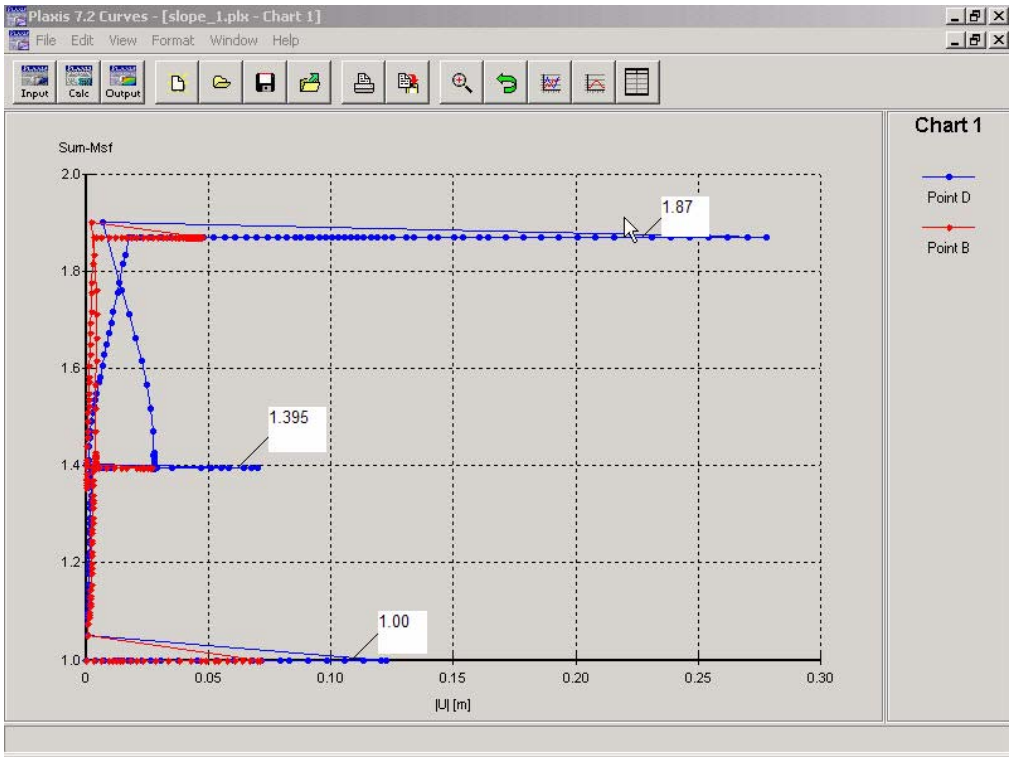

Figure 58: Evaluation of factor of safety for the embankment slope of AuGeo Piled Embankment – Rawang Bidor

4.3.6. Maximum and Differential Settlements

The total and differential settlements at the pile head and at the surface can be found using Plaxis. No other methods have been developed to determine the settlements. For deep mixed columns, settlement calculation methods have been put forward by PWRC (2000) and Ogisako (2002). However, they could not be compared with Plaxis results due to lack of sufficient data. It can be seen that the value for maximum settlement predicted for Case 4.1 is very close to the observed value of 0.0889m. The differential settlement in Case 4.3 was about 0.015m with traffic load. In the absence of the traffic load the differential settlement given by Plaxis was 0.008m. The values given in Table 14 are based on the Updated Mesh Analysis. There is no void considered below the geogrid.

The presence of the void and inclusion of the interfaces increases the settlements significantly. As the interfaces could not be introduced in all cases, the results are not shown here.

Table 14: The predicted maximum and differential settlements at the top of the embankment

Case No	Maximum Settlements(m)	Differential Settlements(m)
4.1	0.1164	0.0137
4.2	0.03544	0.001
4.3	0.03285	0.008
4.4	0.05155	0.015
4.5	0.1339 – w/o void 0.1658 – with void	0.006 – w/o void 0.009 –with void

Table 15: The predicted maximum and differential settlements at the top of the pile

Case No	Maximum Settlements(m)	Differential Settlement(m)
4.1	0.1267	0.01
4.2	0.03484	0.017
4.3	0.03748	0.01
4.4	0.06135	0.03
4.5	0.1218 – w/o void 0.1676 – with void	0.003 – with void 0.064 – w/o void

It can be seen that the differential settlement decreases from the pile head to the top of the embankment. This is due to development of soil arching at the pile heads. In Case 4.3, it can be seen that the maximum settlement at the top of the embankment is less than that at the pile heads. This is because the maximum settlement at the ground surface includes the settlement reflected from the occurring in the soft soil, the compression of the embankment fill under its own weight. However, this portion of reflection is very high when the embankment height is less. This effect reduces with increase in height of embankment.

Geosynthetic reinforced pile supported embankments, represent a complex problem. Many of the factors which are not considered in the other empirical or

analytical methods are handled by Plaxis. A great number of such comparisons are required to establish the degree of reliability. However, the complete complex nature of the system cannot be handled by Plaxis alone. Much research yet needs to be done in this area.

CHAPTER 5
CONCLUSIONS AND RECOMMENDATIONS

5.1.Conclusions

Geosynthetically reinforced pile supported embankments have several technical advantages over other ground improvement techniques. The GRPS techniques can reduce the total, differential and lateral movements. Slope stability of the embankment increases with the use of the GRPS system. Common applications of GRPS embankments are in bridge approaches, railroads, retaining walls and roadway widening over soft soils.

A number of methods have been developed to evaluate embankments placed over soft soil. A few of these have been discussed in this study. The main aim of this study was to make finite element models of the available case histories in Plaxis 2D. There are several case studies where GRPS embankments were used. However, all the data required for developing the finite element model were available in only five case studies. The finite element study shows that factors like tensile stiffness of the geogrid, the pile modulus, the height of the embankment and the position of the geogrid affect the GRPS system significantly. However, these effects are not considered by the other available methods.

There are no methods available for the determination of lateral movements of GRPS embankments. The methods discussed in this study are the ones used for unreinforced piled embankments. Results from the finite element program which gives due consideration to piles and geosynthetic reinforcement seem to be more reliable. The finite element method is able to model the GRPS system without resorting to simplifying

assumptions. The stresses and displacements in the system at all points in the system can be evaluated. However, the finite element analysis requires the soil strength and stiffness data.

The tension in the geosynthetic reinforcement has been compared using the stress reduction factor. BS8006 seems to be a conservative method. Guido's method gives highly under predicted values. The Terzaghi and Hewlett & Randolph methods are very consistent and comparable. However, none of the methods show a consistency with the results obtained from Plaxis. Using the finite element program, the impact of the soil resistance provided by the underlying soil can be studied. The variation in the tensile strength of the geogrid, due to presence or absence of supporting soil, can be seen. However, Plaxis is not able to evaluate the tension in the reinforcement along the width of the embankment. Research is required in this area.

The effect of the position of the geogrid on the top of the pile and the tensile stiffness can be studied using Plaxis 2D. However, making large plane strain models in Plaxis is quite laborious. Plate load tests give reliable values for the parameters, such as spacing between the geogrids, the number of geogrids and the height and width of reinforced fill, required in the design of the geotextile reinforcement.

Several methods are available for determination of lateral deflection of the piles. The bending moment in the pile based on empirical relations is presented by Goh et al. This can be done for initial analysis. However, more detailed analysis should be performed.

The modified boundary method studies the influence of piles in slope stabilization. It follows the conventional Bishop slip circle method. The response of the pile is studied

separately. A program called SLOPIL can be used for analysis of this nature. However, the geosynthetic reinforcement is not considered in this method. The BS8006 method considers both the piles and the geosynthetic reinforcement. It is also based on the Bishop circle method. It can also handle short term stability analysis considering pore water pressures and performing an undrained analysis. The friction circle method was found most convenient for homogenous slopes. This method also does not consider the geoynthetic reinforcement.

The maximum and differential settlements can be calculated using the finite element analysis. The methods put forward by Ogisako (2002) and PWRC (2000) for deep mixed columns need verification from field data. There are no other analytical methods developed for piled embankments.

Considering the current methods available for analysis, the numerical analysis is more reliable. This method considers the effect of the tensile stiffness of the geosynthetic, the pile modulus and the change in height of the embankment on the stress concentration ratio which is neglected by all other methods. Plaxis can calculate the tension in geosynthetic reinforcement in a multi-layer reinforced fill. No other methods are able to handle this situation.

5.2. Recommendations

1. There is a need to develop a method to predict the lateral movements of GRPS embankments. All the available methods are for unreinforced embankments.
2. Research is required in the area of soil resistance provided by the underlying soft soil in calculating the tension in the reinforcement.
3. A method to analyze a multi-layer geosynthetic reinforced fill platform is required.
4. A relation needs to be established between the 2-Dimensional and 3-Dimensional models developed using finite element analysis.

5. An analytical method needs to be developed for the determination of maximum and differential settlements.

6. It is essential to verify the prediction of the bending moments developed in the piles with field data.

7. Research is required in the area of calculating the tensile strength in the geogrid along the width of the embankment using Plaxis.

APPENDIX
SAMPLE CALCULATIONS IN MATHCAD

KPa = 1000 Pa KN = 1000N

Case Study: AuGeo Piled Embankment Railway Track RAWANG – IPOH

Data available:

d = 0.15m	pile diameter
H = 2.5m	height of embankment
s = 1.0m	spacing between adjacent piles
a = 0.3m	size of pile caps
h_s = 6m	thickness of soft clay layer
γ = 19 KN/m^3	unit weight of embankment fill
ϕ` = 30 deg	friction angle of the embankment fill
ε_a = 0.06	axial strain in the reinforcement
w_s = 0 KN/m^2	uniformly distributed surcharge loading
E_p = 2.85 x 10^7 KN/m^2	elastic modulus of the pile

Partial factors used:

f_{fs} = 1.0	load factor for the embankment fill – servicibility limit state
fq = 1.0	load factor for external live loads – servicibility limit state
f_{fs_u} = 1.3	load factor for embankment fill – ultimate limit state
f_{q_u} = 1.3	load factor for external live loads – ultimate limit state

Geosynthetic Reinforcement Design

BS8006 Method

$C_c = 1.95\frac{H}{a} - 0.18$ for end bearing piles

$C_c = 16.07$

$\sigma_v = (f_{fs}\gamma H) + f_q w_s$

$p_c' = \sigma_v'\left(\frac{C_c a}{H}\right)^2$

$S_{3D1} = \frac{2.8s}{(s+a)^2 H}\left(s^2 - a^2\frac{p_c}{\sigma_v}\right)$

$S_{3D1} = 0.441$

$W_{T1} = \frac{S_{3D1}\gamma H(s^2 - a^2)}{2(s-a)}$

$W_{T1} = 13.613$ KN/m

$T_{rp1} = \frac{S_{3D1}\gamma H(s^2 - a^2)}{4a}\sqrt{1 + \frac{1}{6\varepsilon}}$

$T_{rp1} = 30.87$ KN/m

Terzaghi Method

K = 1 ratio between horizontal and vertical pressure assumed to be 1 by Terzaghi

$S_{3D2} = \frac{(s^2 - a^2)}{4HaK\tan(\varphi')} \times \left(1 - e^{\frac{-4aHK\tan(\varphi')}{s^2 - a^2}}\right)$

$S_{3D2} = 0.447$

$$W_{T2}=\frac{S_{3D2}\gamma H(s^2-a^2)}{2(s-a)}$$

$$T_{rp2}=\frac{S_{3D2}\gamma H(s^2-a^2)}{4a}\sqrt{1+\frac{1}{6\varepsilon}}$$

T_{rp2} = 31.3 KN/m

Hewlett and Randolph Method

$$K_p=\frac{1+\sin(\varphi`)}{1-\sin(\varphi`)}$$

K_p = 3

Conditions at the crown lead to a Stress Reduction Ratio

$$S_{3D3}=\left(1-\frac{a}{s}\right)^{2(K_p-1)}\left(1-\frac{s}{2\sqrt{H}}\times\frac{2(K_p-1)}{(2K_p-3)}\right)+\frac{(s-a)}{\sqrt{2}H}\times\frac{2(K_p-1)}{(2K_p-3)}$$

S_{3D3} = 0.414

Conditions at the pile cap lead to another Stress Reduction Ratio

$$S_{3D4}=\frac{1}{\left(\frac{2K_p}{K_p+1}\right)\left(\left(1-\frac{a}{s}\right)^{(1-K_p)}-\left(1-\frac{a}{s}\right)\left(1+\frac{a}{s}K_p\right)\right)+\left(1-\frac{a^2}{s^2}\right)}$$

S_{3D4} = 0.506

$$S_{3D\_hew}:=\begin{cases}S_{3D3} & \text{if } S_{3D3}\geq S_{3D4}\\ S_{3D4} & \text{otherwise}\end{cases}$$

$$W_{T4}=\frac{S_{3D\_hew}\gamma H(s^2-a^2)}{2(s-a)}$$

$$T_{rp3}=\frac{S_{3D\_hew}\gamma H(s^2-a^2)}{4a}\sqrt{1+\frac{1}{6\varepsilon}}$$

T_{rp3} = 35.427 KN/m

Guido's Theory

$$S_{3D5}=\frac{(s-a)}{3\sqrt{2}H}$$

S_{3D5} = 0.066

$$W_{T5}=\frac{S_{3D5}\gamma H(s^2-a^2)}{2(s-a)}$$

$$T_{rp5}=\frac{S_{3D5}\gamma H(s^2-a^2)}{4a}\sqrt{1+\frac{1}{6\varepsilon}}$$

T_{rp5} = 4.621 KN/m

Tension in Reinforcement due to Lateral Sliding

$$x=45deg-\frac{\varphi`}{2}$$

$$K_a=\tan(x)^2$$

$$T_{ds}=0.5K_a(f_{fs}\gamma H+2f_q w_s)H$$

T_{ds} = 19.792 KN/m

Tensile Force in Reinforcement along the width

BS8006	$T_{rp\_w1}=T_{rp1}+T_{ds}$	T_{rp_w1} = 50.661 KN/m
Terzaghi	$T_{rp\_w2}=T_{rp2}+T_{ds}$	T_{rp_w2} = 51.092 KN/m

Hewlett & Randolph	$T_{rp\_w3}=T_{rp3}+T_{ds}$	T_{rp_w3} = 55.219 KN/m
Guido	$T_{rp\_w4}=T_{rp4}+T_{ds}$	T_{rp_w4} = 24.412 KN/m

Pile Design

Efficiency of piles

$\delta = \frac{a}{s}$ $\delta = 0.3$

$K_p = \frac{1+\sin(\varphi`)}{1-\sin(\varphi`)}$

$K_p = 3$

$E = 1-\delta\left(1-\frac{s}{2H}\right)(1-\delta)^{(K_p-1)}$

E = 0.882

When the height of the soil is considered

$\beta_1 = \frac{2K_p}{(K_p+1)} \times \frac{1}{(1+\delta)} \times \left((1-\delta)^{-K_p} - (1+\delta K_p)\right)$

β_1 = 1.172

$E = \frac{\beta_1}{1+\beta_1}$

E = 0.54

Pile Group Capacity

$Q_p = 150$ KN — allowable load carrying capacity of each pile in the pile group

$w_s = 54$ KN/m^2 — external surcharge loading

$$s = \sqrt{\frac{Q_p}{\left(f_{fs\_u}\gamma H + f_{q\_u} w_s\right)}}$$

$s = 1.066$m

Note: The spacing here has been calculated for the actual external loading. However, in the study external loads are not applied.

Pile Group Extent

$n = 0.5$ — side slope of the embankment

$\theta_p = 45^\circ - \varphi`$

$\theta_p = 15$ deg

$L_p = H\left(n - \tan\theta_p\right)$ — horizontal distance between the outer edge of the outside pile cap and the toe of the embankment

$L_p = 0.58$m

KPa = 1000Pa KN = 1000N

Case Study: Timber Pile in-Situ Soil Reinforcement – Polk Parkway

Maximum Bending Moment in the Pile

Data available:

d = 0.3048m	pile diameter
c_u = 37KPa	average undrained shear strength of soil
ϕ` = 30 deg	friction angle for embankment fill
h_s = 12m	thickness of the soft clay layer
H = 6m	height of the embankment
B = 85m	width of the embankment
$E_p = 2.29 \times 10^8$ KN/m^2	elastic modulus of the pile
$\gamma = 19$ KN/m^3	unit weight of the embankment fill
$q=\gamma H$	overburden pressure

$E_{50}=200c_u$

$E_{50} = 7.4 \times 10^6$ Pa

$I_p=\frac{\pi d^4}{64}$ moment of inertia of the pile

$I_p = 4.237 \times 10^{-4}$m^4

$K_R=\frac{E_p I_p}{E_{50} h_s^4}$

$K_R = 6.323 \times 10^{-4}$

$\lambda=1.88\left(K_R\right)^{0.5}$

$\lambda = 0.047$

$\beta=0.18\left(K_R\right)^{-0.1}$

$\beta = 0.376$

$M=\lambda e^{\left[\beta(q/c_u)\right]}$

$M_{max}=Mc_u dh_s^2$

$M_{max} = 244.517$ KNm

Efficiency of piles

a = 0.3048m size of pile caps

s = 1.52m centerline spacing of piles

$\delta=\frac{a}{s}$ $\delta = 0.201$

$K_p=\frac{1+\sin(\varphi`)}{1-\sin\left(\varphi`\right)}$

$K_p = 3$

$E=1-\delta\left(1-\frac{s}{2H}\right)(1-\delta)^{(K_p-1)}$

E = 0.888

When the height of the soil is considered

$\beta_1=\frac{2K_p}{\left(K_p+1\right)}\times\frac{1}{(1+\delta)}\times\left((1-\delta)^{-K_p}-\left(1+\delta K_p\right)\right)$

$\beta_1 = 0.444$

$E=\frac{\beta_1}{1+\beta_1}$

E = 0.308

Pile Group Capacity

$Q_p = 266.88$ KN allowable load carrying capacity of each pile in the pile group

$w_s = 0$ KN/m^2 external surcharge loading

$$s=\sqrt{\frac{Q_p}{\left(f_{fs\_u}\gamma H+f_{q\_u}w_s\right)}}$$

$s = 1.342$m

Note: The spacing here has been calculated for the actual external loading. However, in the study external loads are not applied.

Pile Group Extent

$n = 0.5$ side slope of the embankment

$\theta_p=45^{\circ}-\varphi`$

$\theta_p = 15$ deg

$L_p=H\left(n-\tan\theta_p\right)$ horizontal distance between the outer edge of the outside pile cap and the toe of the embankment

$L_p = 1.392$m

Lateral Movements at the toe of the Embankment

Bourges and Mieussens Method

$$F=\frac{(\pi+2)c_u}{\gamma H}$$

$F = 1.669$

$$a=\frac{h_s}{B}$$

$a = 0.141$

From graph: $\lambda_1 = 2\%$ $\lambda_2 = 3\%$

$y_1 = \lambda_1 h_s$ $y_1 = 0.24m$

$y_2 = \lambda_2 h_s$ $y_2 = 0.36m$

Marche & Chapuis Empirical Method

$E_u = 300c_u$ initial approximation of the undrained modulus

$E_u = 1.11 \times 10^7$ Pa

$q = \gamma H$

$a = 0.141$

$R_1 = 0.0$ $R_2 = 0.025$

$$y_1 = \frac{R_1 qB}{E_u}$$

$y_1 = 0m$

$$y_2 = \frac{R_2 qB}{E_u}$$

$y_2 = 0.022m$

LIST OF REFERENCES

Alzamora, D., Wayne, M.H., and Han, J. (2000). "Performance of SRW supported by Geogrids and Jet Grout Columns." Proceedings of sessions of ASCE Specialty Conference, Amherst, Geotechnical Special Publication No. 94, edited by A.J. Lutenegger and D.J. DeGroot, ASCE, 456-466.

Brinkgreve, R. B. J., and Vermeer, P.A. (1998). Plaxis - Finite Element Code for Soil And Rock Analysis - Version 7, A.A. Balkema Publishers, Netherlands.

British Standard 8006 (1995). Design of Embankments with Reinforced Soil Foundations on Poor Ground. **Section 8:** 98-118.

Cortlever, I. N. G., and Gutter, H.H (2002). "Design of Double Track Railway Bidor-Rawang on AuGeo Piling System according to BS8006 and PLAXIS Numerical Analysis." available at url: http://www.cofra.com/papers/KL2002Augeo.pdf (Accessed Jan 2004).

Gutter, H. H. (2002). "AuGeo Piled Embankment with Fortrac Geogrids Railway Track Rawang -IPOH." OMEGAM Environmental Research Institute, Amsterdam.

Han, J. (1999). "Design and Construction of Embankments on Geosynthetic Reinforced Platforms Supported by Piles." Invited Speaker, Proceedings, 1999 ASCE/PaDOT Geotechnical Seminar, Hershey, PA.

Han, J. (2003). "Development of Design Charts for Geosynthetically Reinforced Embankments on Deep Mixed Columns." Interim Report, Literature Review, Principal Investigator, funded by the FHWA National Deep Mixing Program, 2002-2003, Widener University, Chester, PA.

Han, J., and Akins, K. (2002). "Use of Geogrid Reinforced and Pile-Supported Earth Structures." Proceedings, International Deep Foundations Congress 2002, Orlando, Geotechnical Special Publication No. 116, edited by O'Neill and Towsend, ASCE, 668-679.

Han, J., and Gabr, M.A. (2002). "Numerical Analysis of Geosynthetic-Reinforced and Pile- Supported Earth Platforms over Soft Soil." Journal of Geotechnical and Geoenvironmental Engineering, ASCE, 128(1), 44-53.

Han, J., and Wayne, M.H "Pile-Soil-Geosynthetic Interactions in Geosynthetic Reinforced/Piled Embankments over Soft Soil." Presentation and CD-Rom Paper at 79th Annual TRB meeting.

Hueng, W., Kuo, C.L.,and Roberts, J. (1998). "Surcharge of Phosphatic Waste Clay with Strip Drains." Proceedings of the Conference American Society of Civil Engineers, Boston, Massachusetts, Geotechnical Special Publication No. 81, edited by A. Maher and D.S. Yang, ASCE, 298-312.

Kempton, G., Russell, D., Pierpoint, N.D., and Jones, C.J.F.P. (1998) "Two- and Three-Dimensional Numerical Analysis of the Performance of Piled Embankment." Proceedings of the 6th International Conference on Geosynthetics, Atlanta, available at url: http://www.maccaferri-northamerica.com/downloads/view.php?file=25 (Accessed March 2004).

Kuo, C. L., Heung, W., Tejidor, F.J.,and Roberts, J. (1998). "A Case Study of Timber Pile in-situ soil reinforcement." Proceedings of the Conference American Society of Civil Engineers, Boston, Massachusetts, Geotechnical Special Publication No. 81, edited by A. Maher and D.S. Yang, ASCE, 177-189.

Li, Y., Aubeny, C., and Briaud, J. (2002). "Geosynthetic Reinforced Pile Supported Embakments." Draft submitted to FHWA, Texas A & M University, College Station.

Ostensen, A. K., and Bennett, K.D (2002). Geotechnical Report for Slope Stability Repair Concepts. Williams Earth Sciences, Inc., Polk County, Florida.

BIOGRAPHICAL SKETCH

Rutugandha Gangakhedkar was born in Aurangabad, India, on August 29, 1979. She received her Bachelor of Civil Engineering from V.J.T.I. University of Mumbai. Her desire for education then brought her to the University of Florida, Gainesville. She began working on her master's degree in geotechnical engineering in August 2002. She will pursue her career in the field of geotechnical engineering on graduation.